SPE
Society of Petroleum Engineers

SPE 15431

Oil and Gas Relative Permeabilities Determined From Rate-Time Performance Data

by M.D. Fetkovich, *Phillips Petroleum Co.*; E.T. Guerrero, *U. of Tulsa*; and M.J. Fetkovich and L.K. Thomas, *Phillips Petroleum Co.*

SPE Members

This paper was prepared for presentation at the 61st Annual Technical Conference and Exhibition of the Society of Petroleum Engineers held in New Orleans, LA October 5-8, 1986.

SUMMARY

This paper presents a method of determining k_g/k_o, oil relative permeability, k_{ro}, and gas relative permeability k_{rg}, using oil and gas rate-time performance data from individual wells and from a total field. Advanced decline curve analysis is used to obtain original oil in place, N, and thus saturation; the Δp^2 form of an oil inflow performance equation is used to determine k_{ro} below the bubble point pressure.

The procedure was used on production data from several wells in a North Sea naturally fractured limestone volatile oil field. Results indicate the calculated oil and gas relative permeability curves differ from laboratory and correlation calculated curves. By analyzing the oil and gas relative permeability curves of each of the seven wells in the field, it was found that the degree of natural fracturing of a specific well influences the position of the oil and gas relative permeability curves. The results expressed as k_g/k_o curves appear to be consistent with the field case history findings of Arps for limestone reservoirs - i.e., as the degree of fracturing increases, the k_g/k_o curves become more unfavorable with respect to oil recovery.

Initial pressure surveys on each well determine its degree of fracturing while a later field-wide pressure survey confirms the oil-in-place calculated for each well using rate-time decline curve analysis.

Pressure-time data to make these calculations is seldom available for all wells in a field or, when available, is much less frequent than rate-time data. In contrast, the principal calculation methods shown in this paper use rate-time data, thus taking advantage of the most frequently collected and the most widely available information.

References and illustrations at end of paper.

INTRODUCTION

The conventional approach to calculating gas-oil permeability ratio from field production performance data requires that reservoir pressures as a function of time be available.[1,2,3] Sufficient pressure data as a function of time for all individual wells in a field are seldom available to calculate each individual well's gas-oil permeability ratio. This is largely a result of the expense and loss of production that would be incurred in conducting pressure tests and the lack of reasonably accurate individual well oil and gas production data.

Total field performance derived gas-oil permeability ratio curves are usually based on averaging reservoir pressures from only a few wells and often do not provide adequate areal and time coverage of the entire field. The frequency of conducting pressure survey usually depends on the rate of pressure decline in the field, the expense of conducting the survey, and safety considerations.

When pressure as a function of time data are available, the Schilthius[4] or Tarner[5] conventional "black-oil" material balance equation is used to solve for the original oil-in-place. For volumetric reservoirs, (a necessary assumption for calculation of the gas-oil permeability ratio curve), oil-in-place, N, using the material balance equation will calculate to be essentially constant as a function of time. Once the original oil-in-place is known, the gas-oil permeability ratio and oil or gas saturation can be calculated for each available reservoir pressure value.

Rate-time oil and gas production data should be available for all wells in a field on a monthly basis, either through direct measurement or through allocation based on reasonably accurate monthly separator tests. Rate-time analysis[6,7,8] is made with such production data to develop not only a gas-oil permeability ratio but also the relative permeabilities to oil and gas for individual wells. The method is used

on production data from several wells in the Edda Field, a North Sea naturally fractured limestone volatile oil field in the Greater Ekofisk Development.

Rate-Time Analysis Equations

Before the gas-oil permeability ratio and the oil and gas relative permeabilities can be calculated, the original oil-in-place, N, and productivity factor, PF, must be determined from rate-time performance data. Rate-time[6,7] decline analysis provides a method for calculating both the original oil-in-place and productivity factor on an individual well basis from production data for individual wells. This type of analysis utilizes the concept that once a well and its offsets have reached pseudo-steady state flow, a no flow boundary will result at a distance between all wells. The distance to the no flow boundaries for a well will depend on the flow rate of each offset well. Thus, the drainage volume of each well should remain constant if all wells are on decline and continue producing wide open against a common backpressure with no drastic changes in a well's production rate occurring.

To calculate the pore volume (oil-in-place) and productivity factor (productivity index) a log-log plot of oil production versus time is made. The rate-time plot is overlayed and matched on the Fetkovich type curve.[9] From a type curve match, the match point, $q(t) - q_{Dd}$ and $t - t_{Dd}$ is obtained.

The dimensionless flow rate is defined by

$$q_{Dd} = \frac{q(t)}{\dfrac{kh(P_i - P_{wf})}{141.2(\overline{\mu_o B_o})[\ln(r_e/r_w')-1/2]}} \qquad \text{.....(1)}$$

and the dimensionless time is defined by

$$t_{Dd} = \frac{0.00634kt}{\phi(\mu C_t)_i r_w'^2} \cdot \frac{1}{1/2[(r_e/r_w')^2-1][\ln(r_e/r_w')-1/2]} \qquad (2)$$

($P_i = \overline{P}_R$ at the start of decline analysis.)

The match points are used directly in the calculation of oil-in-place and productivity factor.

Two forms of the rate-time pore volume and productivity factor equations are used in this study. One form assumes the oil decline rate below the bubble point pressure is proportional to $(\overline{P}_R - P_{wf})/\overline{\mu B_o}$.[7] The other form utilizes an m(p) of oil[7,10] approach - i.e., the oil rate with the reservoir pressure, $\overline{P}_R$, below the bubble point pressure declines as a function of $\overline{P}_R^2 - P_{wf}^2$. The first approach evaluates $(\overline{\mu_o B_o})$ at average pressure, $(\overline{P}_R + P_{wf})/2$, and will be called the Δp approach.

The flow rate equation for the Δp approach is

$$q_o = \frac{7.08\ kh}{[\ln(r_e/r_w')-1/2]} \cdot \frac{(\overline{P}_R - P_{wf})}{(\overline{\mu_o B_o})} \qquad \text{...(3)}$$

For the Δp approach, the pore volume can be calculated with the rate-time analysis match points from the following equation

$$V_p = \frac{5.615(\overline{\mu_o B_o})}{(\mu C_t)_{\overline{P}_R}(\overline{P}_R - P_{wf})} \cdot \frac{t}{t_{Dd}} \cdot \frac{q(t)}{q_{Dd}} \qquad \text{....(4)}$$

and oil-in-place is

$$N = \frac{V_p(1 - S_{wi})}{B_{oi}} \qquad \text{.....(5)}$$

The productivity factor, PF, is defined as

$$PF = \frac{7.08\ kh}{\left[\ln\left(\dfrac{r_e}{r_w'}\right) - \dfrac{1}{2}\right]} = \frac{(\overline{\mu_o B_o})}{\overline{P}_R - P_{wf}} \cdot \frac{q(t)}{q_{Dd}} \qquad \text{...(6)}$$

A more rigorous method uses an m(p) of oil or an oil well inflow performance relationship as proposed by Fetkovich.[10] This will be referred to as the Δp^2 approach. The flow-rate equation for the Δp^2 approach is expressed as

$$q_o = \frac{7.08\ kh}{\left[\ln\left(\dfrac{r_e}{r_w'}\right) - \dfrac{1}{2}\right]}\left[\frac{P_b^2 - P_{wf}^2}{2P_b(\mu_o B_o)_{P_b}} + \frac{\overline{P}_R - P_b}{(\overline{\mu_o B_o})_{\overline{P}_R, P_b}}\right] \qquad (7)$$

Using the rate-time match points, pore volume is calculated from the following equation

$$V_p = \frac{5.615\ [q(t)/q_{Dd}](t/t_{Dd})}{(\mu C_t)_{\overline{P}_R}\left[\dfrac{\overline{P}_R - P_b}{(\overline{\mu_o B_o})_{\overline{P}_R, P_b}} + \dfrac{(P_b^2 - P_{wf}^2)}{2P_b\ (\mu_o B_o)_{P_b}}\right]} \qquad \text{..(8)}$$

and oil-in-place is

$$N = \frac{V_p(1 - S_{wi})}{B_{oi}} \qquad \text{.....(5)}$$

The productivity factor is

$$PF = \frac{7.08\ kh}{\left[\ln\left(\dfrac{r_e}{r_w'}\right) - \dfrac{1}{2}\right]} = \frac{q(t)/q_{Dd}}{\left[\dfrac{\overline{P}_R - P_b}{(\overline{\mu_o B_o})_{\overline{P}_R, P_b}} + \dfrac{P_b^2 - P_{wf}^2}{2P_b(\mu_o B_o)_{P_b}}\right]} \qquad \text{..(9)}$$

The oil-in-place calculated from rate-time analysis is then used with a reservoir material balance equation and the actual gas and oil production to calculate reservoir pressure. Then the gas-oil relative permeability ratio and gas saturation can be calculated. The rate-time productivity factor is used to calculate the oil relative permeability. Gas relative permeability values are calculated by multiplying the oil relative permeability by the gas-oil permeability ratio at the same gas saturation. These calculations will be discussed and demonstrated in detail later.

"Black Oil" Approach of Determining the Gas-Oil Permeability Ratio

The term "black oil" normally refers to reservoirs that have reservoir temperatures below 150°F, an initial solution GOR below 500 SCF/STB, and stock tank oil gravities below 35° API. Such a fluid will have little or no liquids drop out of the free gas phase when flashed through a separation process. Under "black oil" conditions, the Schilthius or Tarner material balance equation is used with oil and gas production data and conventional laboratory and/or calculated PVT data to calculate a gas-oil relative permeability ratio for a well or a total field. Laboratory PVT analysis will give the oil viscosity, gas and oil formation volume factors and solution gas-oil ratios as a function of pressure that are needed in the material balance equation. Gas viscosity normally is calculated from a correlation. The laboratory PVT study also determines the bubble point pressure of the reservoir fluid.

When the reservoir pressure is below the bubble point pressure in a solution gas drive reservoir without water influx nor an initial gas cap, the following equation can be used to calculate reservoir pressure, $\bar{P}_R$, as a function of fractional recovery.

$$\frac{N_p}{N} = \frac{B_o - B_{oi} + (R_{si} - R_s)B_g + B_{oi}\left(\frac{C_w S_{wc} + C_f}{1 - S_{wc}}\right)(\bar{P}_{R_{bp}} - \bar{P}_R)}{B_o + (R_p - R_s)B_g} \quad (10)$$

Determining N from rate-time analysis and using reported cumulative gas-oil ratio and cumulative oil production, we iterate on reservoir pressure using the above material balance equation until the right hand side equals the left hand side. We thus obtain reservoir pressure, $\bar{P}_R$, for every cumulative oil production period. After the reservoir pressure has been determined for each monthly production period, the pressure dependent terms, R_s, B_o, B_g, μ_g, and μ_o can be determined to then calculate the liquid saturation and gas-oil permeability ratio using the following equations

$$S_L = \left(1 - \frac{N_p}{N}\right)\frac{B_o}{B_{oi}}(1 - S_{wc}) + S_{wc} \quad \ldots\ldots(11)$$

or

$$S_g = 1 - S_L \quad \ldots\ldots\ldots\ldots\ldots\ldots(12)$$

$$\frac{k_g}{k_o} = (R - R_s)\frac{\mu_g B_g}{\mu_o B_o} \quad \ldots\ldots\ldots\ldots(13)$$

COMPOSITIONAL CALCULATION OF GAS-OIL PERMEABILITY RATIO

The classical black oil calculation of PVT data is based on a two component system (gas and oil) where gas is allowed to dissolve in oil, but oil is assumed to always exist in the liquid phase. This assumption is valid for low to medium gravity oil, but does not hold for volatile oils and gas condensates since substantial amounts of the oil component can exist in the gaseous phase. Thus, black oil PVT data used in conjunction with separator oil and gas rates from a volatile oil reservoir will give incorrect material balance, oil saturations and gas-oil permeability ratios.

A composite (differential and flash) oil formation volume factor and solution gas-oil ratio can be calculated using a one-cell compositional material balance by flashing reservoir oil from each depletion step by itself through the separators. The following equations can be used to determine the oil formation volume factor and solution gas-oil ratio,

$$B_o = \frac{\text{Moles stock tank oil/molar density stock tank oil}}{\text{Moles reservoir oil/molar density reservoir oil}} \quad ..(14)$$

$$R_s = \frac{379(5.615)(\text{moles gas from separators})}{\text{Moles reservoir oil/molar density reservoir oil}} \quad ....(15)$$

The gas formation volume factor and liquid content of the gas phase, r_s, can be calculated by flashing reservoir gas through the separators,

$$B_g = \frac{379(5.615)(\text{moles gas from separators})}{\text{Moles reservoir gas/molar density of reservoir gas}} \quad ....(16)$$

$$r_s = \frac{\text{Moles condensate from separator/molar density of stock tank condensate}}{379(5.615)(\text{moles separator gas})} \quad ....(17)$$

The gas-oil permeability ratio can then be determined at a specific fractional oil recovery by using the following modified black oil equation (see Appendix for derivation),

$$\frac{K_g}{K_o} = \left(\frac{R - R_s}{1 - r_s R_s}\right)\frac{\mu_g B_g}{\mu_o B_o} \quad .....(18)$$

A compositional material balance can also be used to directly calculate the gas-oil permeability ratio for a volatile oil reservoir using rate-time depletion data. At each time step the oil rate is set and K_g/K_o is varied until the computed gas-oil ratio equals the producing gas-oil ratio. The corresponding gas saturation is obtained from the flash of remaining fluids at the end of the time step. The compositional material balance program was used to directly calculate the K_g/K_o and S_g results reported for the Edda Field study.

Oil and Gas Relative Permeability

With the reservoir pressure, $\overline{P}_R$, oil formation volume factor, and the historical oil flow rates (excluding condensate for volatile oil reservoirs) now available, the relative permeability to oil, K_{ro}, can be calculated. Rate-time analysis matching will give the $q(t)$ and q_{Dd} needed to calculate the productivity factor using equations 6 or 9.

Once the productivity factor, PF, has been determined, the relative permeability to oil can be calculated by using the following equation for the Δp^2 approach.

$$k_{ro} = \frac{2\overline{P}_R(\mu_o B_o)_{\overline{P}_R} q_o}{PF\ (\overline{P}_R^2 - P_{wf}^2)} \qquad \text{.....(19)}$$

and for the Δp approach

$$k_{ro} = \frac{q_o(\overline{\mu_o B_o})}{PF(\overline{P}_R - P_{wf})} \qquad \text{.....(20)}$$

For each production period - monthly for this study - an oil relative permeability value is calculated. The corresponding gas saturation is calculated by using equations 11, 12 for black oil systems or obtained from a compositional material balance run for volatile oil systems. Rate data immediately after a shut-in period is normally not used for low permeability reservoirs. After an extended shut-in, transient flow behavior will cause the production to be higher than would occur under pseudo-steady state flow conditions. This leads to invalid oil relative permeability values being calculated. After the relative permeability to oil and gas-oil permeability ratio have been calculated, a value for gas relative permeability can be obtained. This is accomplished by multiplying the gas-oil permeability ratio by the oil relative permeability at the same gas saturation

$$K_{rg} = \frac{K_{rg}}{K_{ro}} \cdot K_{ro} \qquad \text{.....(21)}$$

In reality, the productivity factor, PF, could also include a rate dependent skin $s(q, t)$ and a non-darcy flow term, $D_o q_o$, for completeness.[10] For simplicity, we have assumed these terms to be zero in calculating the relative permeability to oil. An $s(q, t)$ term that would exist when $\overline{P}_R$ is above the bubble point pressure with drawdown below the bubble point pressure would vanish once the total reservoir pressure dropped below the bubble point pressure. In contrast the D_o term if present should increase in the presence of an increasing gas saturation with depletion.

PRODUCTION PERFORMANCE DATA FROM THE EDDA FIELD

Production performance data from the Edda Field, which is the smallest of four overpressured volatile oil fields within the Greater Ekofisk development in the Norwegian Sector of the North Sea, is used in this study. Production from the Edda Field started in December of 1979. Fig. 1 shows the wells and their location. The production data used in this study covers the same time period as that used in reference 6 to study the total Edda Field decline.

Perforations in some of the Edda Field wells are in the Ekofisk (Danian) chalk and Upper Cretaceous (Tor) chalk or Tor formation at approximately 11,000 feet. As indicated by production logs, the Tor formation provide the majority of the production with only a very small fraction coming from the Ekofisk formation when both formations are perforated. The Tor formation is considered to be much more highly fractured than the Ekofisk formation in the Greater Ekofisk area. The wells in the Edda Field had calculated fracture intensities ranging from 28 in well C-2 to 1 in well C-5 Table 2. Fracture intensity is defined as the effective permeability determined from a pressure build-up test divided by the effective permeability of the matrix.

Initial gas-oil ratios and pressure buildup test results suggested that the Edda Field may consist of two separate accumulations. The compositions of the reservoir fluid used for each of these two areas in this study are shown in Table 1. The PVT properties for the South Edda Field (the field we will concentrate on) are shown in Figure 2. Examining the initial reservoir fluid compositions along with the initial solution gas-oil ratios and noticing the high fraction of low and intermediate hydrocarbon fractions, it was concluded that a black oil approach of calculating K_g/K_o, K_{ro}, and K_{rg} performance from the North and South Edda Fields may not be appropriate.

Oil and gas-oil ratio production performance data are shown in Figures 3 through 9 for each of the seven producing wells in the Edda Field. The allocated oil production (including condensate) is in stock tank barrels per day. The allocated gas-oil ratio is in standard cubic feet per stock tank barrel while the separator test GOR is in standard cubic feet per separator barrel.

The individual well peak oil production rates ranged from approximately 13500 BOPD to 2000 BOPD. The gas-oil ratio for five of the South Edda Field wells (wells C-2, C-5, C-9, C-11, and C-14) was initially around 1700 SCF/STB while the other two wells in the North Edda Field (wells C-10 and C-15) had initial gas-oil ratios of approximately 2000 SCF/STB. This initial difference in GOR first suggested that the Edda Field may consist of two separate reservoirs. (Also, when the only field wide pressure buildup tests were performed on the wells of the Edda Field in September 1983, the two wells with the higher initial gas-oil ratios had significantly higher average reservoir pressures than the other five wells.) In the rate-time analysis evaluations, a bubble point pres-

sure of 6067 psi was used for the higher initial solution gas-oil ratio wells (2000 SCF/STB) and a bubble point pressure of 5045 psi was used for the lower initial solution gas-oil ratio wells (1700 SCF/STB). Initial gravities of the oil were approximately 41° API, ultimately increasing to 44° API. The producing gas-oil ratio increased steadily with time for wells C-2, C-5, and C-14, but increased only marginally for wells C-9, C-11, and C-15, and stayed approximately the same for well C-10.

EDDA FIELD INDIVIDUAL WELL RESERVOIR PARAMETERS

The connate water saturation for each well in the Edda Field was determined from resistivity logs. Log calculated average water saturations for the seven wells ranged from a low of 33.8% in well C-11 to a high of 47.8% in well C-5. The pay thickness of the oil zone for each well was calculated using a water saturation cutoff of 70%. Pay zone thickness ranged from a high of 120 feet in well C-9 to a low of 70 feet for well C-15. Porosity ranged from 20.8% to 25.3% and was calculated from a compensated neutron log. Table 2 summarizes these results for each well.

Total irreducible liquid saturation - water saturation plus residual oil - was determined from laboratory water flood tests on several Cretaceous core samples of different porosities. A plot was made which showed the effect of porosity on the total irreducible liquid saturation. Total irreducible liquid saturation for each well was determined by matching the compensated neutron log determined average porosity with the laboratory derived total irreducible liquid saturation versus porosity curve. The total irreducible liquid saturation values ranged from 63.5% for well C-15 to 53.5% for well C-2 (see Table 2). Residual oil saturation was approximated by subtracting the resistivity log determined irreducible water saturation from the laboratory determined total irreducible liquid saturation.

Because the fluids in the Edda Field are contained in a fractured limestone rock system and the fracture permeability dominates fluid flow, a fracture intensity FI was calculated for each well. This was done to determine if the degree of fracturing in the well would affect the gas-oil permeability ratio curve and oil and gas relative permeability curves for each well. In order to calculate fracture intensity, the initial well test effective permeability and matrix effective permeability were determined. The reservoir effective permeability was determined from the initial pressure buildup tests. Effective permeabilities calculated from the build-up tests ranged from a high of 18 md to a low of 0.5 md. The effective permeability of the matrix was determined by flowing oil through core samples at irreducible water saturation. These permeabilities ranged from 0.66 md to 0.28 md. Each of the cores had different porosities from which a plot of porosity versus effective permeability was made. The effective matrix permeability for each well was then determined by using its average log derived porosity with the laboratory determined effective matrix permeability versus porosity plot. The fracture intensity was calculated by dividing the reservoir effective permeability from the pressure buildup test by the laboratory derived value. Well C-2 had the highest fracture intensity of 28 and well C-5 had the lowest value of 1. As should be expected; well C-2 had much greater production rates than well C-5. All well test effective permeability results, laboratory derived matrix permeability values, and fracture intensities for each of the seven Edda wells are given in Table 2.

DISCUSSION OF RESULTS

Rate-Time Analysis

Rate-time analysis for each of the wells in the Edda Field was performed by plotting and matching the oil production rate versus time to the log-log composite type curve of reference[9]. The log-log plots with their corresponding match point are shown in Figures 10 through 16 and summarized in Table 3. The oil production rate used on the log-log plot is the oil rate, excluding condensates, not the total liquid as would be measured from the separator. Note that the log-log plot of the oil rate, excluding condensate, and the oil rate, including condensate, for well C-9, indicates that the b exponent matched was 0.5 and 0.6 respectively. Further note that the match point would be the same for both curves.

This observation was used to obtain a first estimate of reservoir pore volumes for each of the wells in the Edda Field. A compositional material balance computer run with rate-time calculated pore volume as input, calculated the historical K_g/K_o and gas saturation to match the actual rate and GOR performance. From the run we also obtained the surface oil production rate excluding condensate. A log-log plot of the rate-time data with the oil rate, excluding the condensate, was then made to confirm or recalculate a new reservoir pore volume. Changes were usually negligible since much of the early time data used for the initial match did not have much free gas associated with it.

From an analysis of the individual well rate-time plots, five of the wells indicated a decline exponent b of 0.5, while well C-5 had a b exponent of 0 (exponential), and well C-14 had a b exponent of 0.2. References[6,7] suggest that all wells in the same reservoir should be expected to have approximately the same value of b exponent. Well C-14's b exponent of 0.2 cannot be readily explained, but well C-5's exponent of 0 is thought to be caused by the well flowing at an insufficient velocity to prevent wellbore liquid loading i.e., a high bottomhole backpressure, P_{wf}, has existed for the well for a long time. A well's decline exponent b is a function of the level of backpressure.[9,11] (As P_{wf} approaches $\overline{P}_{Ri}$, b approaches 0.)

To determine the dimensionless flow rate, q_{Dd}, and dimensionless time, t_{Dd}, a match point is chosen. For convenience, the match points in this study were at a time of 1 month and a rate of 1000 BOPD for every well in the field. The dimensionless flow rates, q_{Dd}, ranged from a value of 0.64 for well C-5 to a value of 0.068 for well C-2, and the dimensionless time, t_{Dd}, ranged from 0.065 for well C-10 to 0.19 for well C-2. From the match point values, pore volume and the productivity factor for each well were calculated. The pore volume calculated using rate-time data was largest for well C-9, with 47,359,000 reservoir barrels and smallest for well C-5 with 11,210,000 reservoir barrels. The productivity factor was highest for well C-2 and lowest for well C-5, having values of 1.161 Darcy-ft and 0.123 Darcy-ft, respect-

ively. All pertinent results obtained from rate-time analysis are shown in Table 3.

To confirm that the pore volume for each well from rate-time analysis was reasonable, the average reservoir pressure, $\bar{P}_R$, calculated from a compositional material balance, using the rate-time calculated pore volume and actual oil and gas production rates, was compared with the average reservoir pressure obtained from the 1983 field-wide pressure buildup survey. See Figures 17-23. Pressure buildup results, in terms of P_{max}, P^* and $\bar{P}_R$, for each of the seven wells are shown in Table 3.

Separate compositional material balance runs were made with oil-in-place calculated from both the Δp and and Δp^2 pore volume equations (equations 4 and 8). The Δp pore volume equation always gave a calculated pore volume lower than the one calculated using the Δp^2 pore volume equation. (The area under the curve of $1/(\mu_o B_o)$ versus P from P_{wf} to $\bar{P}_R$ results in a smaller value than $\overline{(\mu_o B_o)}$ evaluated at $(\bar{P}_R + P_{wf})/2$ used with the Δp equation.) When using the pore volume calculated from the Δp pore volume equation, the compositional material balance computer program runs calculate a consistently lower average reservoir pressure.

Figures 17 through 23, show that when using the pore volume derived from the Δp^2 pore volume equation the material balance calculated average reservoir pressure for each well fell within the pressure buildup survey maximum shut-in pressure and P^* range. Good matches between the average reservoir pressure determined from the compositional material balance and buildup tests were found in wells C-9, C-11, and C-15 (Figures 19, 20, and 23). Pore volumes calculated using the Δp approach resulted in pressures which were always much less than the pressure found from the pressure buildup tests. The compositional material balance calculated average reservoir pressures for wells C-2 and C-14, using the pore volume obtained from the Δp pore volume equation, were even below the observed maximum shut-in pressure. Wells C-5, C-11, and C-14 fell within the maximum shut-in pressure and the P^* range using the Δp^2 calculated pore volume. Only Δp^2 calculated pore volume runs were made for the two wells in the North Edda Field (wells C-10 and C-15).

Relative Permeability Ratio, K_g/K_o

To determine a gas-oil permeability ratio curve for each of the wells in the volatile oil Edda Field, compositional material balance runs were made using the reported gas and oil production rates and the Δp^2 calculated pore volume determined from the rate-time match for each well. The gas-oil permeability ratio was determined by iterating on the gas-oil permeability ratio until the gas-oil ratio from production data matched the gas-oil ratio calculated from the material balance program. (For black oil reservoirs, K_g/K_o would be calculated directly using equation 13.) Gas-oil permeability ratio values were calculated for each monthly production period. When the reservoir pressure is above the bubble point pressure, the gas-oil permeability ratio is assumed equal to zero.

The calculated gas-oil permeability ratio versus gas saturation curves determined from the compositional material balance run for each of the wells in the Edda Field are shown in Figures 24 through 30. Only for wells C-5 and C-10 were the gas-oil permeability ratio versus gas saturation curves demonstrating unusual behavior. Well C-5's gas-oil permeability ratio curve (see Figure 25) is considered unreliable because the well tended to load up with liquid and produced erratically. Well C-10 had an unusual curve (Figure 27) because the producing gas-oil ratios for the well remain nearly constant (see also Figure 7). No explanation for this well's behavior has been found except that it appears to be in the North Edda Field and exhibits the same flat GOR behavior as the C-15 well which is also in the North Edda Field.

The most interesting result obtained from the individual well gas-oil permeability ratio curve study is that they all appear to be a function of fracture intensity. All of the well gas-oil permeability ratio curves have been normalized to the same average water saturation and plotted on Figure 31. Note that as the fracture intensity of the wells increase, the gas-oil permeability ratio curves become less favorable to oil flow, i.e., shift to the left. As can be seen from Figure 31, wells C-2 and C-14 which had fracture intensities of 28 and 18 respectively have the most unfavorable gas-oil permeability ratios. Well C-11 and C-15 have the lowest fracture intensities, and as would be expected, their relative permeability ratios are more favorable (were shifted more towards the right). The fact that gas-oil permeability ratio curves become unfavorable with higher fracture intensity suggests that capillary "end effects" may become a greater factor in naturally fractured reservoirs than in nonfractured systems. This end effect is caused by the capillary pressure discontinuity between the fracture and the matrix.

An average total South Edda Field gas-oil permeability ratio curve was determined as a function of gas saturation, using the total gas and oil production of the South Edda Field and the sum of the rate-time calculated individual well pore volumes, (Figure 32). The South Edda compositionally derived gas-oil permeability ratio curve was then compared using two different averaging methods, (Figure 33). The two averaging methods were least squares linear regression and volume averaging, as proposed by Guerrero.[3] (Actually Guerrero used a thickness weighted instead of volume weighted approach but the logic for using volume is similar.)

The linear regression technique attempts to make a best fit straight line from the individual well curves. The data from the wells in the South Edda Field used to develop a total field gas-oil permeability ratio using the linear regression technique is shown in Table 5. As can be seen in Figure 33, the linear regression method's gas-oil permeability ratio approximation falls within the general area of the compositionally derived gas-oil permeability curve. However, because the gas-oil permeability ratio determined with this method forms a straight line, the gas-oil permeability ratio would be incorrect at high and low gas saturations.

The volume averaging technique averages the individual gas-oil permeability ratio curves by weighting each by pore volume. The data used to derive this curve are also shown in Table 5. At the same gas-oil permeability ratio an average field gas saturation is generated by using the following equation,

$$S_{gavg} = \frac{\sum_{i=1}^{n} S_{gi} V_{pi}}{\sum_{i=1}^{n} V_{pj}} \quad \text{.....(22)}$$

A gas-oil permeability ratio curve generated using the volume averaged technique appears more reasonable than the linear regression method for two reasons: the curve will show characteristic curvature and the wells with the lower production rates (smaller drainage volumes) will not influence the shape of the curve as much as the wells with higher production rates (larger drainage volumes). As can be seen from Figure 33, the volume averaged gas-oil permeability ratio curve has almost the same shape as the compositional material balance derived gas-oil permeability ratio curve, but is shifted slightly towards higher gas saturation values. A volume averaged curve was also determined by normalizing each wells' curve to the South Edda Field's average connate water saturation of 36.4 percent with virtually no difference.

K_g/K_o Determined From Correlations

The use of Corey's correlation[12] to develop a gas-oil permeability ratio curve requires a value for the pore size distribution index, λ, be known. The pore size distribution index can be determined from either an air-brine capillary pressure laboratory test or a log calculated capillary pressure curve. A log calculated capillary pressure curve was made by plotting water saturation as a function of depth for the C-9 well. The pore size distribution index for both the log and laboratory derived capillary pressure curve was calculated from a plot of capillary pressure versus effective water saturation. A λ of 2.063 was found using the laboratory capillary pressure curve.

The field performance compositionally and black oil derived gas-oil permeability ratio curve for well C-9 are compared with Corey's correlation and laboratory (unsteady-state) derived gas-oil permeability ratio curve (Figure 34). The laboratory curve was generated from the unsteady-state gas drive method on a Cretaceous core with 25.3% porosity and an effective permeability to oil at connate water saturation of 0.38 millidarcies. Corey's gas-oil permeability ratio curve was calculated using the pore size distribution index of 2.063. Neither the laboratory nor Corey's calculated gas-oil permeability ratio curves resembled well C-9's compositionally or black oil derived gas-oil permeability ratio curve. Laboratory and Corey's calculated gas-oil permeability ratio curves have almost no curvature and fall within a small gas saturation range. This suggests that laboratory and Corey derived gas-oil permeability ratio curve should not be used for naturally fractured reservoirs, as would be expected.

In order to show the effect of condensate production from a volatile oil reservoir on the gas-oil permeability ratio curve, both the black oil and compositionally calculated curves are plotted on Figure 34. The black oil gas-oil permeability ratio curve for well C-9 is shown to be below the compositional derived gas-oil permeability ratio curve. The calculated values for black oil and the compositionally derived gas-oil permeability ratio for each monthly production period of well C-9 is given in Table 4. As more free gas is produced from this volatile oil well, the calculated black oil and compositional gas-oil permeability ratio curves deviate to a much greater extent. This is primarily due to the increased amount of condensate being produced from the free gas phase as the reservoir pressure is lowered. When the black oil approach is used to calculate a gas-oil permeability ratio curve from field production data, a more favorable curve than actually exists in the reservoir will be obtained.

K_g/K_o Compared With Other Fields

One objective of this study was to determine if naturally fractured solution gas drive fields producing from the same formation would have gas-oil permeability ratio curves located in approximately the same region on a gas-oil permeability ratio versus gas saturation plot. In Figure 35, the South Edda Field K_g/K_o curve is compared with Arps's limestone-dolomite-chert formations minimum, maximum and average curves.[13] All K_g/K_o curves in Figure 35 have been normalized to the same connate water saturation. Note that the total South Edda Field gas-oil permeability ratio curve lies in approximately the same location as the fractured reservoirs found in Arps's limestone curves. To further emphasize this point, total field curves from other naturally fractured fields in the Greater Ekofisk area are compared with the Edda Field curve, and are also shown on Figure 35. The Edda Field is the only oil field in the Greater Ekofisk Area that produces exclusively from the more highly fractured Tor (Cretaceous) formation. This would explain why the Edda Field K_g/K_o is the most adverse curve. All of the Greater Ekofisk field gas-oil permeability ratio curves, normalized to the same water saturation, are in approximately the same location on a gas-oil permeability ratio versus gas saturation plot. All generally fall between Arps' average and maximum curves. The minimum Arps limestone curve represents highly naturally fractured reservoirs (fractured chert), and the average limestone curve represents a medium degree of fracturing.

RELATIVE PERMEABILITY TO OIL (K_{ro}) AND GAS (K_{rg})

Relative permeability to oil, K_{ro}, was calculated in this study using an oil well inflow performance or Δp^2 backpressure equation (equation 19) and rate-time performance data for the seven individual wells in the Edda Field. Calculating the relative permeability to oil curves for individual wells gives some insight into how natural fractures influence fluid flow. An "average well" concept for a field would be required to calculate them from total field performance data. In the past, the only methods in which gas and oil relative permeability curves could be determined for naturally fractured reservoirs was by laboratory flooding of a fractured core,[14] using pseudo functions[15,16] or individual well history matching with simulation models. Very little information is given in any previously published literature on the shape of the oil relative permeability curve in an actual solution gas drive naturally fractured field case.

Relative permeability to oil curves were calculated for six of the wells in the Edda Field using a constant bottomhole flowing pressure of 1500 psi. Results of these calculations are shown in Figures 36 through 41. The one well that did not have its oil relative permeability calculated was well C-10, because the gas-oil ratio was virtually constant. The C-10 well is considered to be in the North Edda Field. The other North Edda well, C-15, also did not give a good relative permeability curve. The five wells which are located in the South Edda Field, however, gave calculated oil relative permeability values that had distinguishable trends. Of these five wells, only C-2 seemed to have some oil relative permeability points which were scattered.

Calculating the gas relative permeability was the next step. This was accomplished by multiplying the calculated oil relative permeability by the previously determined gas-oil permeability ratio at the same gas saturation. One interesting result noticed by examining the gas relative permeability curves was that no critical gas saturation exists. This, however, should be expected for wells in a naturally fractured reservoir.

The conventional productivity index or Δp backpressure equation was also used to derive a relative permeability to oil equation (equation 20). One way in which to determine whether the Δp or the Δp^2, inflow performance, method of calculating oil relative permeability should be used is to conduct an isochronal test on a well in the field of interest. The Edda Field and the Ekofisk Field have similar fluid and rock characteristics. An Ekofisk Field isochronal test was analyzed in a paper by Fetkovich.[10] The isochronal curve of the 2/4-2X well in the Ekofisk Field was shown to give the Δp^2 oil backpressure equation for flows below the bubble point pressure. These results suggest that the Δp^2 form of the oil backpressure equation should be used to calculate the relative permeability to oil in the Edda Field study.

Calculation of oil relative permeability was made on well C-9's production data using both the Δp and Δp^2 oil relative permeability equations. However, both were based on saturations and pressures, $\overline{P}_R$, determined from the Δp^2 calculated pore volume since the pore volume could also be determined from pressure performance data. The saturations are therefore the same for both the Δp and Δp^2 K_{ro} calculations. Data for these two calculations are shown in Table 6. A comparison of the oil relative permeability curves obtained using both the Δp and Δp^2 oil relative permeability equation is shown in Figure 42. The oil relative permeability calculated using the Δp equation gives lower oil relative permeability values than the Δp^2 equation. Therefore, if the Δp method is used for a reservoir exhibiting Δp^2 flow characteristics, a lower estimation of the oil and gas flow rates will be made.

The oil relative permeabilities of every well in the South Edda Field, all normalized to the same water saturation and using the Δp^2 oil relative permeability equation, are plotted on Figure 43. The wells with the higher fracture intensity generally gave more favorable oil relative permeability curves at high gas saturations. Well C-2 had the highest fracture intensity of 28 and almost had the appearance of a straight line. This would indicate that the fractures are dominating flow because the oil relative permeability curve for fracture flow is normally represented by a straight line. Well C-5 had a fracture intensity of 1, indicating little or no natural fractures, and had an unfavorable oil relative permeability curve at high gas saturations. From well C-5's performance derived oil relative permeability curve, it is concluded that flow in this well is dominated by matrix flow. It resembles the oil relative permeability curves found in an unsteady-state matrix core plug, (see Figure 45).

In order to determine whether Corey's correlation derived gas and oil relative permeabilities can be used to approximate actual field oil and gas flow rates, they are compared to wells C-2 and C-14 performance derived relative permeabilities (Figure 44). The relative permeabilities for oil and gas calculated using Corey's correlation are normalized to the same average water saturation that is used to normalize the performance calculated gas and oil relative permeability curves. The pore size distribution index varied between 0.1 to 1000. These values of 0.1 and 1000 were chosen to represent the most diverse cases of an extremely heterogeneous and homogeneous rock system, respectively. Calculated oil relative permeabilities for well C-2, which had the most favorable oil relative permeability curve, and well C-14, which had the least favorable oil relative permeability curve, are shown and compared on Figure 44. The dashed lines on Figure 44 represent the performance derived oil relative permeability curves of wells C-2 and C-14. Well C-14 matched fairly well with the homogeneous Corey's derived oil relative permeability curve which used a pore size distribution index of 1000. Well C-2 was to the left of Corey's derived oil relative permeability curves calculated using both pore size distributions of 0.1 and 1000. Note that only the oil relative permeability curve of well C-14 matched Corey's derived curve. The C-14 well fracture intensity of 18, and b exponent of 0.2, are lower than well C-2's fracture intensity of 28 and b exponent of 0.5. The major influence behind the difference between these two wells' oil relative permeability curve is thought to be the degree of fracturing. The gas relative permeability, shown also on Figure 44, calculated from Corey's equation deviated from performance derived gas relative permeability in that a critical gas saturation is assumed in Corey's equation and was not found in the performance derived values. Also, the gas relative permeability curve is much lower using Corey's equation as compared with the performance calculated gas relative permeability curve at low gas saturations. (For examples see Figures 45 and 46.)

Corey's correlation, laboratory, and performance calculated gas and oil relative permeability curves are compared for wells C-2 and C-9 in the Edda Field on Figures 45 and 46. A water-wet laboratory calculated oil and gas relative permeability curve was used. The pore size distribution value of 2.063 was used in Corey's oil and gas relative permeability equations.

The performance derived gas relative permeability curves are significantly different from Corey's or laboratory derived gas relative permeability curves. This difference is partly caused by the laboratory and Corey's derived gas relative permeability curves always having a critical gas saturation. In the case of production performance from our naturally fractured solution gas drive reservoir, no critical gas satura-

tion is seen to occur. Corey's and laboratory derived gas relative permeability curves might be used when attempting to approximate gas flow in an unfractured system, but should not be used in a naturally fractured system.

Both the oil relative permeability and gas-oil permeability ratio versus gas saturation curves derived from performance data for well C-9 were entered into a compositional material balance program along with pore volume from the rate-time analysis. A forecast was then made with the well producing wide-open against a minimum bottomhole flowing pressure of 1500 psia. A comparison between the actual oil production rate and gas-oil ratio and that computed from the compositional material balance program are shown in Figure 47. The comparison is excellent. The oil inflow performance equation used in the compositional material balance computer program to predict flow below the bubble point pressure is,

$$q_o = \frac{PF(\overline{P}_R^2 - P_{wf}^2)K_{ro}}{2\overline{P}_R(\overline{\mu_o B_o})_{\overline{P}_R}} \quad \text{.....(23)}$$

CONCLUSIONS

1. Rate-time analysis can be used to determine the original oil in place, N, for an individual well. It was found that by entering the Δp^2 calculated pore volume obtained by rate-time analysis and the gas and oil production for each of the wells in the Edda Field into the compositional material balance program, the average pressure computed from the compositional material balance matched quite well with pressure buildup average reservoir pressures.

2. Use of the black oil gas-oil permeability ratio equation for a volatile oil reservoir results in the calculation of a low gas-oil permeability ratio. In order to determine the gas-oil permeability ratio for a volatile oil reservoir, a correction term, designated r_s, can be introduced into the denominator of the black oil gas-oil permeability ratio equation, to correct for the amount of condensate being produced from the free gas phase.

3. As the fracture intensity is increased, the gas-oil permeability ratio becomes more unfavorable. Capillary end effects become more significant as the fracture intensity increases.

4. The Edda total field gas-oil permeability ratio curve was found to be in the same region as fractured limestone gas-oil permeability ratio curves shown in Arps' paper. Highly naturally fractured field gas-oil permeability ratio curves are closest to the minimum limestone Arps curve. Moderately naturally fractured reservoirs give gas-oil permeability ratio curves closer to the Arps average limestone curve.

5. The Δp^2 oil backpressure equation can be used to determine the relative permeability to oil from performance data.

6. Oil relative permeability curves derived from unsteady-state laboratory tests and Corey's correlation were found to be less favorable to oil flow than performance calculated oil relative permeability curves in the fractured limestone Edda Field. The unsteady-state and Corey's correlation calculated oil relative permeabilities are not applicable to naturally fractured reservoirs.

7. As fracture intensity increases, the performance derived oil relative permeability curve approaches a straight line between 0% gas saturation and the irreducible liquid saturation. Low fracture intensity wells have oil relative permeability curves similar to laboratory determined matrix curves. Intermediate fracture intensity wells have oil relative permeability curves somewhere between the straight line found in highly naturally fractured reservoirs and the oil relative permeability curve of an unfractured system.

8. It was found that the unsteady-state and Corey's correlation derived gas relative permeability curves were much lower at small gas saturations than performance derived gas relative permeability curves.

NOMENCLATURE

b	= reciprocal of decline curve exponent
B_g	= gas formation volume factor, RB/SCF
B_o	= oil formation volume factor, RB/STB
B_{oi}	= initial oil formation volume factor, RB/STB
C_f	= effective rock compressibility, psi^{-1}
C_t	= total compressibility, psi^{-1}
C_w	= water compressibility, psi^{-1}
GOR	= gas-oil ratio, SCF/STB
h	= oil zone thickness, ft
K_g/K_o	= gas-oil permeability ratio
K_{mat}	= effective fluid permeability of the matrix, md
K_{rg}	= relative permeability to gas, fraction
K_{ro}	= relative permeability to oil, fraction
N	= initial oil initially in place, STB
N_p	= cumulative oil production, STB
$\overline{P}$	= average pressure, psia $(\overline{P}_R + P_{wf})/2$
P_b	= bubble point pressure, psia
PF	= productivity factor, md-ft, equations 6 and 9
P_{max}	= maximum shut-in pressure, psia
$\overline{P}_R$	= reservoir average pressure, psia
P^*	= pseudo pressure obtained from pressure buildup test, psia
PVT	= pressure, volume, temperature variables (μ_o, μ_g, B_o, B_g)
P_{wf}	= bottomhole flowing pressure, psia
q_{Dd}	= decline curve dimensionless rate
q_o	= average oil production rate, excluding condensate, STB/Day
$q(t)$	= surface rate of flow at time t, STB/Day
Q_o	= average oil production rate, including condensate, STB/Day
r_e	= external boundary radius, ft
r_s	= condensate correction term, STB/SCF
r_w	= wellbore radius, ft
r_w'	= effective wellbore radius $r_w e^{-s}$, ft
R	= instantaneous gas-oil ratio, SCF/STB
R_p	= cumulative gas-oil ratio, SCF/STB
R_s	= solution gas-oil ratio, SCF/STB
s	= skin effect, dimensionless
S_g	= gas saturation

S_L = total liquid saturation
S_o = oil saturation
S_{wc} = water saturation
t = time, days
t_{Dd} = decline curve dimensionless time
μ_g = gas viscosity, cp
μ_o = oil viscosity, cp
$(\overline{\mu_o B_o})$ = viscosity - formation volume factor product evaluated at $(\overline{P}_R + P_{wf})/2$, RB-cp/STB
$(\mu_o B_o)_{\overline{P}_R, P_b}$ = oil viscosity - formation volume factor, product evaluated at $(\overline{P}_R + P_b)/2$, RB-cp/STB
$(\mu_o B_o)_{\overline{P}_R}$ = oil viscosity - formation volume factor product evaluated at P_b, or $\overline{P}_R$ if below bubble point, RB-cp/STB
V_p = reservoir volume, ft^3
λ = pore size distribution index
ϕ = porosity, fraction of bulk volume

Subscripts

g = gas
i = initial
o = oil

ACKNOWLEDGEMENTS

We wish to thank Phillips Petroleum Company for permission to publish this paper. We also wish to thank our Stavanger Office and our co-venturers in the Greater Ekofisk Development for permission to publish the Edda Field data.

REFERENCES

1. Amyx, J. W., Bass, D. M., and Whiting, R. L.: "Petroleum Reservoir Engineering," McGraw-Hill, (1960).

2. Craft, B. C. and Hawkins, M. F., Jr.: "Applied Petroleum Reservoir Engineering," Prentice Hall, Inc., Englewood Cliffs, N. J. (1959).

3. Guerrero, E. T. and Stewart, F. M.: "Practical Reservoir Engineering #1," Oil and Gas Journal.

4. Schilthius, R. J.: "Active Oil and Reservoir Energy," Trans AIME (1936) 118: 33-52.

5. Tarner, J.: "How Different Size Gas Caps and Pressure Maintenance Affect Ultimate Recovery," Oil Weekly (June 1944) 32.

6. Fetkovich, M. J., Vienot, M. E., Bradley, M. D., and Kiesow, U. G.: "Decline Curve Analysis Using Type Curves: Case Histories," paper SPE 13169 presented at the 59th Annual Fall Meeting of SPE of AIME, Houston, Texas, September 1984.

7. Fetkovich, M. J., Vienot, M. E., Johnson, R. D., and Bowman, B. A.: "Case Study of a Low Permeability Volatile Oil Field Using Individual-Well Advanced Decline Curve Analysis," paper SPE 14237 presented at the 60th Annual Technical Conference and Exhibition of the SPE, Las Vegas, NV, Sept. 1985.

8. Fetkovich, M. D.: "Oil and Gas Relative Permeabilities From Well and Reservoir Performance Data," Masters Thesis, U. of Tulsa, Tulsa, OK (1985).

9. Fetkovich, M. J.: "Decline Curve Analysis Using Type Curves," JPT (June 1980) 1065-1077.

10. Fetkovich, M. J.: "The Isochronal Testing of Oil Wells," paper SPE 4529 presented at the 48th Annual Fall Meeting, Las Vegas, Nev., Sept. 30 - Oct. 3, 1973.

11. Carter, R. D.: "Characteristic Behavior of Finite Radial and Linear Gas Flow Systems - Constant Terminal Pressure Case," SPE/DOE 9887 presented at the 1981 SPE/DOE Low Permeability Symposium, Denver, CO, May 27-29, 1981.

12. Corey, A. T., Rathjens, C. H., Henderson, J. H., and Wylie, M. R. J: "Three Phase Relative Permeability," Trans AIME (1956) 207, 349-351.

13. Arps, J. J. and Roberts, T. G.: "The Effect of the Relative Permeability Ratio, the Oil Gravity, and the Solution Gas-Oil Ratio on the Primary Recovery From a Depletion Type Reservoir," Trans AIME (1955) 204, 120-127.

14. Erlich, Robert: "Relative Permeability Characteristics of Vugular Cores - Their Measurement and Significance," paper SPE 3553 presented at the 46th Annual Fall Meeting of SPE of AIME, New Orleans, LA, Oct. 1971.

15. Jack, Hugh H., Smith, Owen J. E. and Matlax, C. C.: "The Modeling of a Three-Dimensional Reservoir With a Two-Dimensional Reservoir Simulator - The Use of Dynamic Pseudo Functions," paper SPE 4701 presented at the SPE-AIME 47th Annual Fall Meeting, San Antonio, Tex., Oct. 1973.

16. Kyte, J. R. and Berry, D. W.: "New Pseudo Functions to Control Numerical Dispersion," paper SPE 5105 presented at the SPE-AIME 49th Annual Fall Meeting, Houston, Tex., Oct., 1974.

SI METRIC CONVERSION FACTORS

bbl	x 1.589873	E-01	= m^3
bbl/D	x 1.589873	E-01	= m^3/D
c_p	x 1.0*	E-03	= Pa·s
ft	x 3.048*	E-01	= m
ft^3/D	x 2.831685	E-02	= M^3/D
md	x 9.869233	E-04	= μm^2
psi	x 6.894757	E-03	= MPa

* conversion factor is exact

APPENDIX

Modified Black-Oil Gas-Oil Permeability Ratio Equation For a Volatile Oil

Gas Rate $q_g = q_g \text{ free} + (q_o \text{ free})R_s$ ...A-(1)

Oil Rate $q_o = q_o \text{ free} + (q_g \text{ free}) r_s$ ....A-(2)

GOR $$GOR = \frac{q_g}{q_o} = \frac{\text{free} + q_o \text{ free } R_s}{\text{free} + q_g \text{ free } r_s} \quad ..A-(3)$$

For black oil, r_s is equal to zero and the above equation reduces to:

$$GOR = \frac{q_g \text{ free}}{q_o \text{ free}} + R_s \quad .....A-(4)$$

$$= \frac{K_g \mu_o B_o}{K_o \mu_g B_g} + R_s \quad ....A-(5)$$

The K_g/K_o for the black oil gas can be calculated as follows:

$$\frac{K_g}{K_o} = \frac{\mu_g B_g}{\mu_o B_o} (GOR - R_s) \quad ....A-(6)$$

For a volatile oil case K_g/K_o can be calculated by rearranging equation A-3.

$$GOR = \frac{(q_g \text{ free}/q_o \text{ free}) + R_s}{1 + (q_g \text{ free}/q_o \text{ free}) r_s} \quad ....A-(7)$$

$$GOR + GOR \left(\frac{q_g \text{ free } r_s}{q_o \text{ free}} \right) = \frac{q_g \text{ free}}{q_o \text{ free}} + R_s \quad ..A-(8)$$

$$GOR - R_s = \frac{q_g \text{ free}}{q_o \text{ free}} (1 - GOR * r_s) \quad .....A-(9)$$

$$\frac{K_g}{K_o} = \frac{\mu_g B_g (GOR - R_s)}{\mu_o B_o (1 - GOR * r_s)} \quad .....A-(10)$$

Note than when r_s is equal to zero (black oil), equation A-10 reduces to equation A-6.

TABLE 1

EDDA FIELD
INITIAL RESERVOIR COMPOSITIONS
(MOLE FRACTION)

COMPONENT	SOUTH EDDA	NORTH EDDA
C_1	0.5745	0.6210
C_2	0.0882	0.0826
C_3	0.0509	0.0471
i-C_4	0.0090	0.0078
n-C_4	0.0253	0.0236
i-C_5	0.0096	0.0075
n-C_5	0.0153	0.0125
C_6	0.0288	0.0098
C_{7+}	0.1917	0.1802
H_2S	0.0000	0.0000
N_2	0.0034	0.0035
CO_2	0.0033	0.0044
AVG. MOL. WT.	62.94	60.49
C_{7+} AVG. MW.	220.76	230.62
C_{7+} SP. GR.	0.8408	0.8430

	SEPARATOR CONDITIONS		
	1st STAGE	2nd STAGE	STOCK TANK
PRESSURE - psia	1015	265	15
TEMPERATURE - °F	155	80	60

TABLE 2

RESERVOIR PARAMETERS OF THE EDDA FIELD

WELL NO.	OIL ZONE THICKNESS (feet)	POROSITY FRACTION	WATER SATURATION FRACTION	IRREDUCIBLE LIQUID SATURATION FRACTION	BUBBLE POINT PRESSURE (psia)	BUILD-UP k-md	k_{matrix} (ϕ-K PLOT) md	FRACTURE INTENSITY (FI) k_{bu}/k_{matrix}
C-2	110	0.253	0.372	0.535	5045	18.4	0.66	28
C-5	70	0.238	0.478	0.565	5045	0.7	0.50	1
C-9	120	0.246	0.347	0.550	5045	9.3	0.58	16
C-10	82	0.240	0.400	0.562	6067	2.7	0.50	5
C-11	90	0.241	0.338	0.560	5045	5.7	0.52	11
C-14	114	0.226	0.363	0.600	5045	7.3	0.40	18
C-15	115	0.208	0.412	0.635	6067	1.7	0.28	6

INITIAL RESERVOIR PRESSURE - 7115 psia
RESERVOIR TEMPERATURE - 270°F

TABLE 3

RATE TIME ANALYSIS RESULTS FOR THE EDDA FIELD WELLS

WELL NO.	MATCH POINTS FOR t=1 mo; q(t)=1000 BPD q_{Dd}	t_{Dd}	DECLINE EXPONENT "b"	PORE VOLUME 1000 BBLS	PRODUCTIVITY FACTOR (Darcy-ft)
C-2	0.068	0.190	0.5	42,520	1.161
C-5	0.640	0.072	0.0	11,210	0.123
C-9	0.080	0.145	0.5	47,359	0.984
C-10	0.350	0.065	0.5	29,113	0.166
C-11	0.220	0.080	0.5	31,214	0.359
C-14	0.135	0.100	0.2	41,757	0.588
C-15	0.285	0.067	0.5	33,818	0.203

1983 PRESSURE BUILD-UP SURVEY RESULTS FOR THE EDDA FIELD WELLS

WELL NO.	MAXIMUM SHUT-IN PRESSURE P_{max}-psia	P* psia	AVERAGE RESERVOIR PRESSURE $\bar{P}_R$-psia
C-2	1757.5	2414	2359
C-5	3460.6	--	--
C-9	1977.8	2776	2737
C-10	2685.2	4108	4053
C-11	2483.5	3689	3637
C-14	2686.9	3550	3511
C-15	2740.4	4204	4171

TABLE 4

COMPARISON OF BLACK OIL AND COMPOSITIONAL DERIVED RELATIVE PERMEABILITY RATIOS FOR WELL C-9 (IN THE EDDA FIELD)

N_p Oil & Cond STK/BBL	N_p Oil STK/BBL	$\bar{P}_R$ psia	GOR SCF/STB	R_s	r_s STB/MMSCF	B_o RB/STB	B_g RB/MSCF	μ_o cps	μ_g cps	Black-Oil K_g/K_o	Modified Black Oil K_g/K_o	Compositional K_g/K_o	S_L * Black-Oil Fraction	S_L Compositional Fraction
196227	196227	6791	1725	1725		1.9075		0.1934					1.0	1.0
579532	579532	6184	1725	1725		1.933		0.184					1.0	1.0
838408	838408	5804	1725	1725		1.952		0.179					1.0	1.0
1040251	1040251	5516	1725	1725		1.967		0.174					1.0	1.0
1194430	1194430	5319	1725	1725		1.980		0.171					1.0	1.0
1396393	1396393	5057	1725	1725		1.997		0.167					1.0	1.0
1576129	1576118	4889	1724	1641	73.9	1.954	0.785	0.180	0.0301	0.0056	0.0064	--	0.9774	0.9754
1679089	1679083	4804	1691	1596	71.2	1.931	0.792	0.186	0.0302	0.0063	0.0072	0.0063	0.9657	0.9620
1841146	1836008	4652	2266	1514	66.7	1.888	0.807	0.196	0.0303	0.0497	0.0585	0.0538	0.9453	0.9403
1942400	1929488	4556	2544	1463	64.0	1.861	0.817	0.202	0.0287	0.0674	0.0805	0.0805	0.9326	0.9271
2074118	2052821	4438	2518	1401	60.9	1.829	0.829	0.210	0.0283	0.0682	0.0806	0.0783	0.9173	0.9113
2196255	2165392	4329	2648	1345	58.2	1.800	0.842	0.218	0.0276	0.0772	0.0913	0.0903	0.9035	0.8972
2311216	2271062	4231	2669	1295	55.8	1.774	0.854	0.225	0.0270	0.0794	0.0933	0.0926	0.8911	0.8848
2415426	2364360	4137	3049	1248	53.7	1.749	0.867	0.232	0.0264	0.1016	0.1215	0.1217	0.8795	0.8734
2503709	2442579	4057	3170	1208	51.9	1.729	0.879	0.238	0.0258	0.1081	0.1294	0.1308	0.8701	0.8641
2585398	2513989	3981	3417	1171	50.3	1.709	0.890	0.244	0.0254	0.1218	0.1471	0.1491	0.8610	0.8556
2663909	2582055	3907	3575	1135	48.8	1.691	0.902	0.249	0.0250	0.1307	0.1583	0.1607	0.8527	0.8475
2737785	2642587	3835	3800	1101	47.3	1.673	0.914	0.254	0.0247	0.1434	0.1748	0.1775	0.8447	0.8400
2807114	2704020	3767	4007	1070	46.0	1.657	0.926	0.259	0.0243	0.1540	0.1888	0.1927	0.8374	0.8331
2874283	2760625	3700	4131	1039	44.7	1.641	0.938	0.264	0.0240	0.1607	0.1971	0.2014	0.8303	0.8265
2912327	2795038	3673	2766	1027	44.2	1.635	0.943	0.266	0.0235	0.0886	0.1009	0.1042	0.8272	0.8234
2984690	2858209	3610	3661	999	43.1	1.620	0.956	0.270	0.0236	0.1373	0.1630	0.1646	0.8203	0.8171
3034825	2900435	3562	4169	978	42.2	1.610	0.966	0.274	0.0232	0.1621	0.1967	0.2028	0.8156	0.8126
3093637	2949622	3504	4422	953	41.2	1.597	0.978	0.278	0.0231	0.1765	0.2158	0.2210	0.8098	0.8072
3139604	2986011	3450	5391	930	40.3	1.585	0.990	0.282	0.0228	0.2253	0.2878	0.2979	0.8047	0.8028
3188189	3025197	3396	5142	907	39.4	1.574	1.003	0.286	0.0226	0.2133	0.2675	0.2762	0.7999	0.7983
3231875	3060947	3351	4895	889	38.6	1.564	1.014	0.289	0.0224	0.2013	0.2482	0.2559	0.7955	0.7944
3277559	3097609	3299	5360	868	37.8	1.554	1.027	0.293	0.0222	0.2249	0.2820	0.2917	0.7911	0.7903
3319943	3132265	3255	5005	850	37.1	1.545	1.038	0.296	0.0220	0.2075	0.2548	0.2634	0.7871	0.7867
3354327	3159899	3217	5372	835	36.5	1.537	1.048	0.299	0.0218	0.2255	0.2805	0.2913	0.7837	0.7838
3398654	3197595	3177	4323	820	35.9	1.529	1.059	0.302	0.0216	0.1735	0.2054	0.2125	0.7800	0.7804
3441335	3226627	3139	5283	805	35.4	1.522	1.070	0.304	0.0215	0.2226	0.2738	0.2835	0.7766	0.7775
3480089	2358334	3098	5180	790	34.8	1.514	1.082	0.308	0.0213	0.2170	0.2647	0.2754	0.7731	0.7744
3515226	3287305	3063	5047	777	34.2	1.507	1.092	0.311	0.0212	0.2109	0.2549	0.2652	0.7699	0.7716
3548618	3315577	3033	4487	766	33.8	1.502	1.102	0.313	0.0210	0.1832	0.2160	0.2241	0.7675	0.7692
3581559	3343089	3001	4843	754	33.4	1.496	1.112	0.316	0.0209	0.2010	0.2398	0.2492	0.7647	0.7668
3614022	3369446	2967	5485	742	32.9	1.490	1.123	0.319	0.0208	0.2331	0.2844	0.2965	0.7620	0.7643
3644481	3394617	2937	5124	731	32.5	1.484	1.133	0.322	0.0207	0.2156	0.2587	0.2693	0.7593	0.7621
3670745	3416140	2910	5320	721	32.1	1.479	1.142	0.324	0.0205	0.2247	0.2710	0.2834	0.7571	0.7601
3699590	3439852	2881	5300	711	31.7	1.474	1.153	0.327	0.0205	0.2250	0.2704	0.2816	0.7548	0.7580
3727006	3462561	2854	5146	702	31.4	1.470	1.163	0.329	0.0203	0.2169	0.2587	0.2704	0.7528	0.7561
3753304	3484115	2827	5443	692	31.0	1.465	1.173	0.332	0.0202	0.2315	0.2785	0.2919	0.7506	0.7542

* S_L Based on N_p (Oil & Cond.) Surface Measured Production

TABLE 5

CALCULATED FIELD AVERAGE K_g/K_o CURVE USING THE LINEAR REGRESSION METHOD (SOUTH EDDA FIELD)

S_g FRACTION	INDIVIDUAL WELL K_g/K_o					TOTAL FIELD K_g/K_o
	C-2	C-5	C-9	C-11	C-14	
0.05	0.100	0.185	0.037	0.0230	0.0745	0.0818
0.06	0.116	0.210	0.051	0.0266	0.0968	0.0899
0.07	0.133	0.241	0.059	0.0298	0.117	0.0988
0.08	0.155	0.273	0.069	0.0351	0.140	0.108
0.09	0.175	0.310	0.078	0.0400	0.167	0.119
0.10	0.197	0.350	0.090	0.0445	0.194	0.131
0.11	0.218	0.387	0.111	0.0509	0.224	0.144
0.12	0.259	0.442	0.115	0.0576	0.251	0.158
0.13	0.278	0.543	0.125	0.0639	0.285	0.174
0.14	0.298	0.624	0.141	0.0676	0.320	0.191
0.15	0.318	0.800	0.153	0.0780	0.355	0.209
0.16	0.337	--	0.168	0.0870	0.391	0.230
0.17	0.355	--	0.182	0.100	0.426	0.253
0.18	0.375	--	0.199	0.105	0.466	0.278
0.19	0.393	--	0.215	0.111	0.505	0.305
0.20	0.412	--	0.230	0.120	0.562	0.335

$$\text{LOG } (K_g/K_o)' = - 0.0408\ S_L + 2.789$$

CALCULATED FIELD AVERAGE K_g/K_o CURVE USING THE VOLUMETRIC AVERAGE METHOD (SOUTH EDDA FIELD)

K_g/K_o	INDIVIDUAL WELL GAS SATURATION - S_g					PORE VOLUME AVERAGED S_g
	C-2	C-5	C-9	C-11	C-14	
0.06	0.030	0.010	0.070	0.123	0.042	0.0589
0.07	0.035	0.014	0.080	0.138	0.049	0.0675
0.08	0.040	0.018	0.090	0.151	0.052	0.0747
0.09	0.043	0.020	0.099	0.163	0.059	0.0819
0.10	0.050	0.021	0.108	0.177	0.061	0.0890
0.11	0.055	0.025	0.116	0.189	0.064	0.0954
0.12	0.060	0.029	0.122	0.200	0.067	0.1012
0.13	0.065	0.031	0.131	0.208	0.071	0.1073
0.14	0.071	0.035	0.139	0.218	0.074	0.1136
0.15	0.078	0.039	0.148	0.226	0.079	0.1206
0.16	0.083	0.042	0.155	0.235	0.083	0.1265
0.17	0.089	0.045	0.161	0.242	0.089	0.1325
0.18	0.094	0.049	0.169	0.251	0.091	0.1381
0.19	0.100	0.052	0.178	0.259	0.095	0.1445
0.20	0.105	0.065	0.183	0.267	0.100	0.1506

TABLE 6

SOUTH EDDA FIELD'S WELL C-9's CALCULATED K_{ro} USING Δp^2 AND Δp METHOD

MONTH	S_L	$\bar{P}_R$ psia	q_o STB/Day	Δp^2 METHOD $(\mu_o\beta_o)\bar{P}_R$ STB-CP/RB	K_{ro}	Δp METHOD* $(\mu_o\beta_o)$ STB-CP/RB	K_{ro}
1	1.0	6791.3	6455	0.3689	1.0	0.4033	1.0
2	1.0	6184.4	12609	0.3564	1.0	0.4224	1.0
3	1.0	5804.1	8516	0.3487	1.0	0.4342	1.0
4	1.0	5516.3	6640	0.3427	1.0	0.4425	1.0
5	1.0	5319.3	5072	0.3388	1.0	0.4480	1.0
6	1.0	5056.9	6644	0.3339	1.0	0.4559	1.0
7	0.9754	4888.9	5912	0.3514	0.953	0.4603	0.816
8	0.9620	4803.5	3387	0.3585	0.569	0.4631	0.483
9	0.9403	4652.1	5162	0.3699	0.931	0.4672	0.777
10	0.9271	4555.5	3075	0.3767	0.580	0.4700	0.481
11	0.9113	4437.5	4057	0.3850	0.808	0.4741	0.665
12	0.8972	4329.3	3703	0.3927	0.776	0.4771	0.634
13	0.8848	4231.3	3476	0.3996	0.763	0.4801	0.621
14	0.8738	4136.7	3069	0.4061	0.706	0.4835	0.572
15	0.8641	4056.9	2573	0.4061	0.615	0.4859	0.497
16	0.8556	3980.7	2349	0.4162	0.586	0.4884	0.470
17	0.8475	3906.7	2239	0.4208	0.575	0.4908	0.464
18	0.8400	3835.4	2080	0.4250	0.533	0.4930	0.446
19	0.8331	3767.0	1932	0.4291	0.532	0.4961	0.430
20	0.8265	3700.3	1862	0.4329	0.530	0.4981	0.429
21	0.8234	3673.3	1132	0.4345	0.327	0.4986	0.264
22	0.8171	3610.1	2078	0.4381	0.620	0.5005	0.501
23	0.8126	3562.1	1389	0.4407	0.425	0.5024	0.344
24	0.8072	3503.5	1618	0.4439	0.510	0.5051	0.414
25	0.8028	3449.9	1197	0.4468	0.389	0.5063	0.316
26	0.7983	3396.2	1289	0.4497	0.431	0.5081	0.351
27	0.7944	3350.6	1176	0.4520	0.403	0.5110	0.330
28	0.7903	3299.4	1206	0.4547	0.426	0.5122	0.349
29	0.7867	3255.0	1140	0.4570	0.413	0.5135	0.339
30	0.7838	3217.0	909	0.4591	0.337	0.5151	0.277
31	0.7804	3176.8	1240	0.4610	0.471	0.5170	0.389
32	0.7775	3138.6	955	0.4631	0.371	0.5189	0.307
33	0.7744	3098.3	1043	0.4655	0.416	0.5204	0.345
34	0.7716	3062.9	953	0.4682	0.389	0.5217	0.323
35	0.7692	3032.8	930	0.4705	0.388	0.5224	0.322
36	0.7668	3001.3	905	0.4728	0.386	0.5240	0.321
37	0.7643	2966.9	867	0.4753	0.379	0.5246	0.315
38	0.7621	2936.7	828	0.4776	0.370	0.5260	0.308
39	0.7601	2910.0	708	0.4796	0.323	0.5263	0.267
40	0.7580	2880.9	780	0.4818	0.364	0.5281	0.303
41	0.7561	2854.1	747	0.4838	0.356	0.5285	0.297
42	0.7542	2827.3	709	0.4856	0.344	0.5295	0.287

* K_{ro} Δp method based on pressures, $\bar{P}_R$, determined from Δp^2 pore volume method

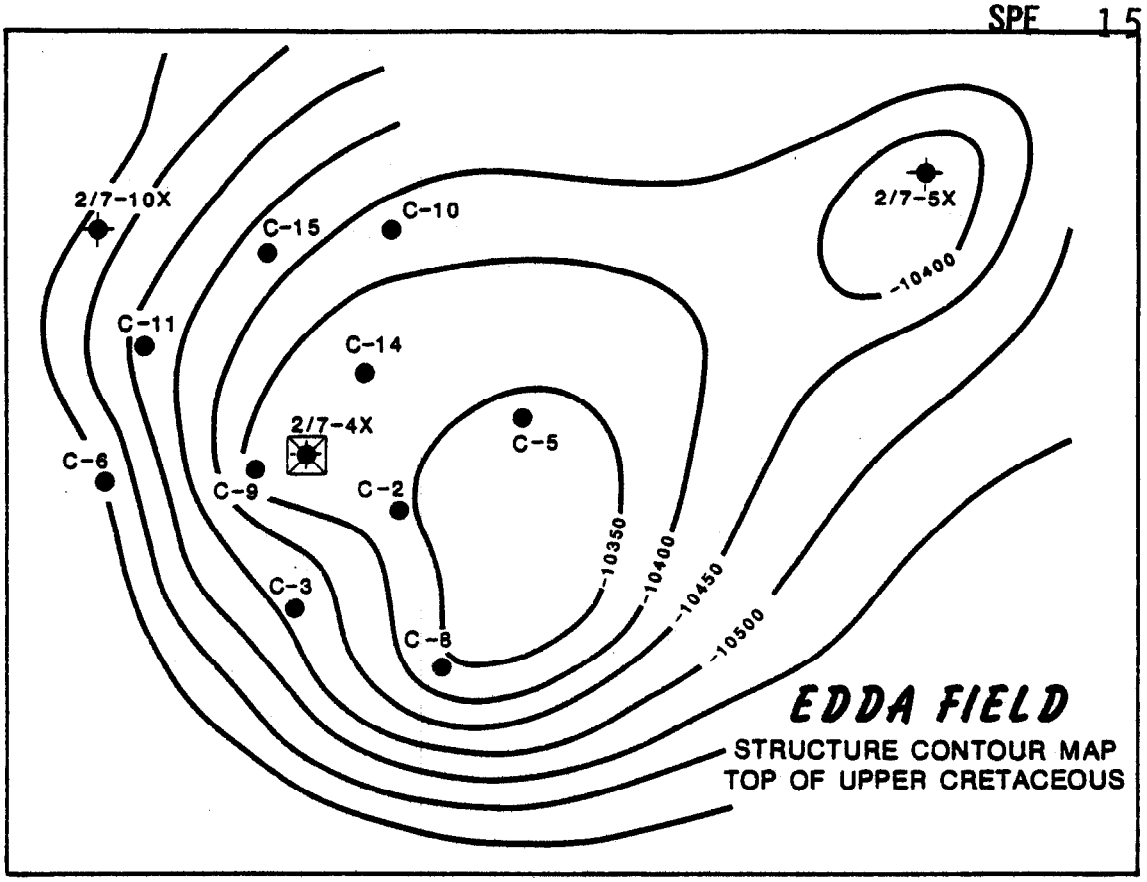

Fig. 1—Edda field well location map.

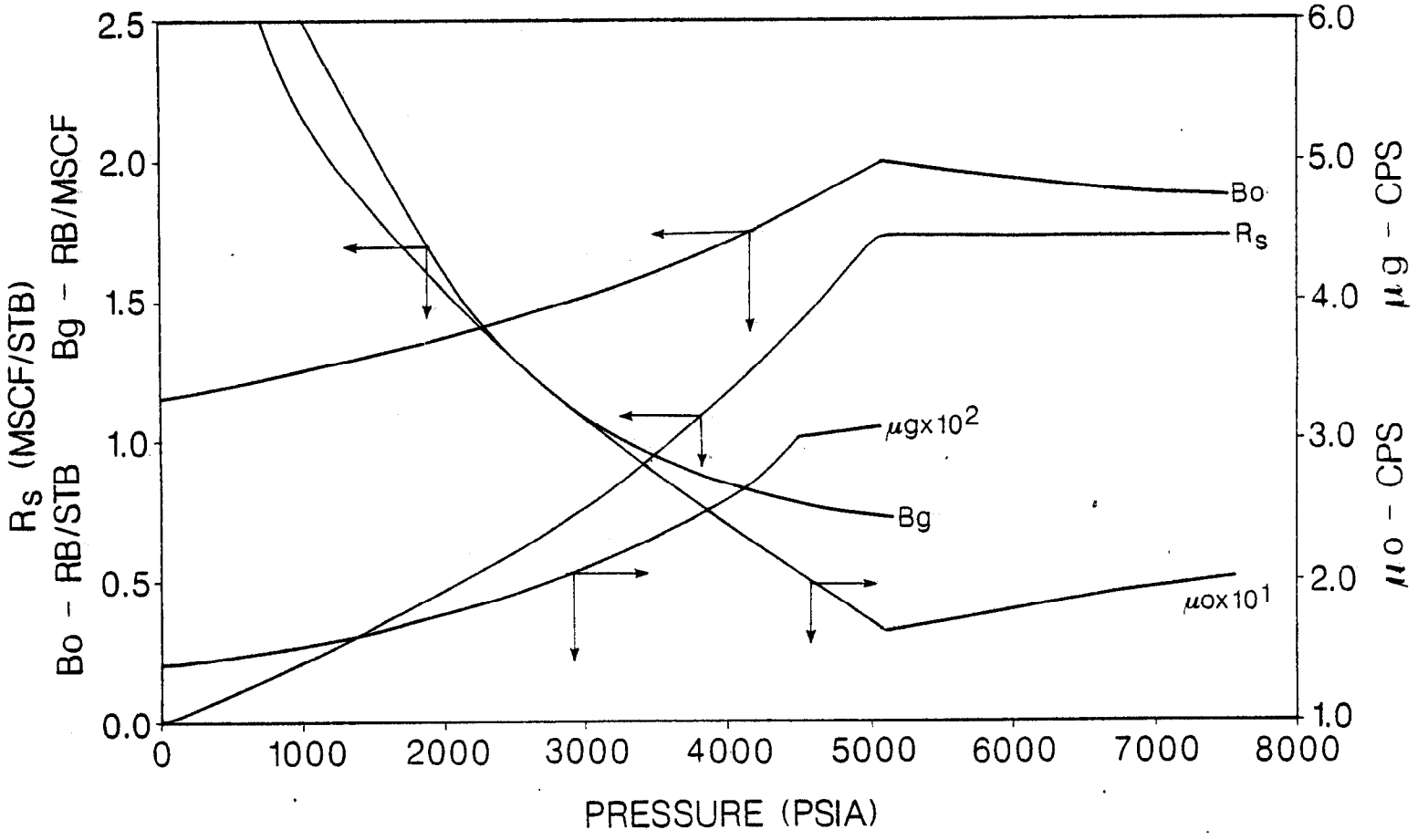

Fig. 2—South Edda field PVT data.

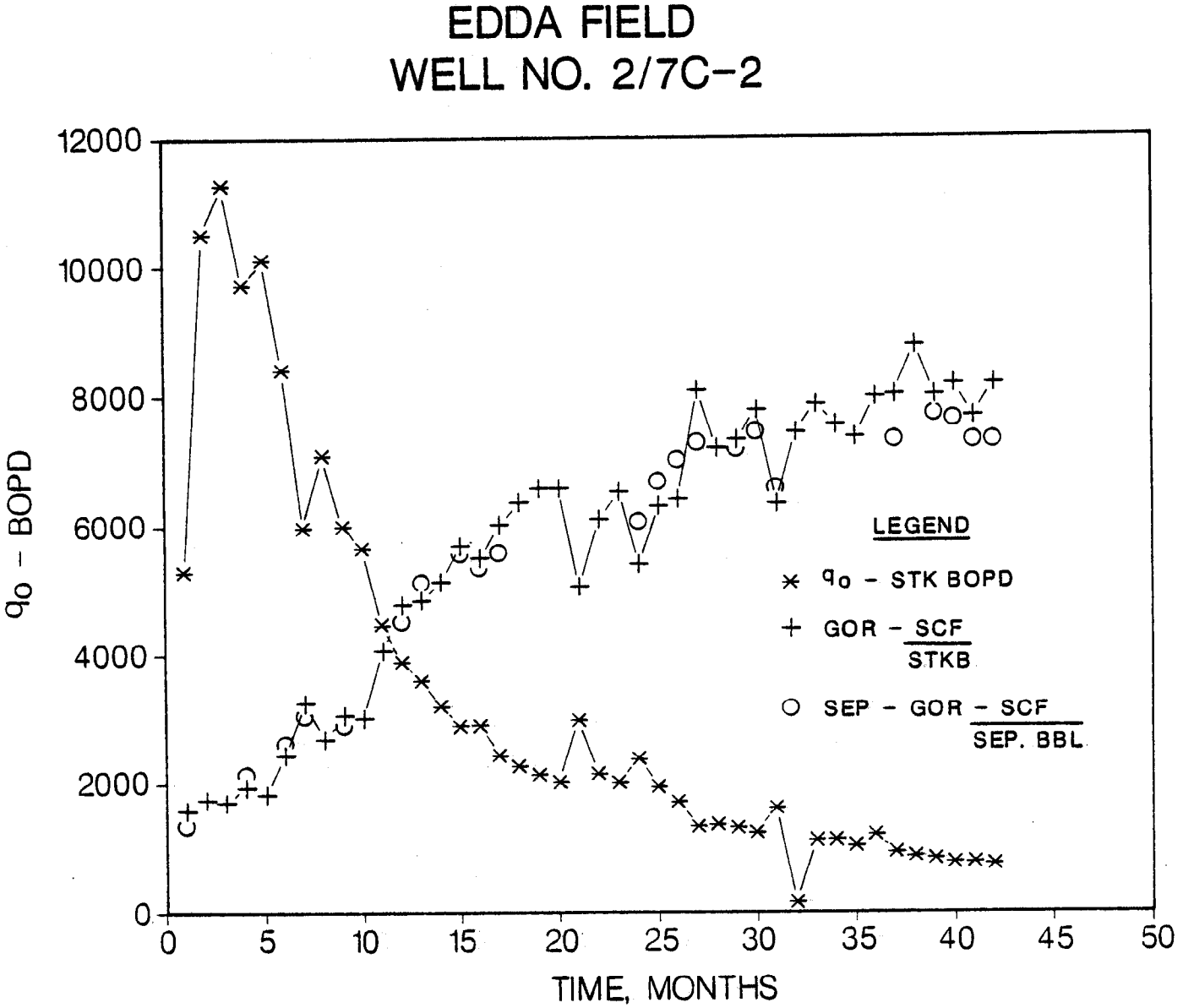

Fig. 3—Allocated GOR—production performance and separator test GOR's.

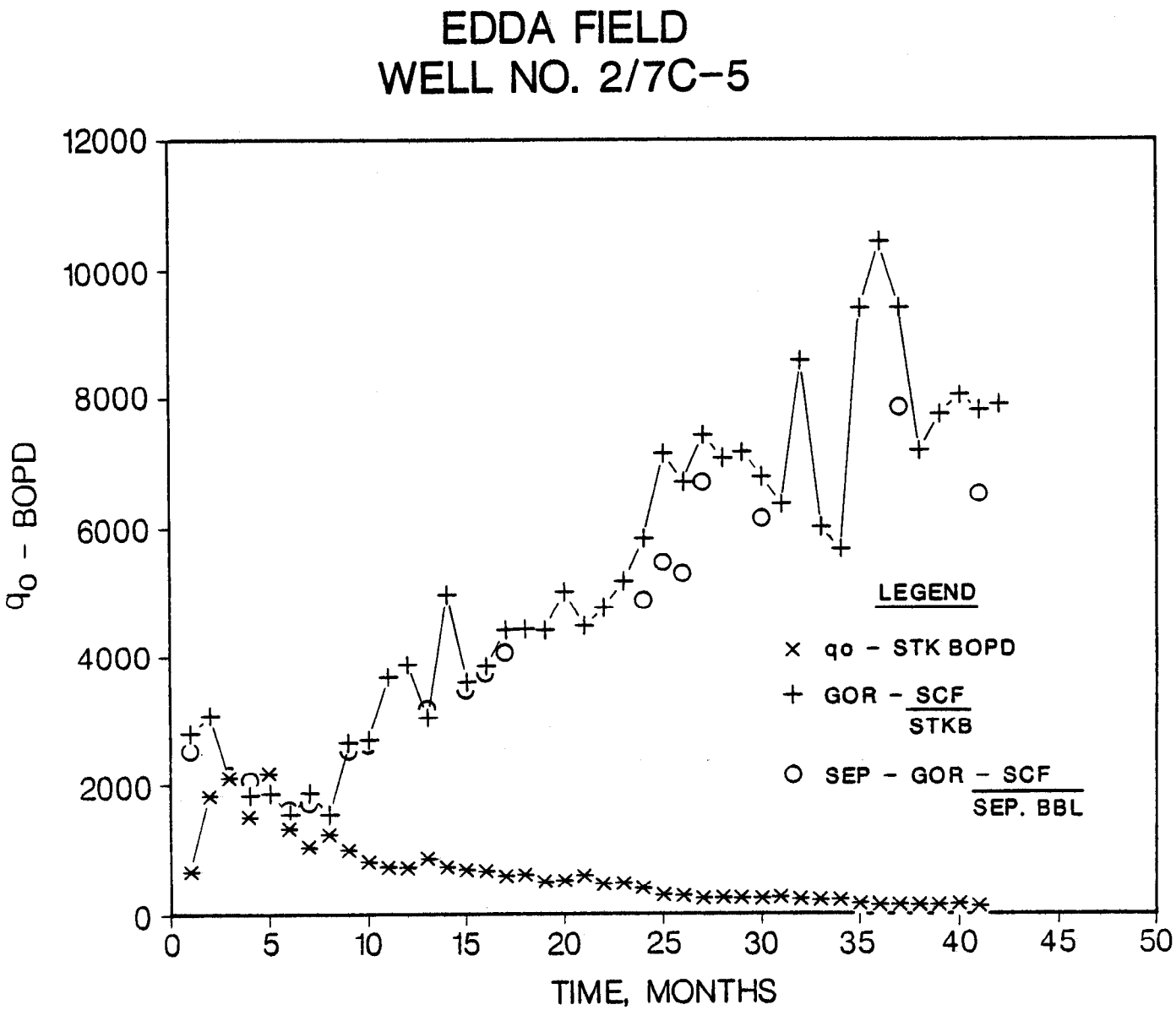

Fig. 4—Allocated GOR—production performance and separator test GOR's.

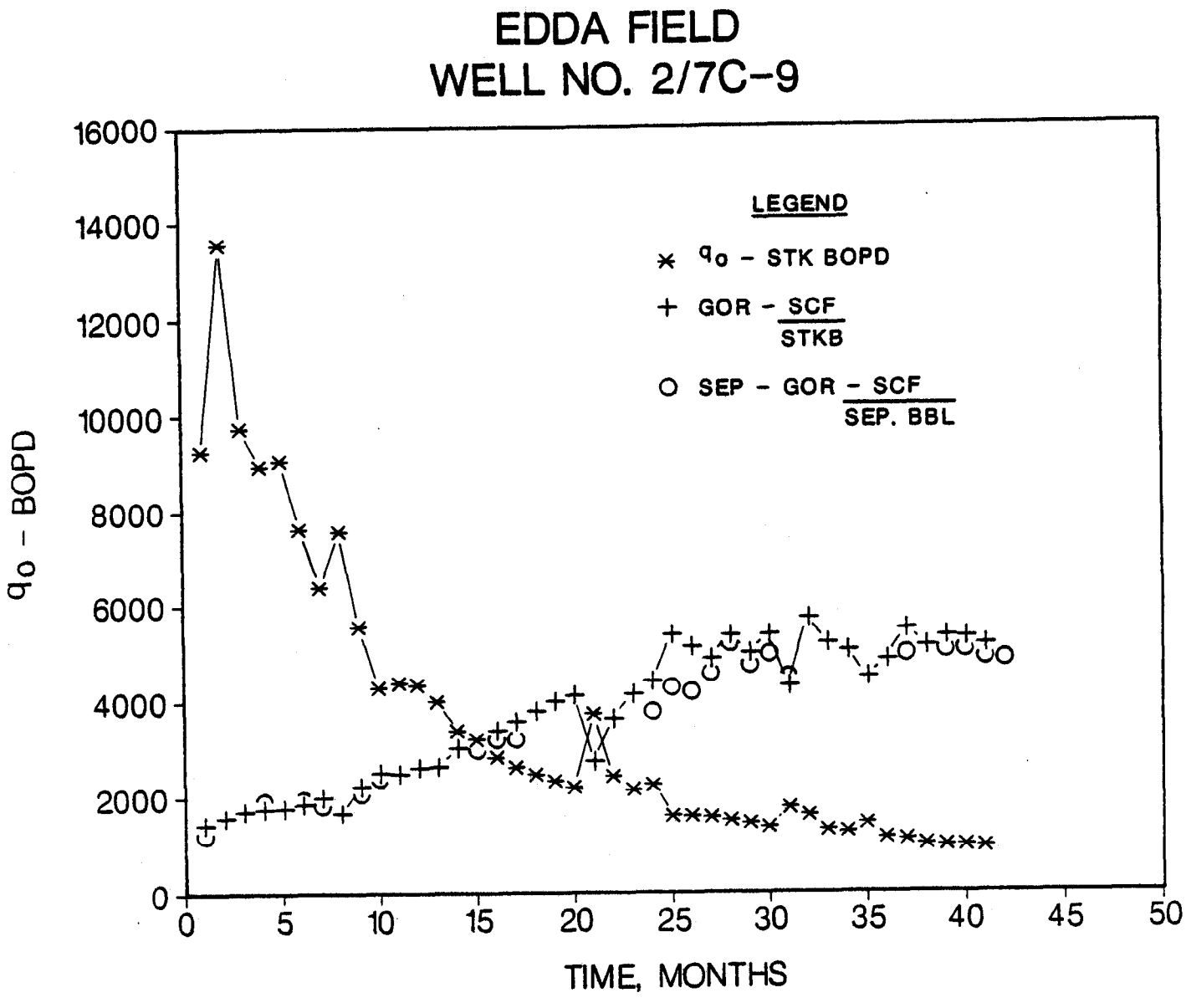

Fig. 5—Allocated GOR—production performance and separator test GOR's.

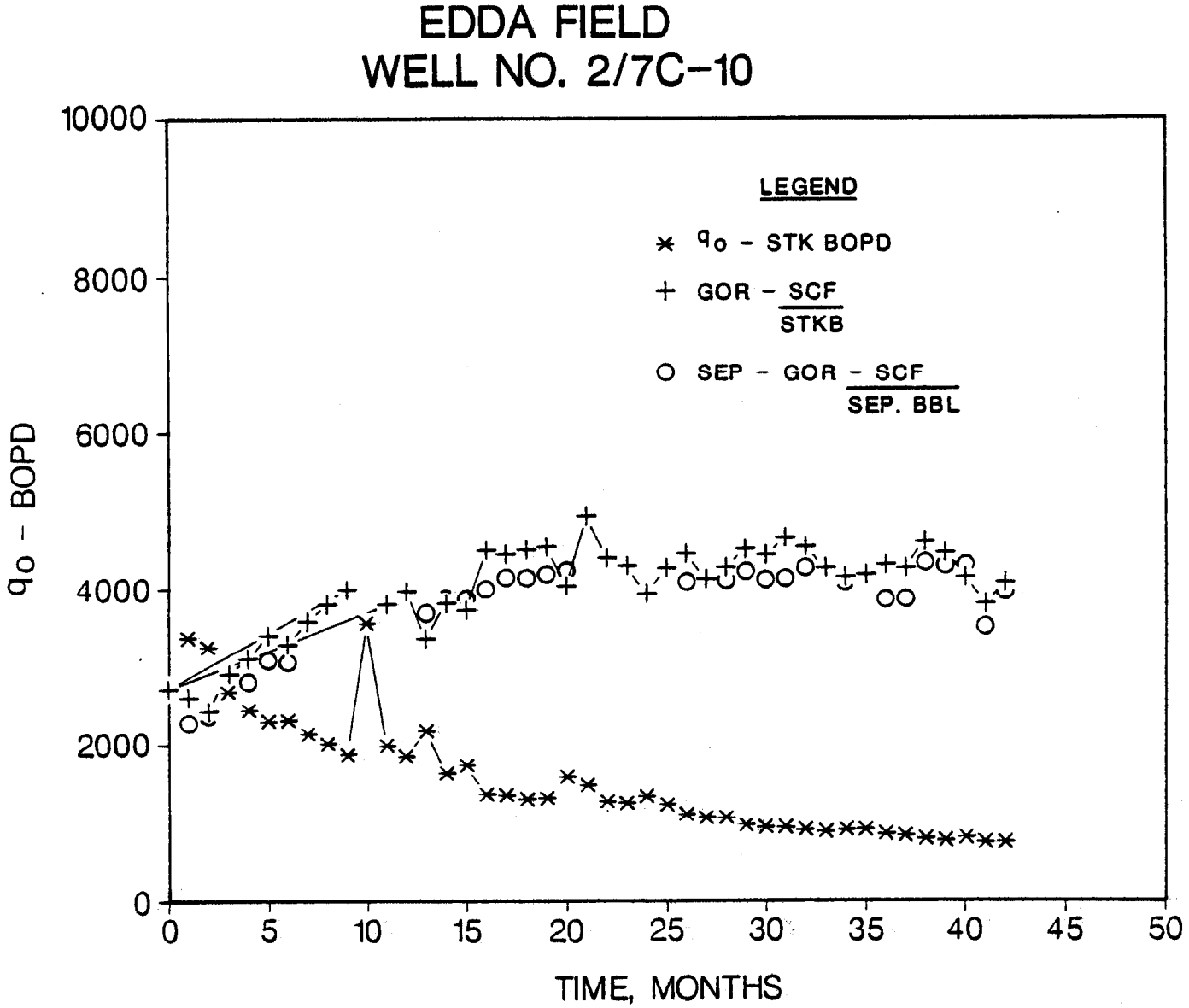

Fig. 6—Allocated GOR—production performance and separator test GOR's.

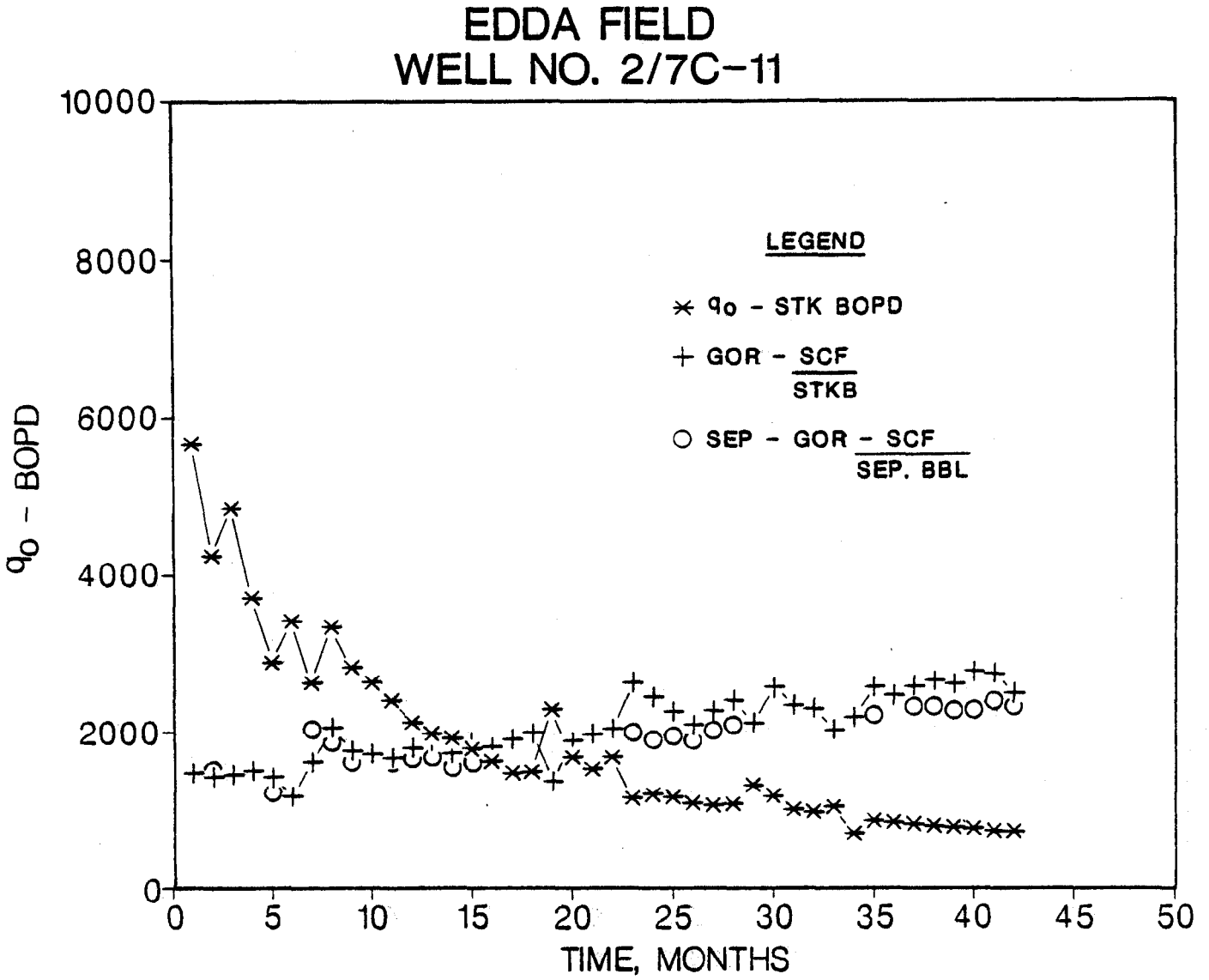

Fig. 7—Allocated GOR—production performance and separator test GOR's.

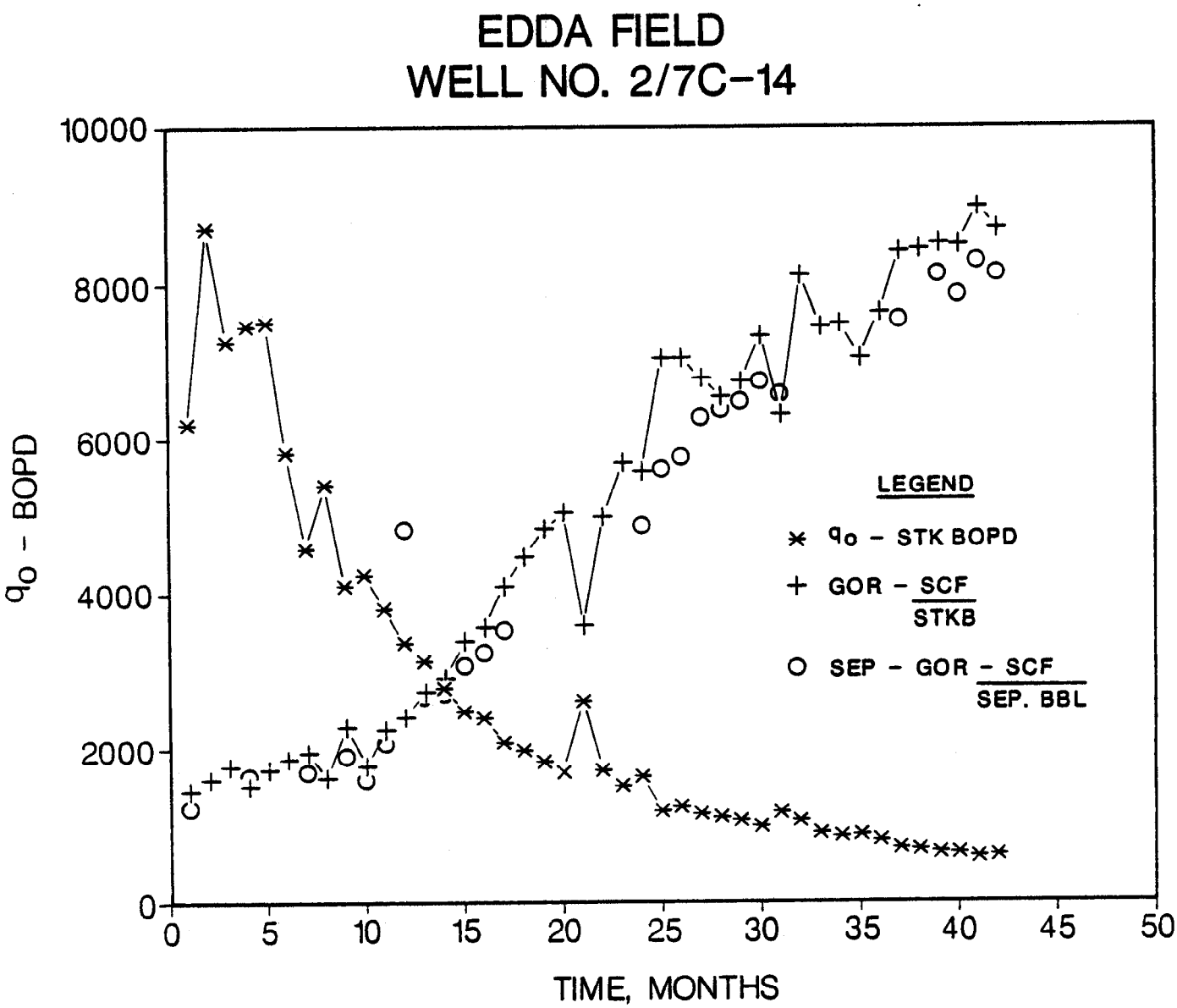

Fig. 8—Allocated GOR—production performance and separator test GOR's.

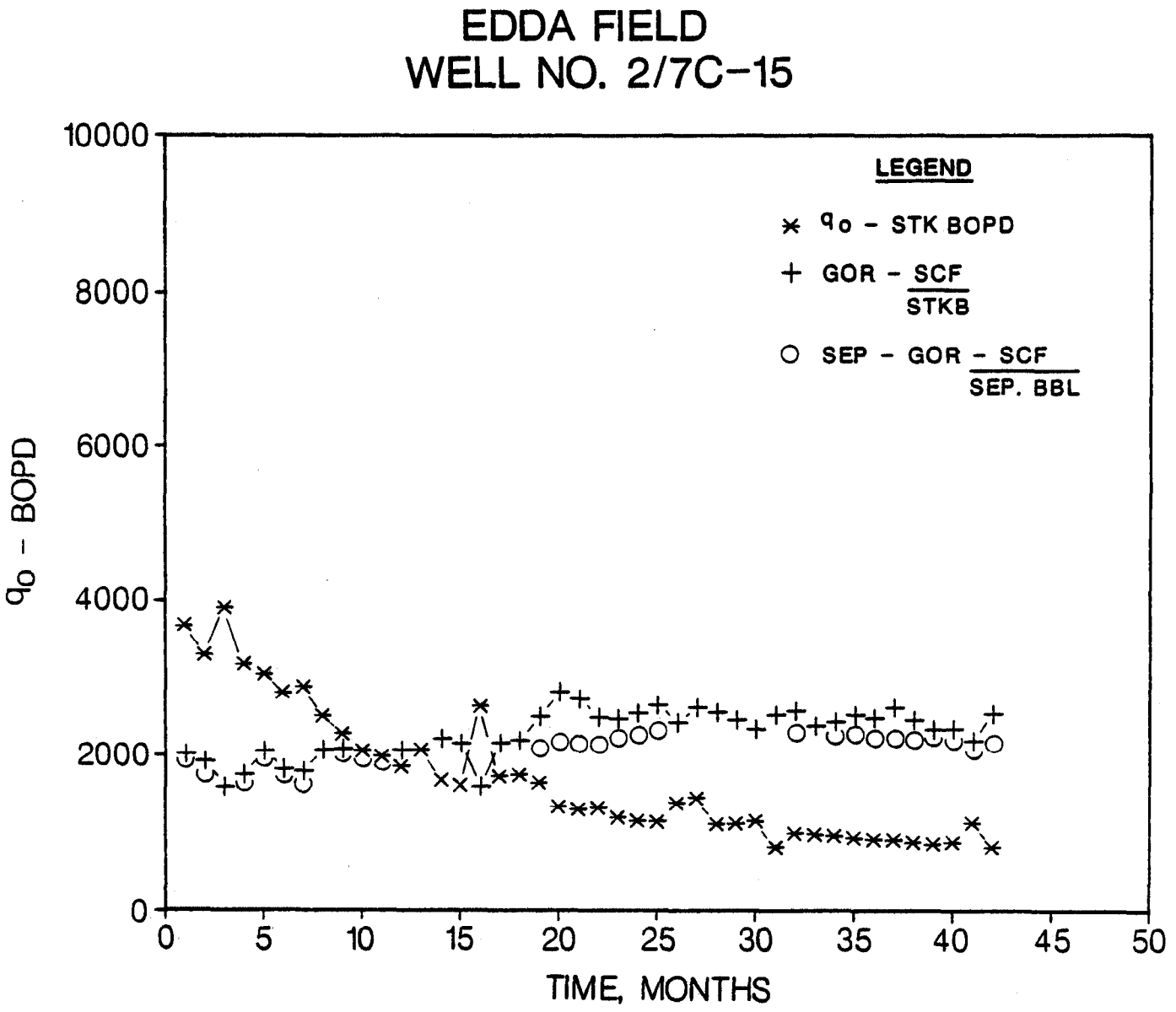

Fig. 9—Allocated GOR—production performance and separator test GOR's.

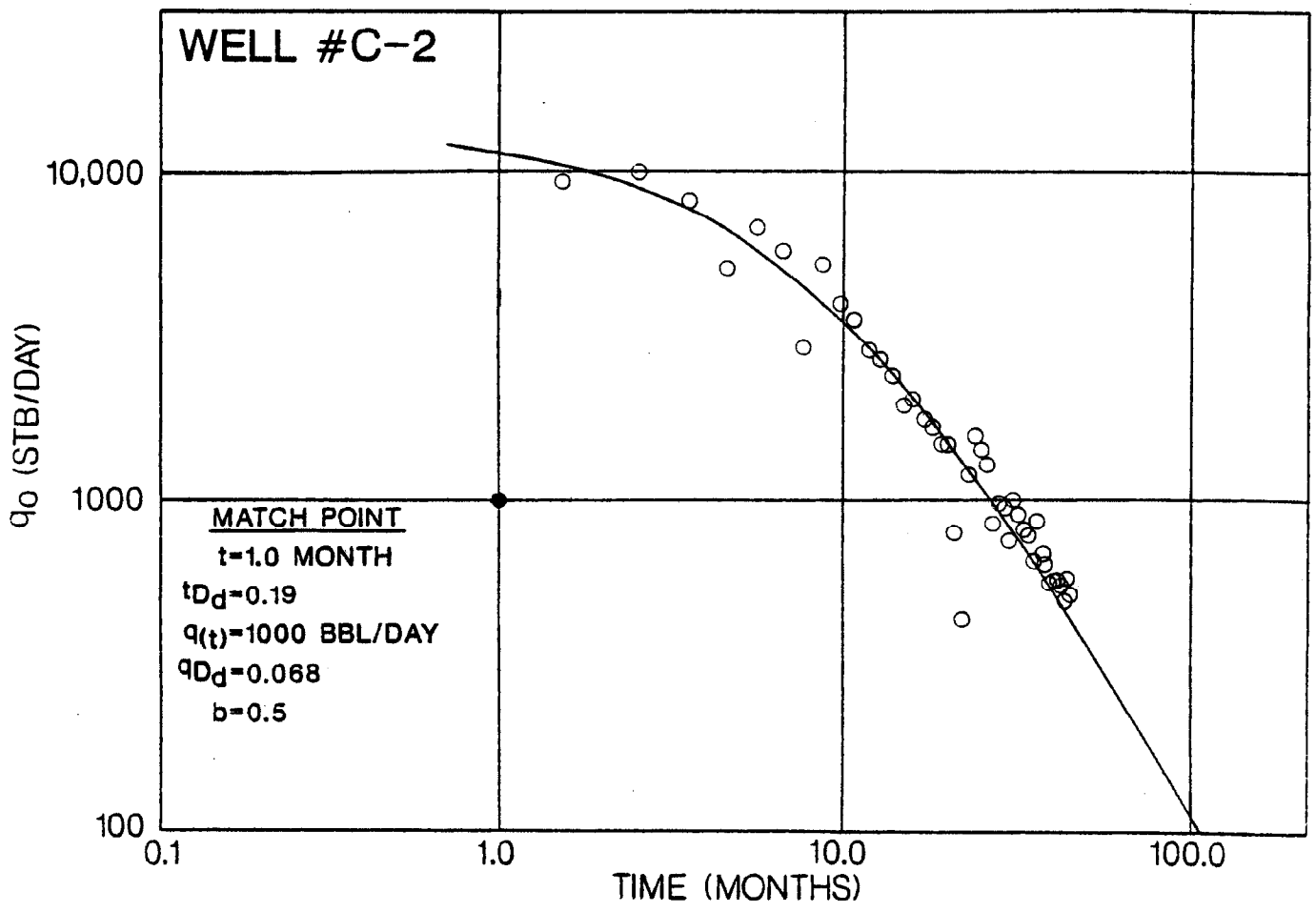

Fig. 10—Log rate vs. log time plot, oil rate excludes condensate.

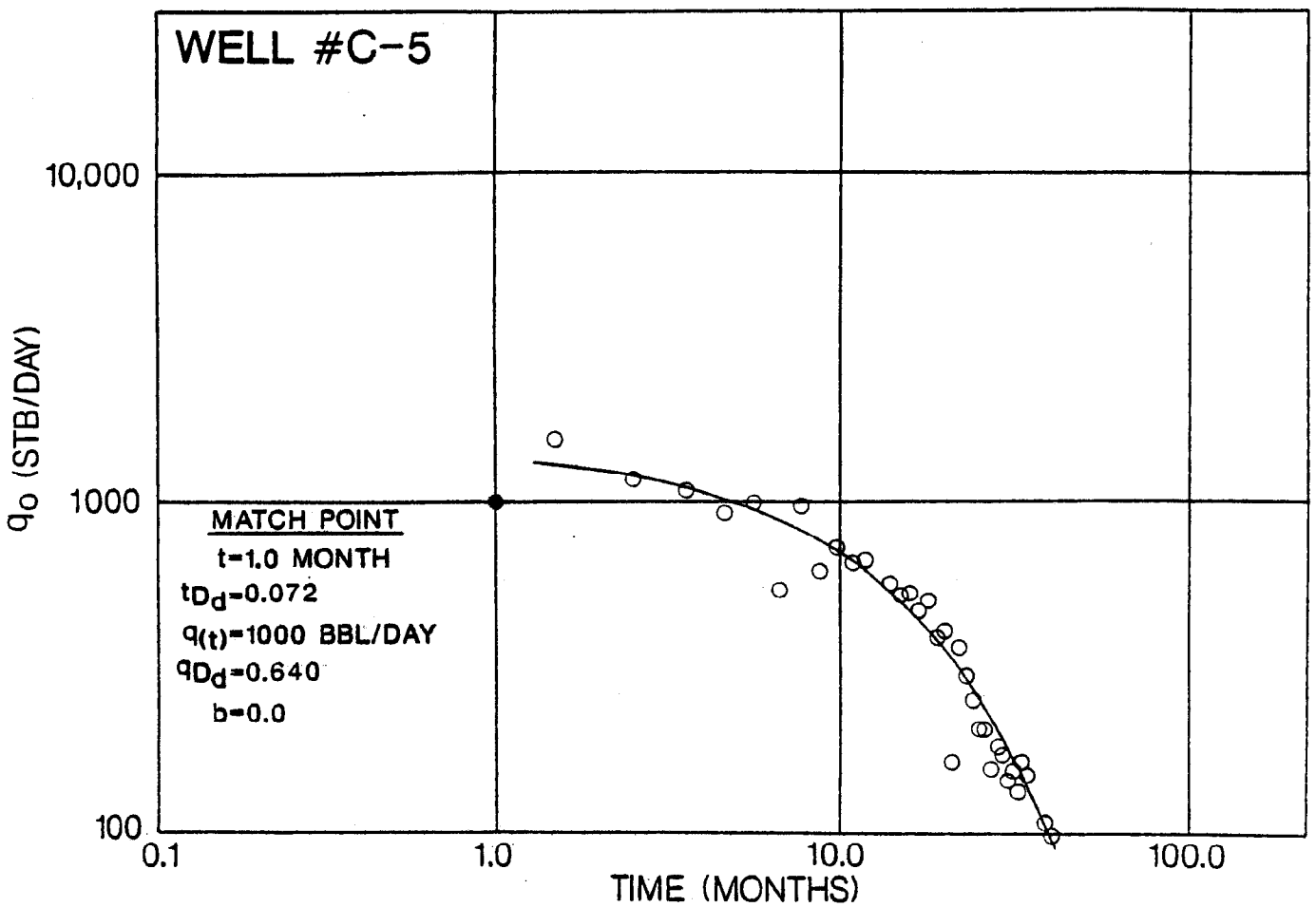

Fig. 11—Log rate vs. log time plot, oil rate excludes condensate.

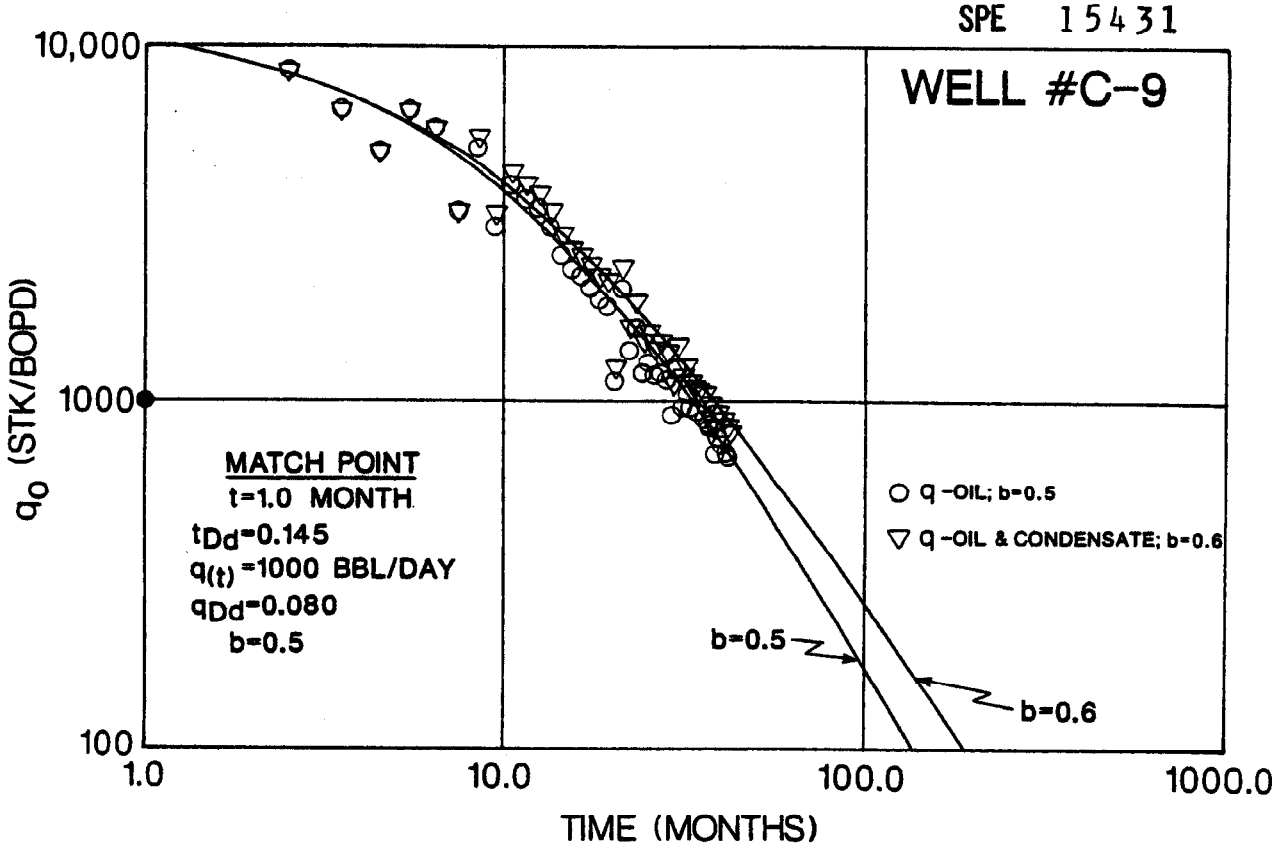

Fig. 12—Log rate vs. log time plots, oil rate including and excluding condensate.

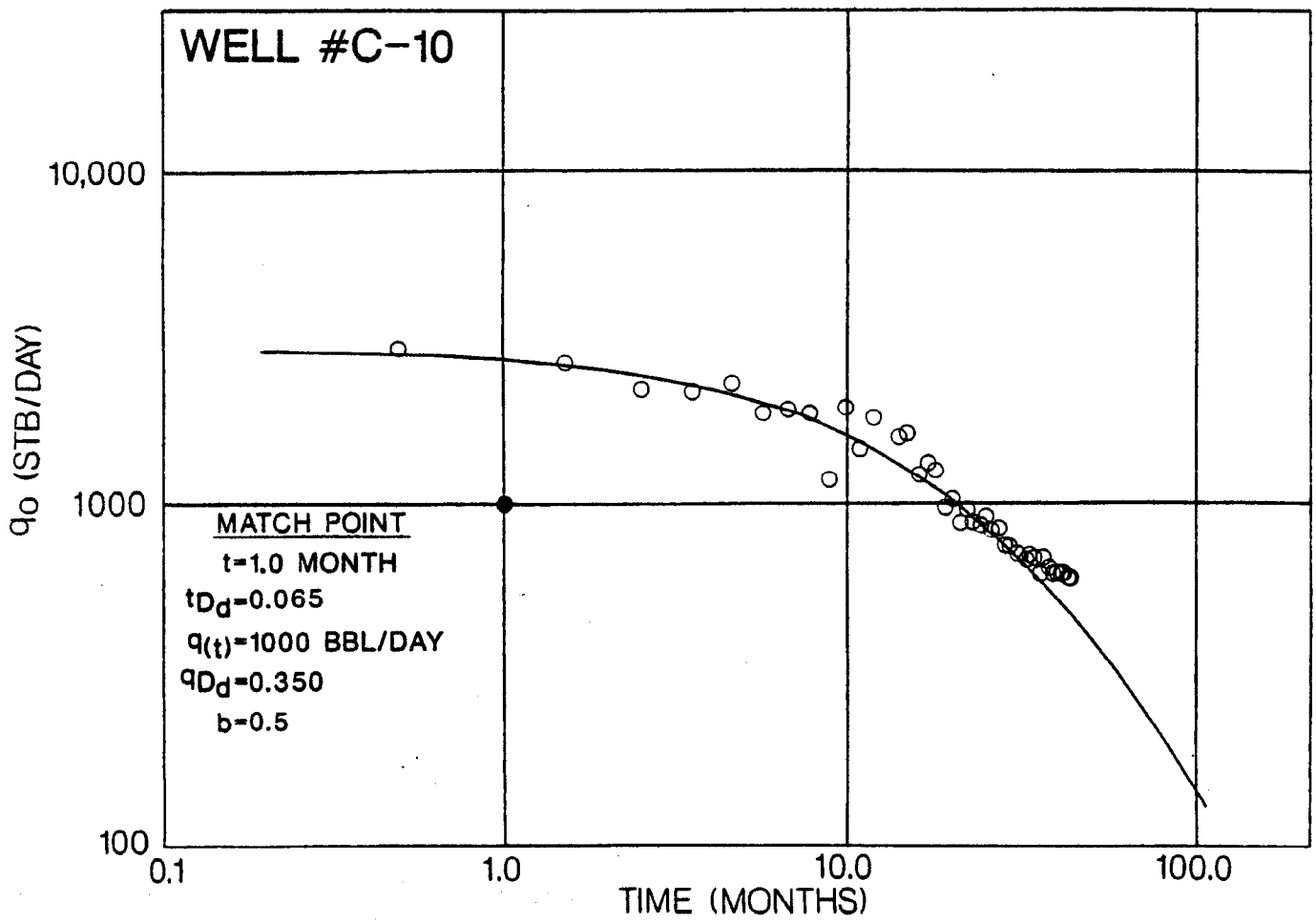

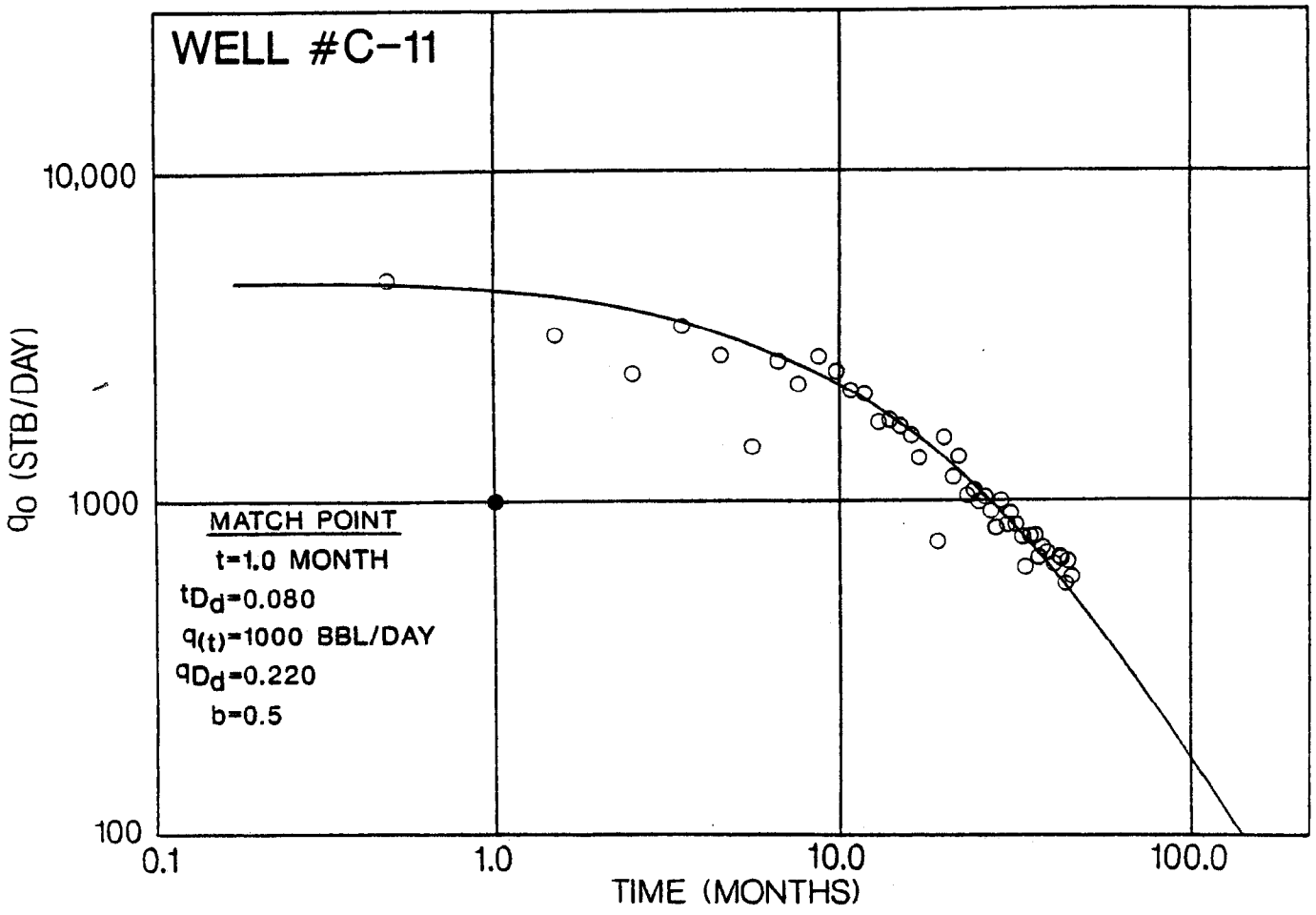

Fig. 14—Log rate vs. log time plot, oil rate excludes condensate.

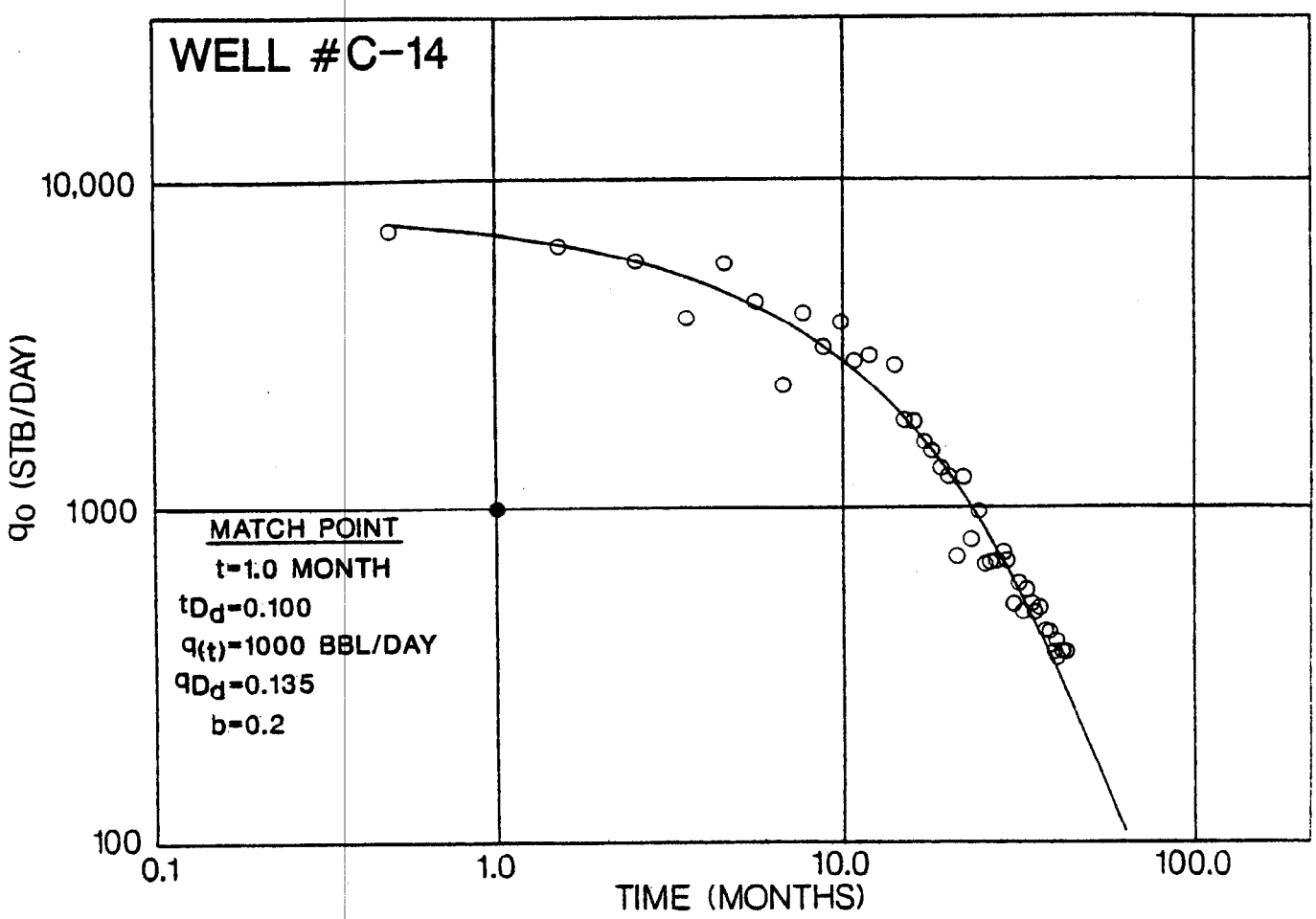

Fig. 15—Log rate vs. log time plot, oil rate excludes condensate.

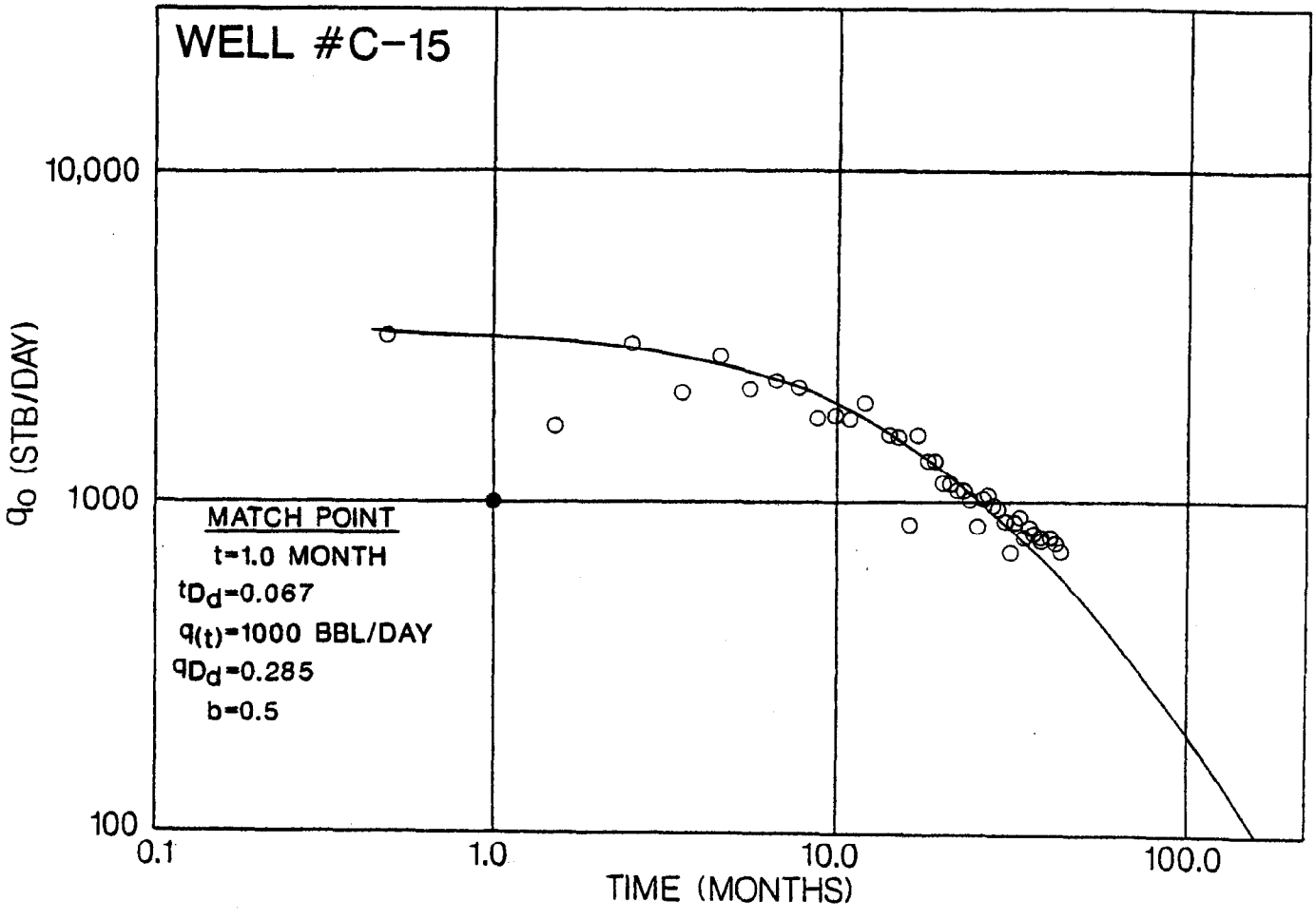

Fig. 16—Log rate vs. log time plot, oil rate excludes condensate.

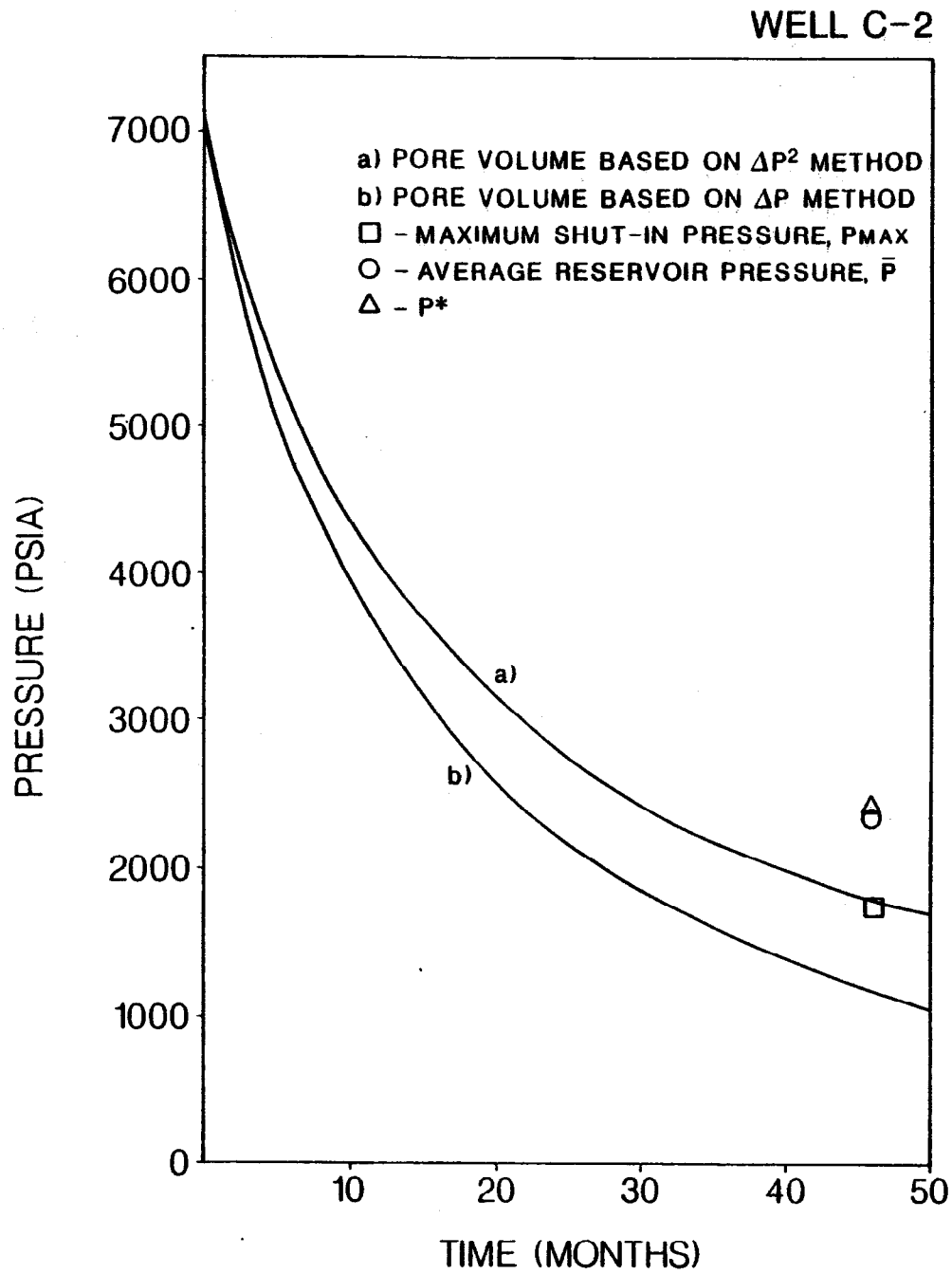

Fig. 17—Match of pressure buildup data and compositional material balance pressure based on rate-time calculated pore volume.

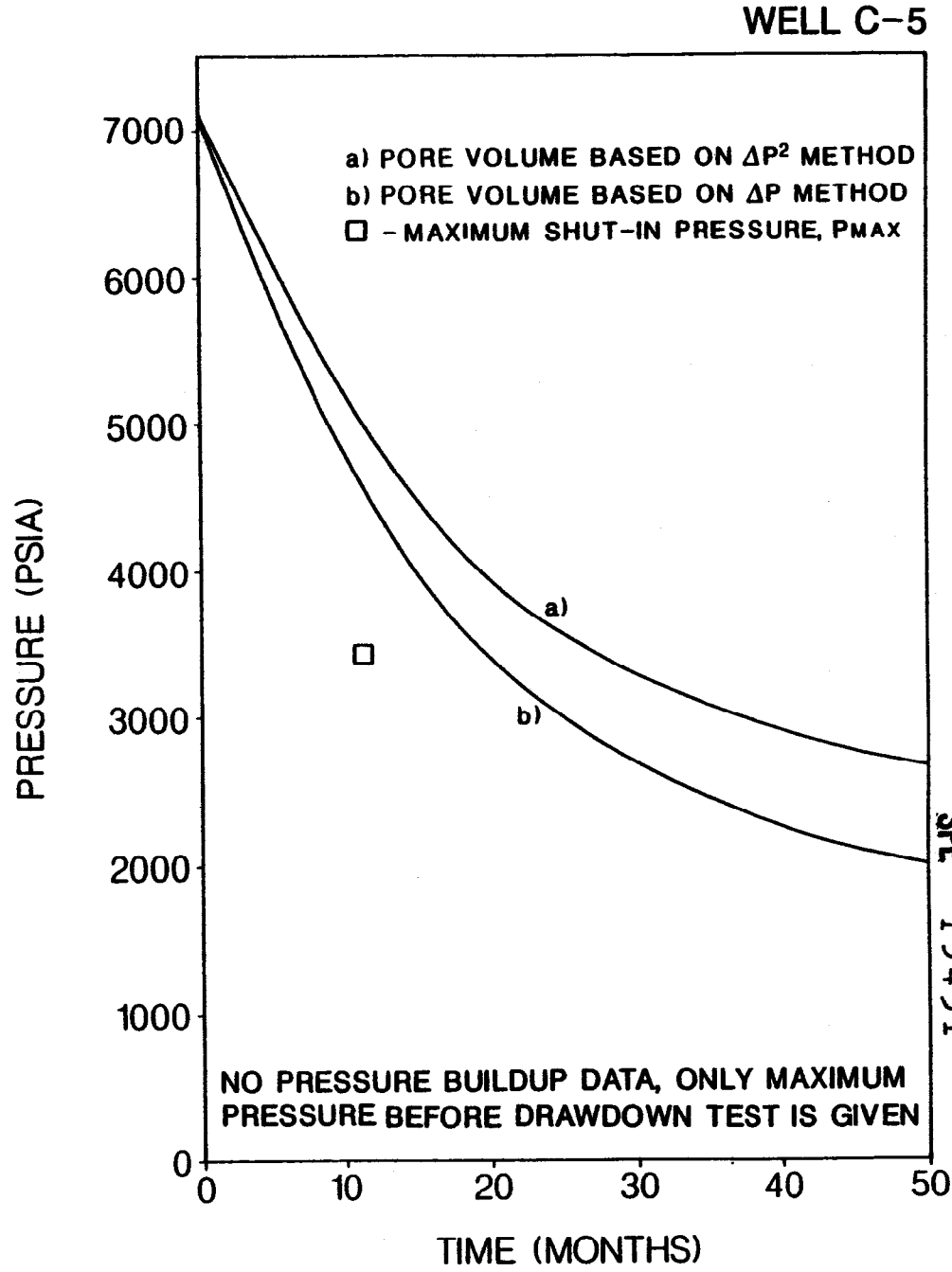

SPE 15431

Fig. 18—Match of pressure buildup data and compositional material balance pressure based on rate-time calculated pore volume.

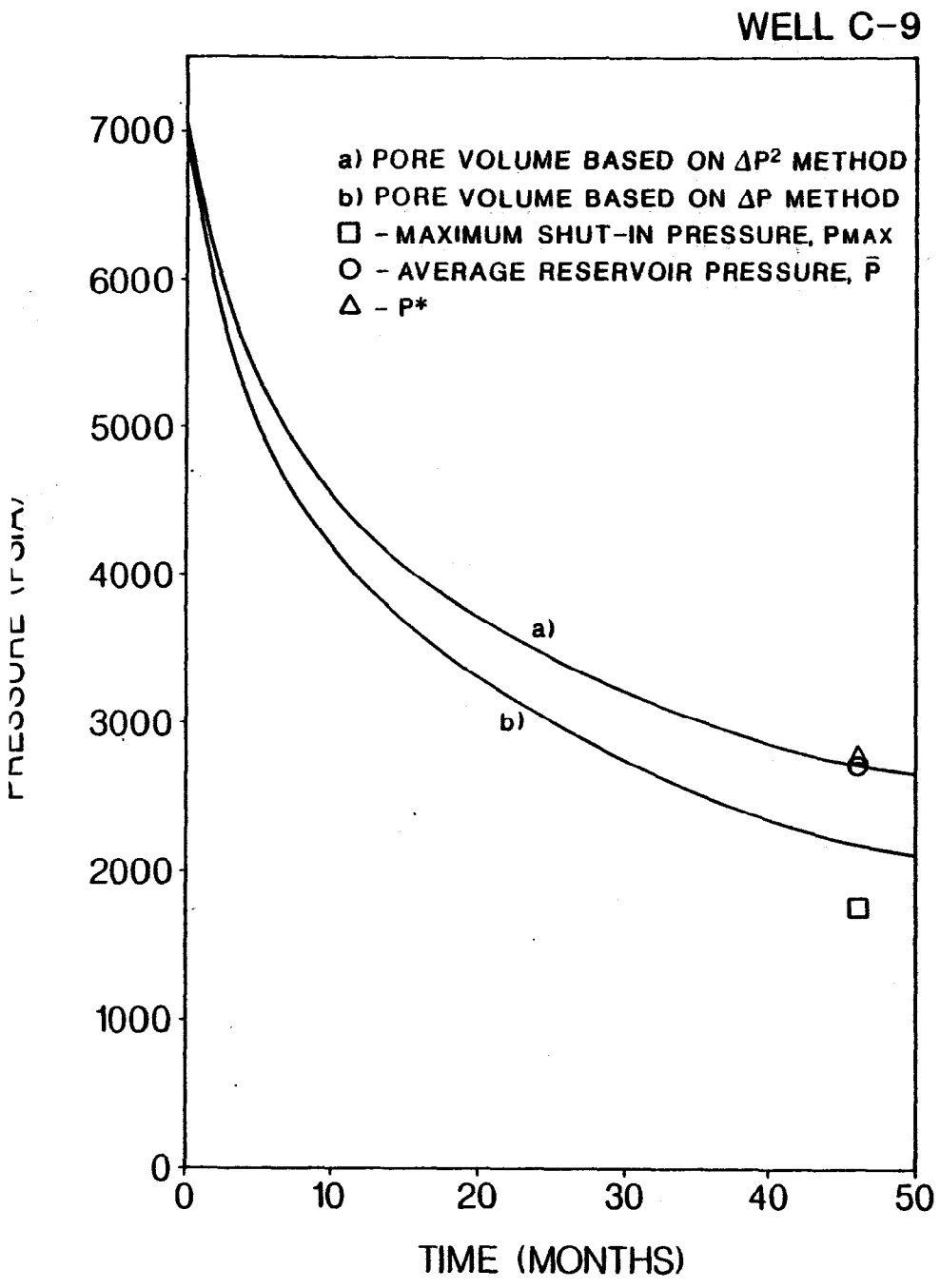

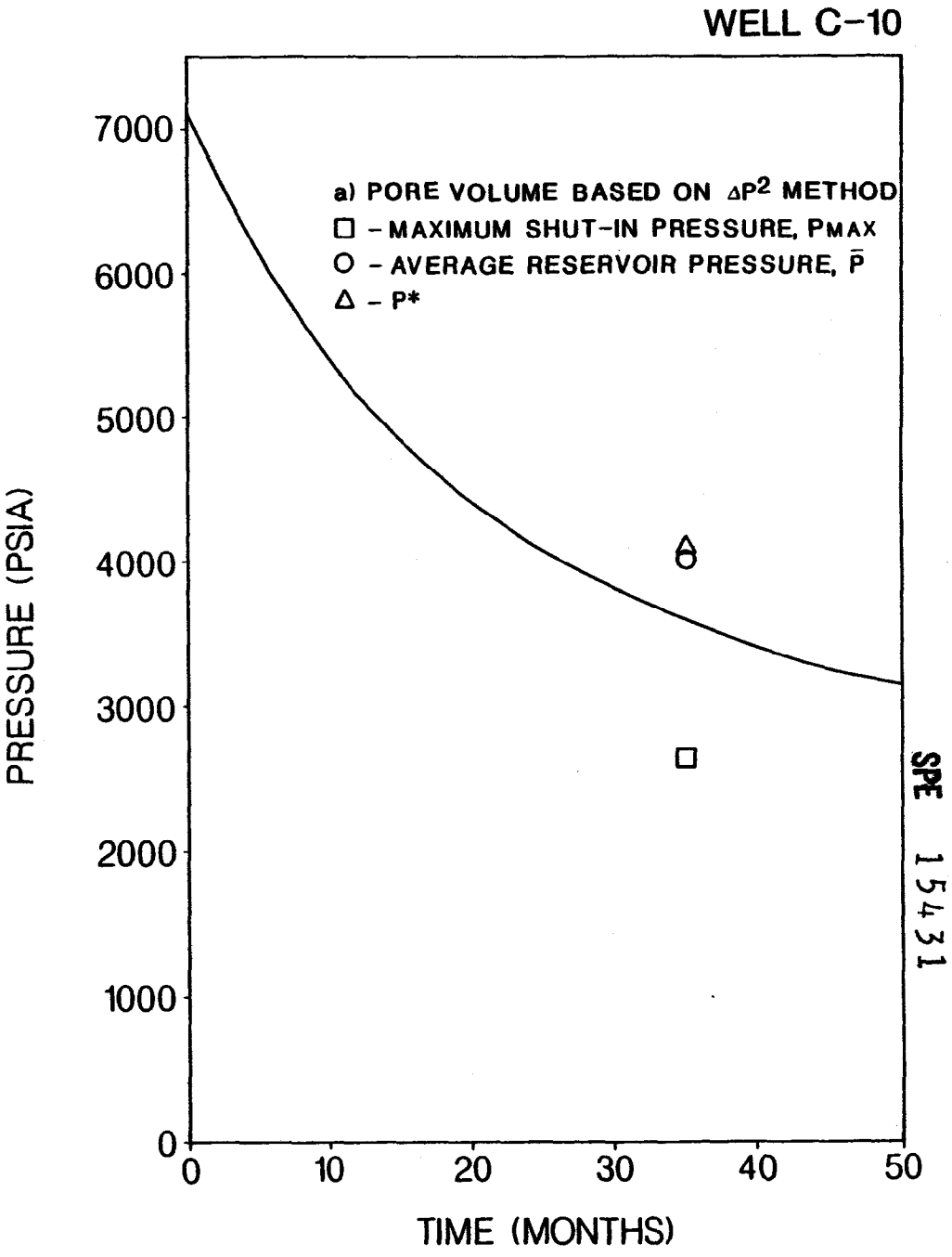

ig. 19—Match of pressure buildup data and compositional material balance pressure based on rate-time calculated pore volume.

Fig. 20—Match of pressure buildup data and compositional material balance pressure based on rate-time calculated pore volume.

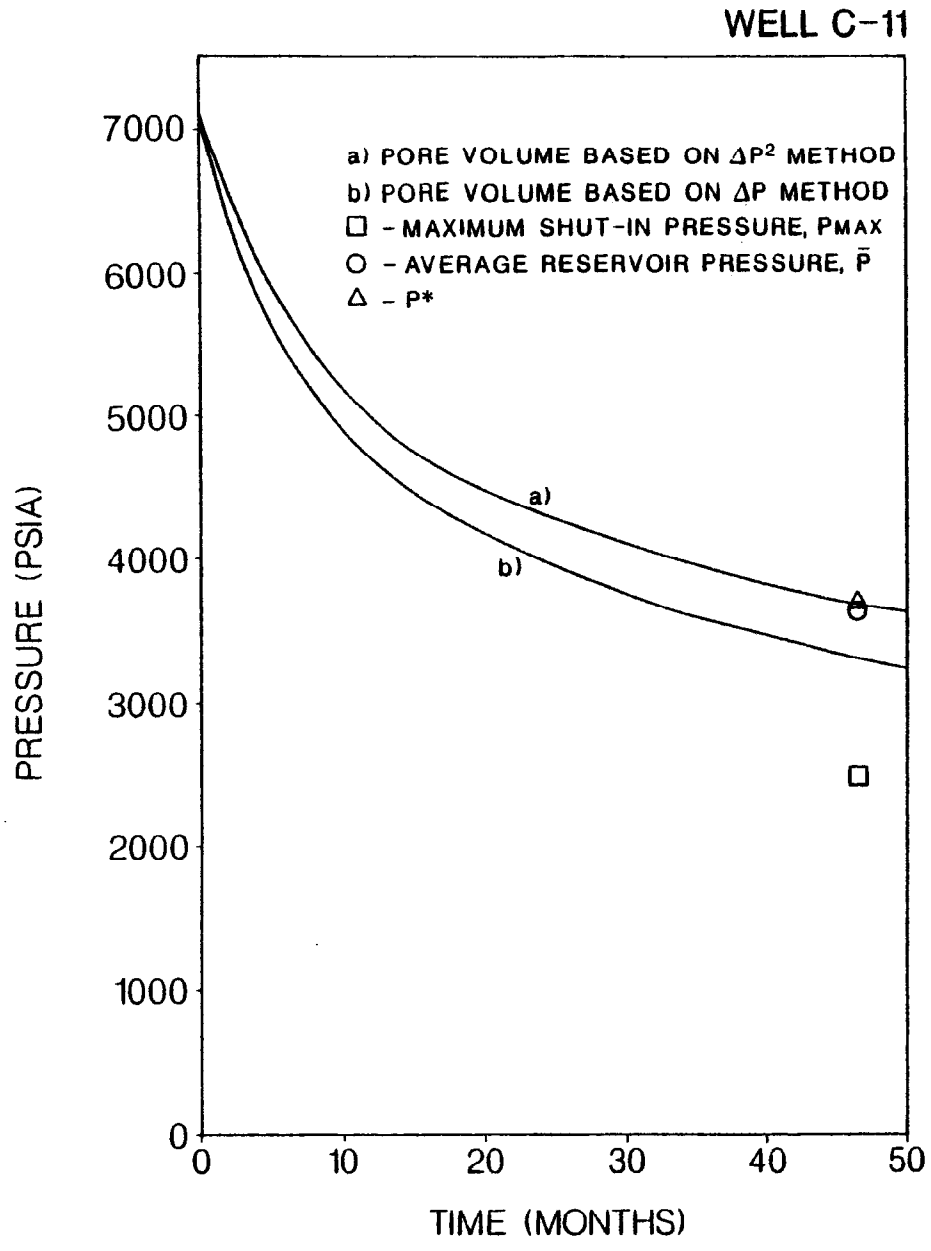

Fig. 21—Match of pressure buildup data and compositional material balance pressure based on rate-time calculated pore volume.

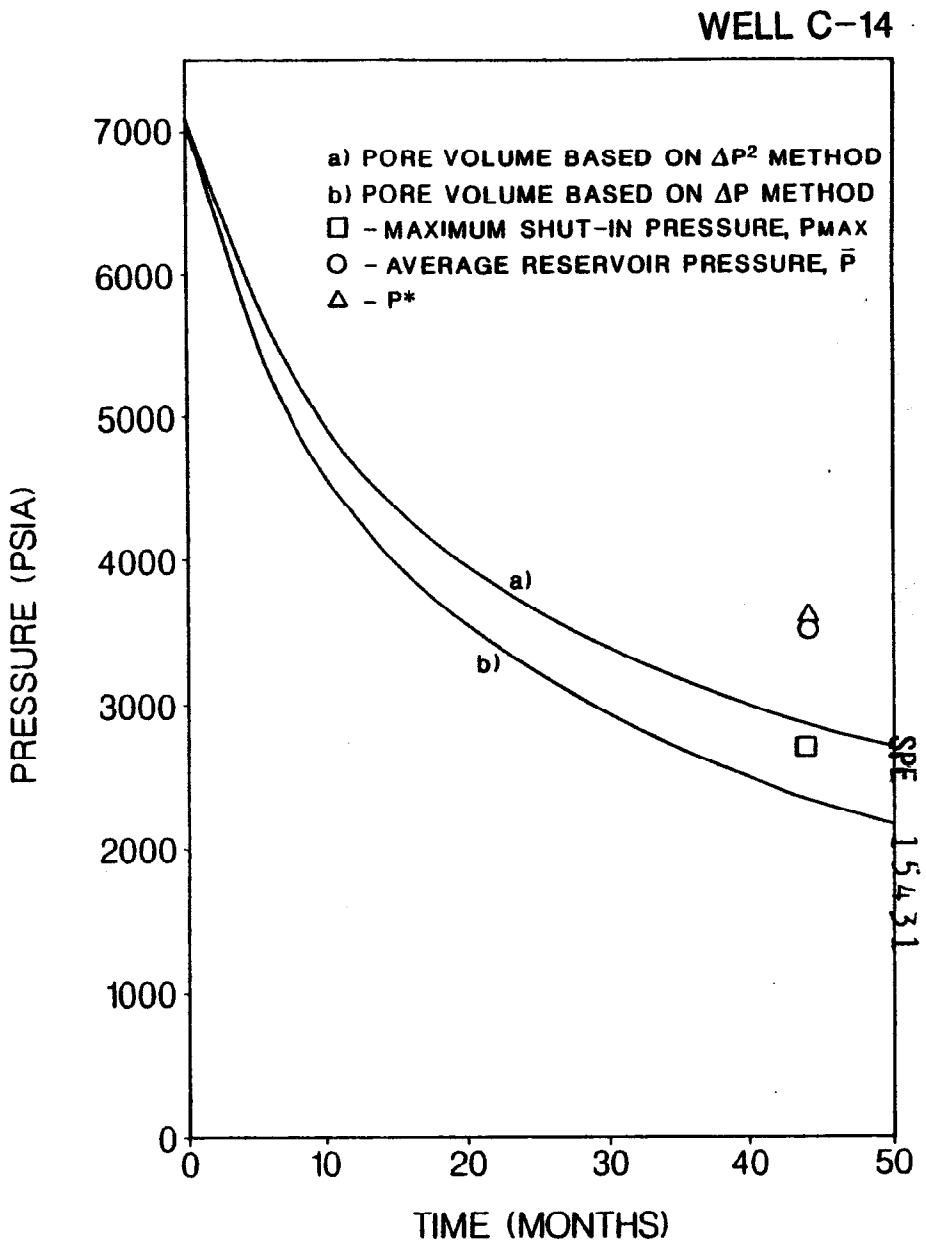

Fig. 22—Match of pressure buildup data and compositional material balance pressure based o rate-time calculated pore volume.

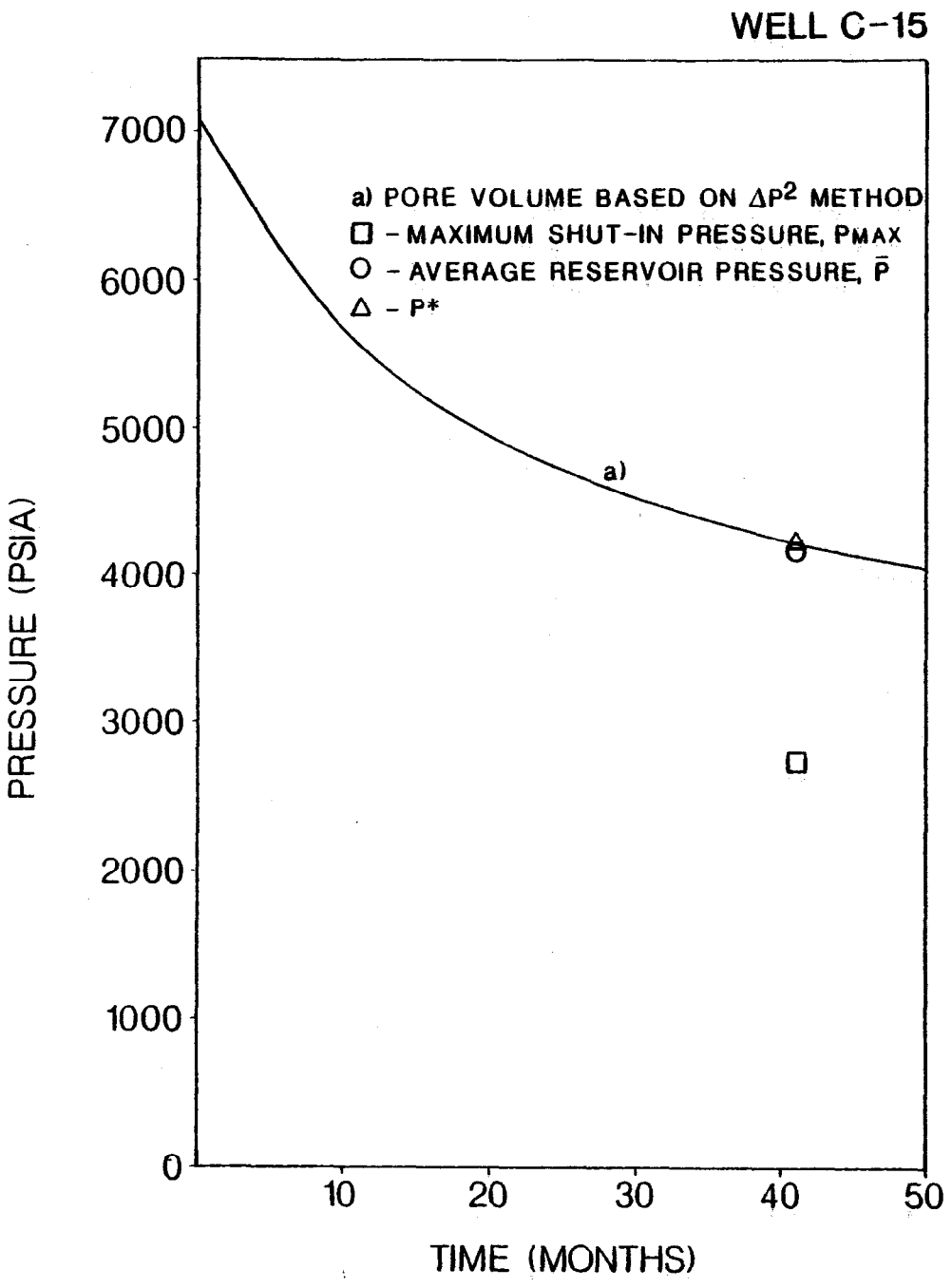

Fig. 23—Match of pressure buildup data and compositional material balance pressure based on rate-time calculated pore volume.

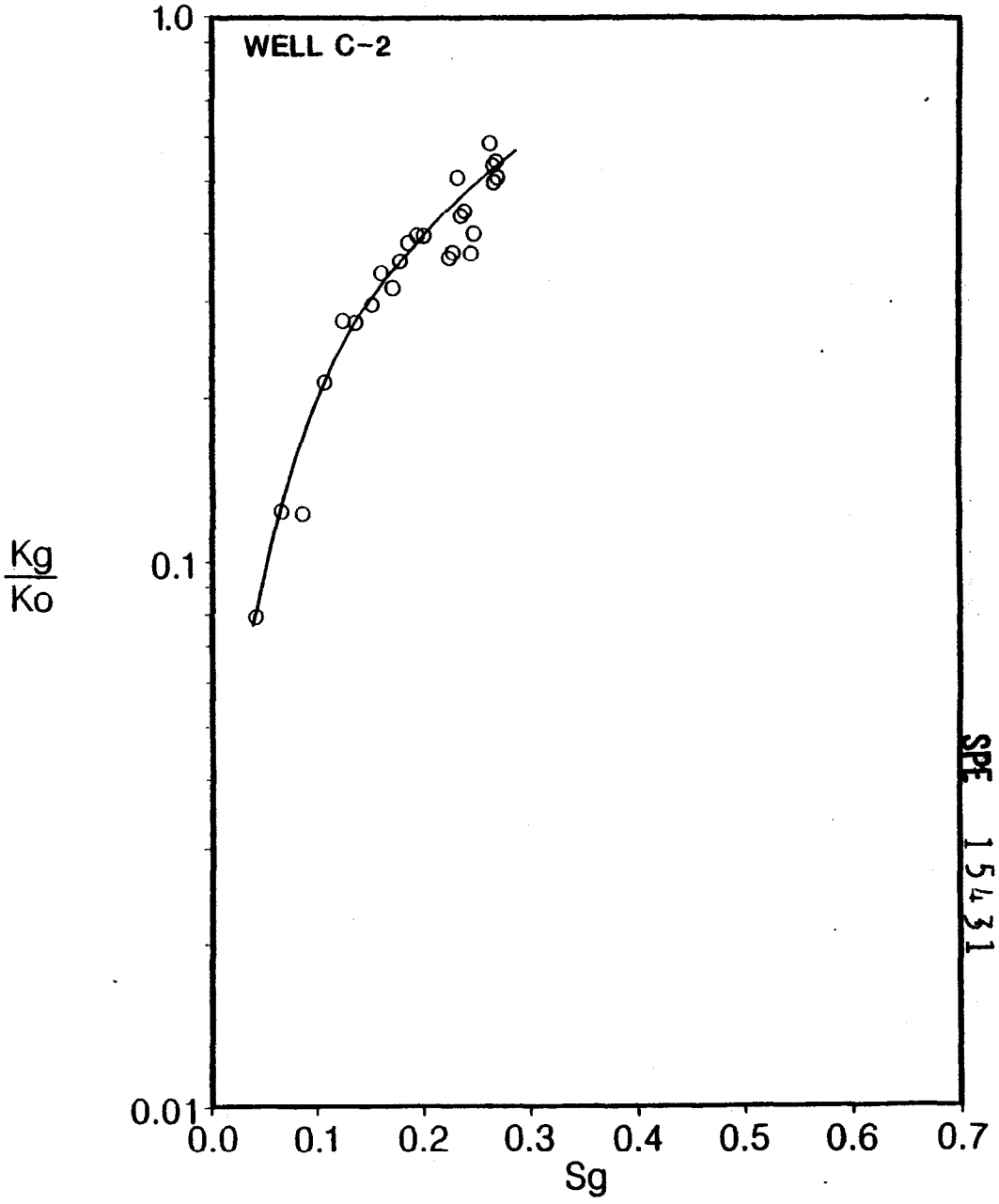

Fig. 24—Individual well performance derived K_g/K_o calculated using a compositional material balance with rate-time calculated pore volume.

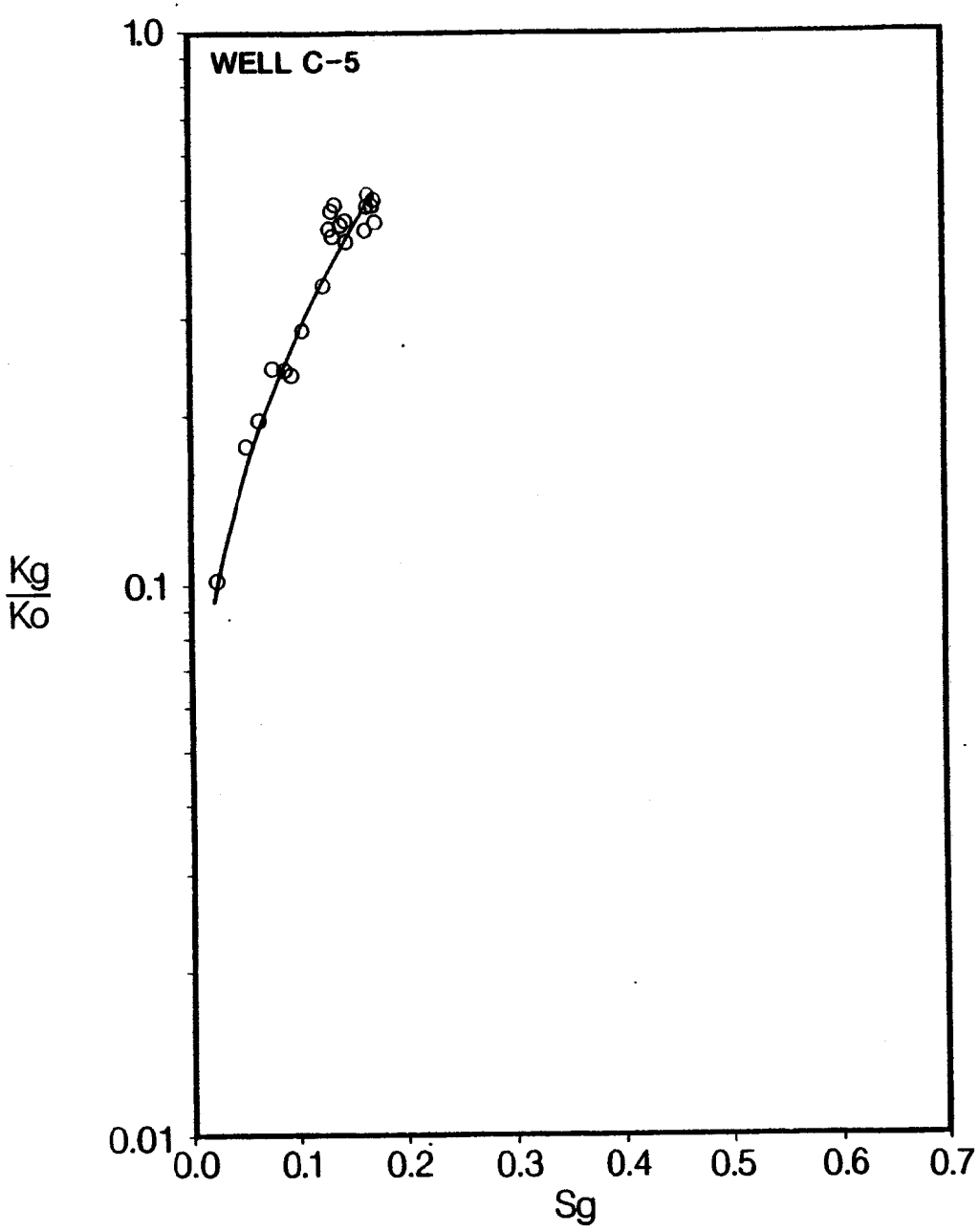

Fig. 25—Individual well performance derived K_g/K_o calculated using a compositional material balance with rate-time calculated pore volume.

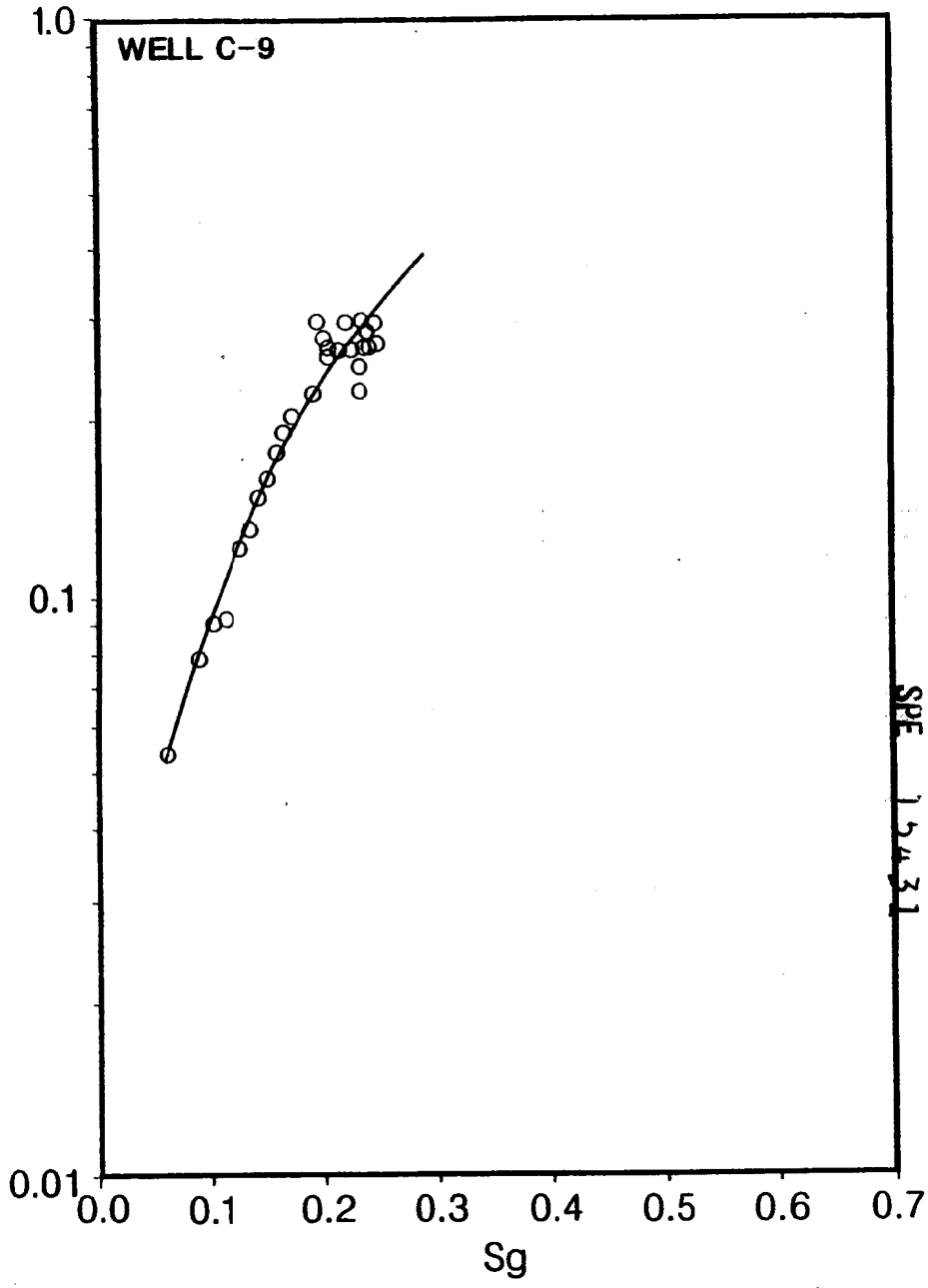

Fig. 26—Individual well performance derived K_g/K_o calculated using a compositional materi balance with rate-time calculated pore volume.

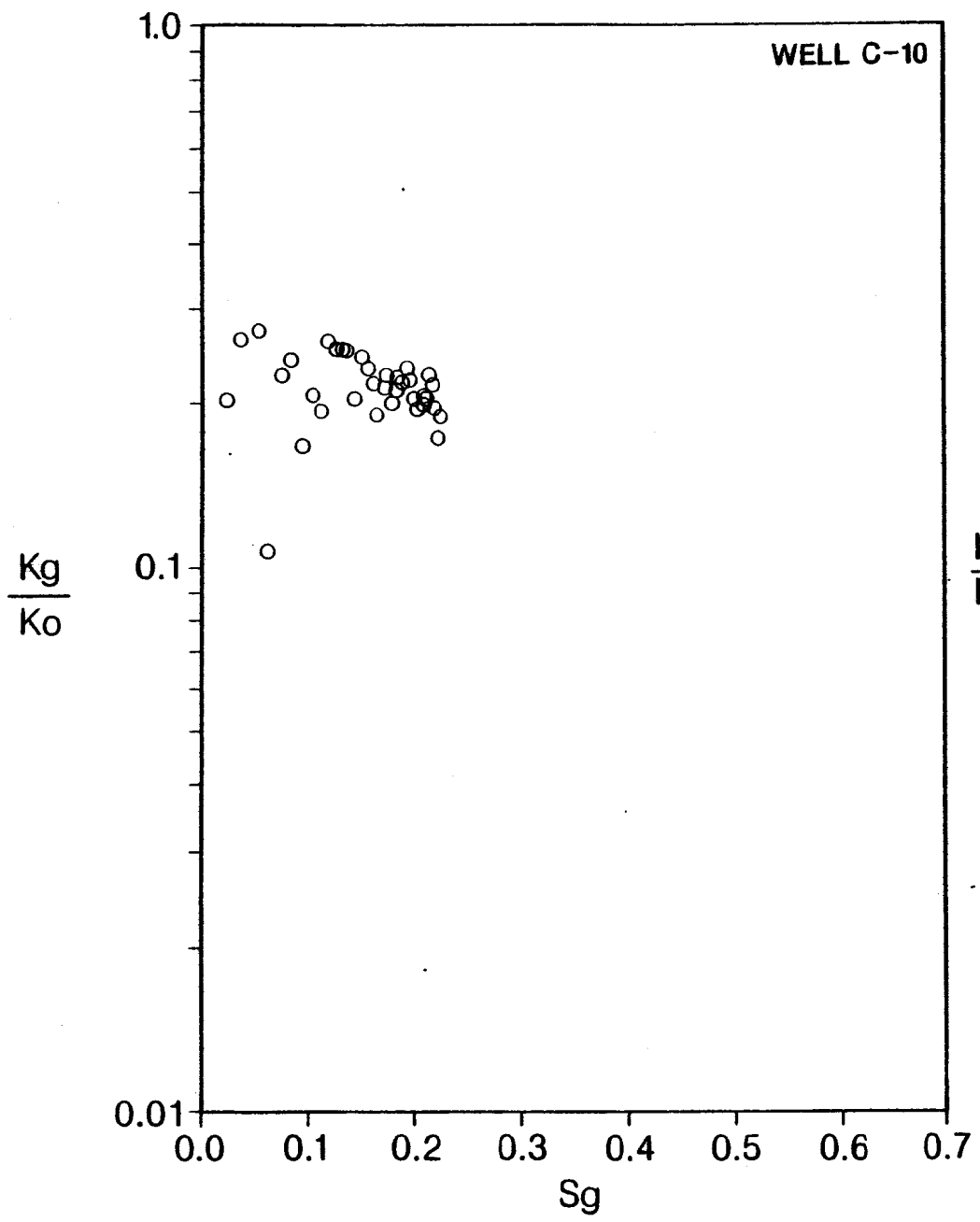

Fig. 27—Individual well performance derived K_g/K_o calculated using a compositional material balance with rate-time calculated pore volume.

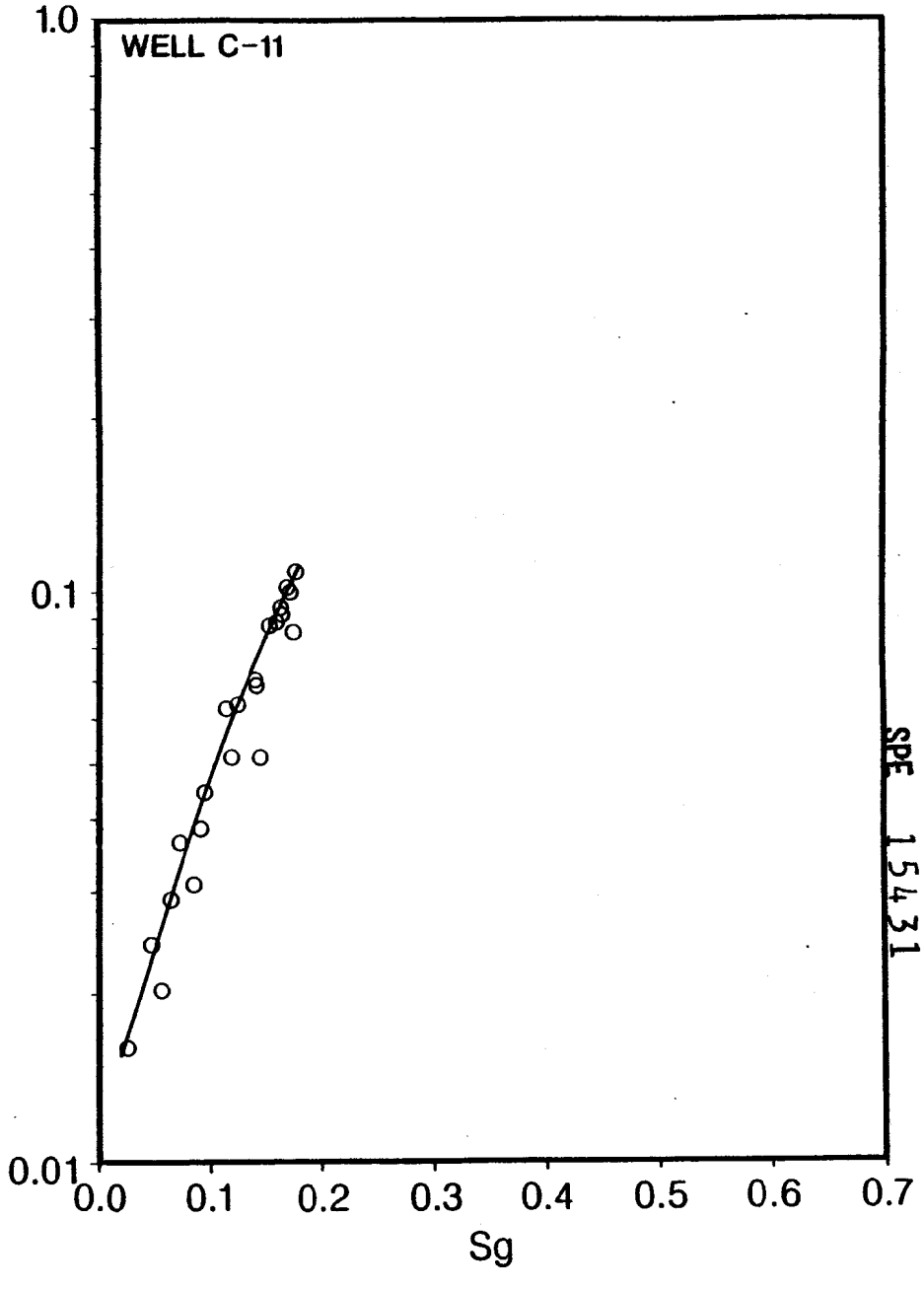

Fig. 28—Individual well performance derived K_g/K_o calculated using a compositional materia balance with rate-time calculated pore volume.

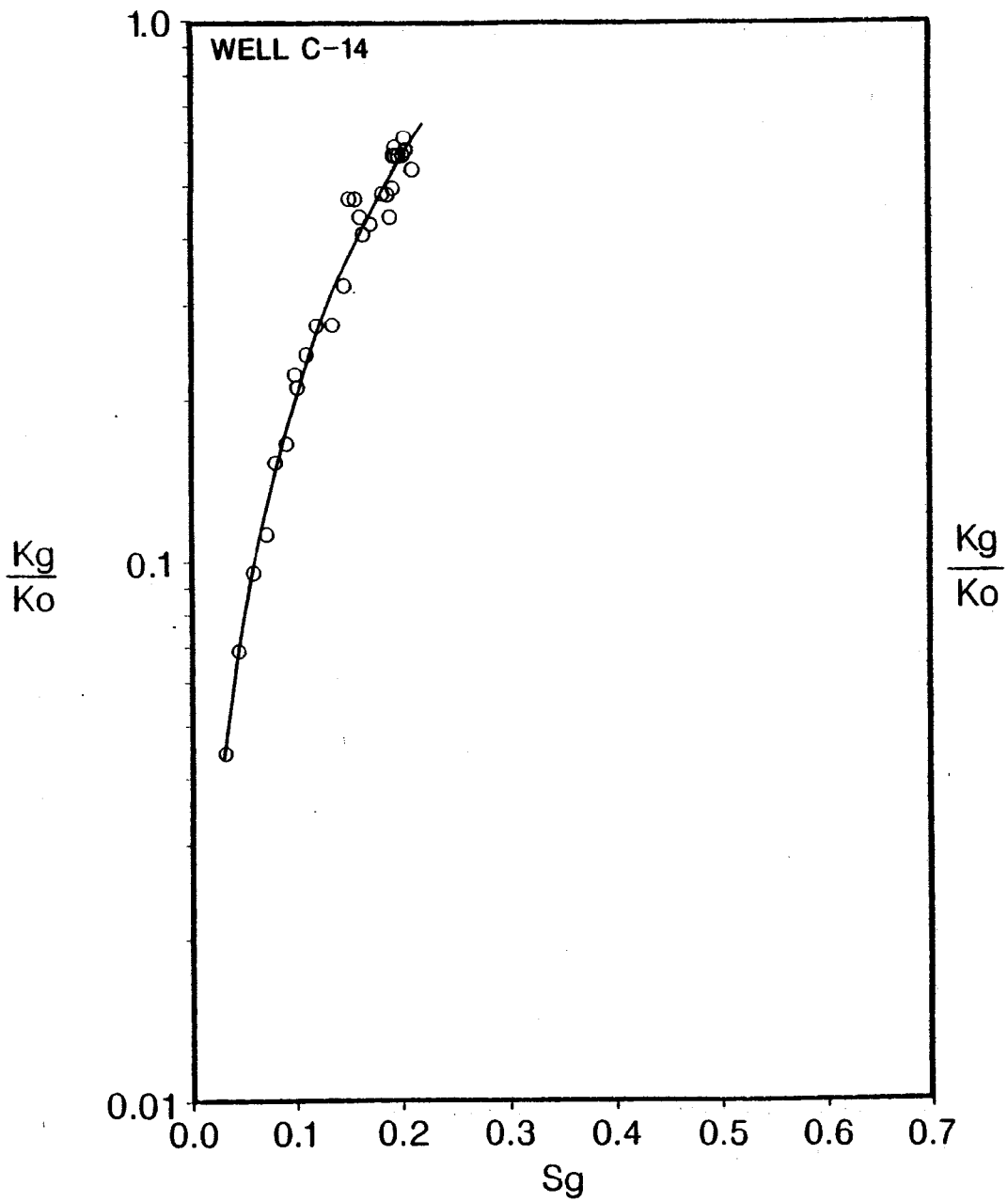

Fig. 29—Individual well performance derived K_g/K_o calculated using a compositional material balance with rate-time calculated pore volume.

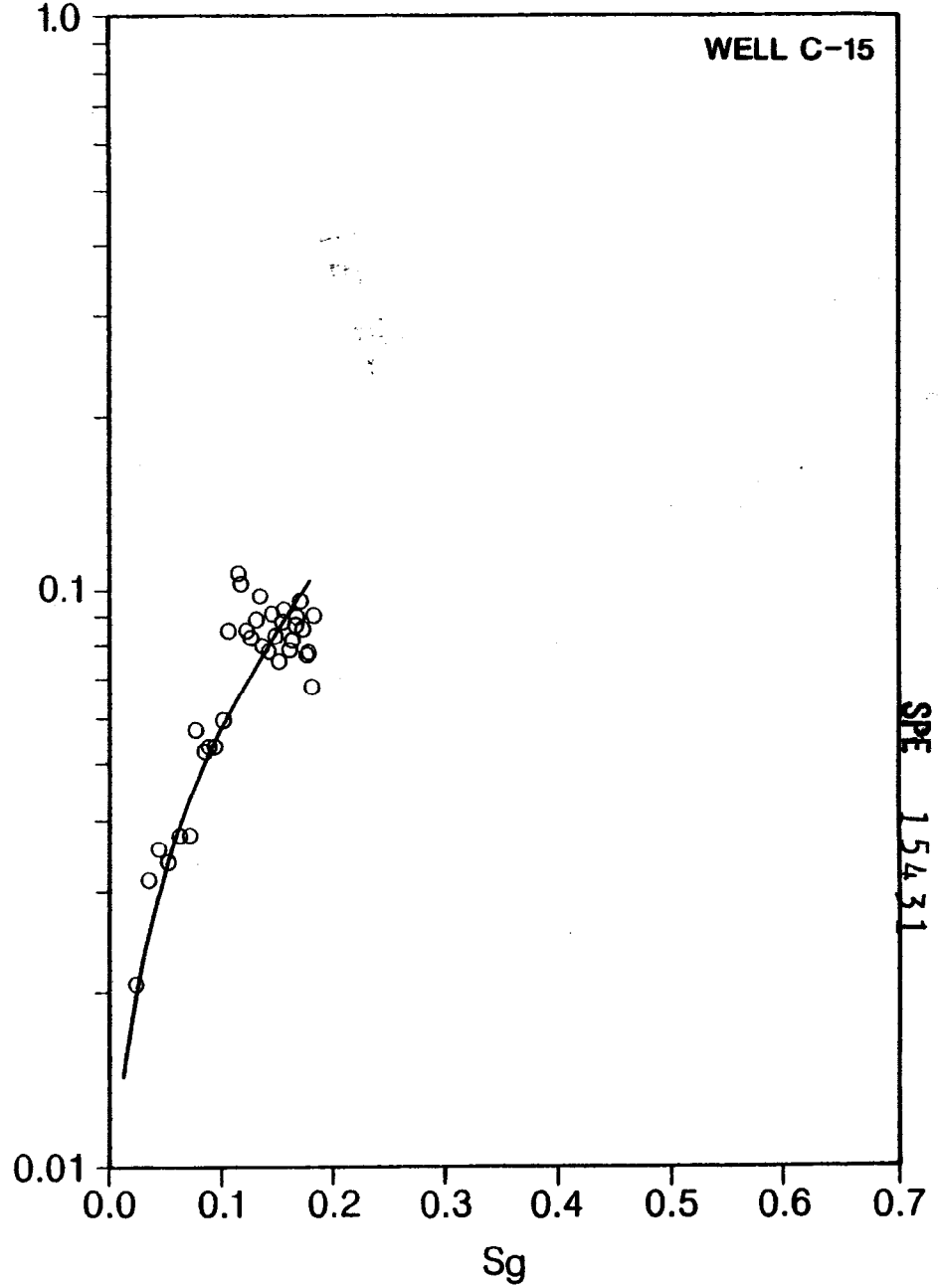

Fig. 30—Individual well performance derived K_g/K_o calculated using a compositional materia balance with rate-time calculated pore volume.

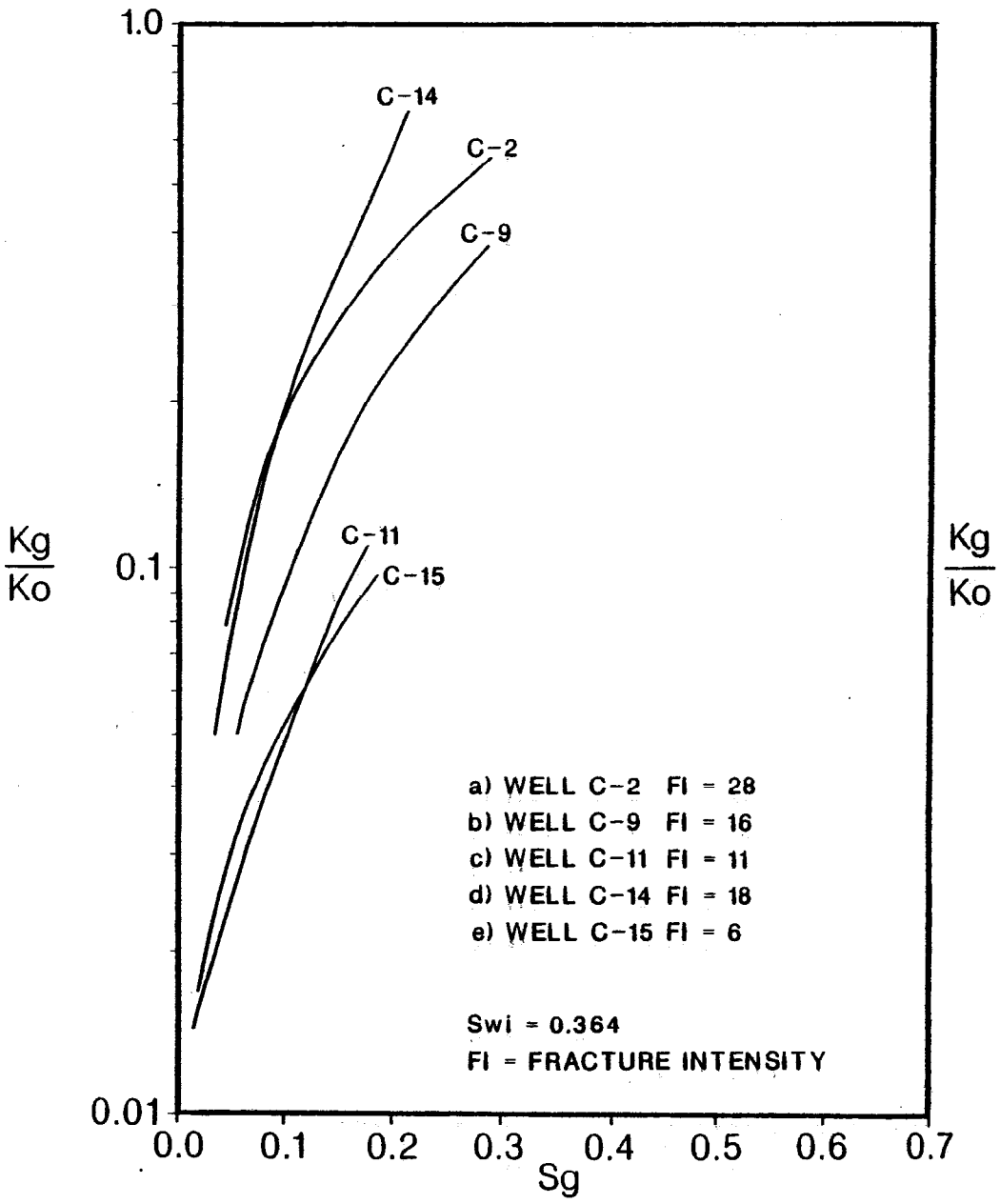

Fig. 31—Comparison of individual well performance derived K_g/K_o curves normalized to the same connate water saturation.

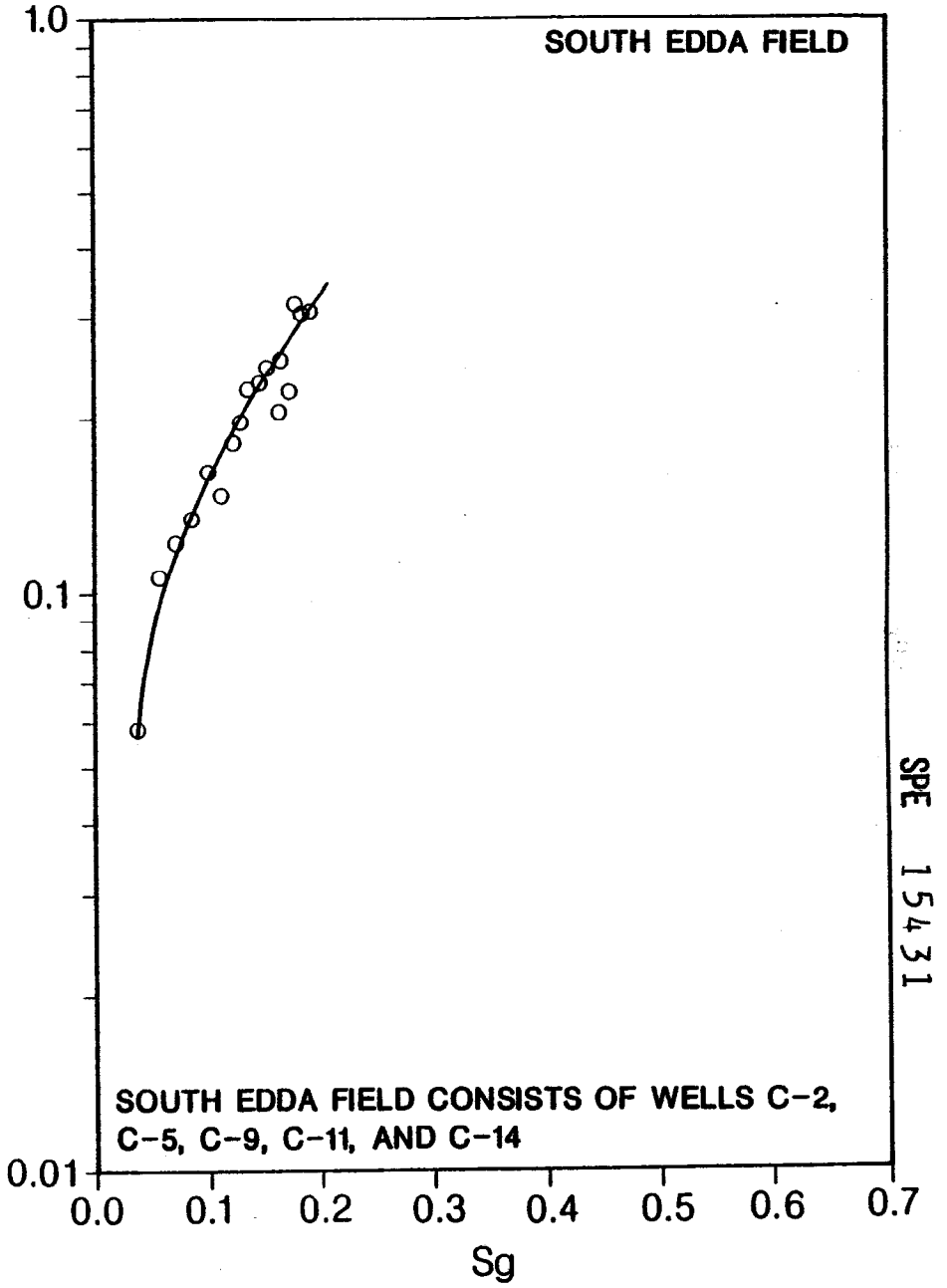

Fig. 32—Total field performance derived K_g/K_o calculated using a compositional materia balance.

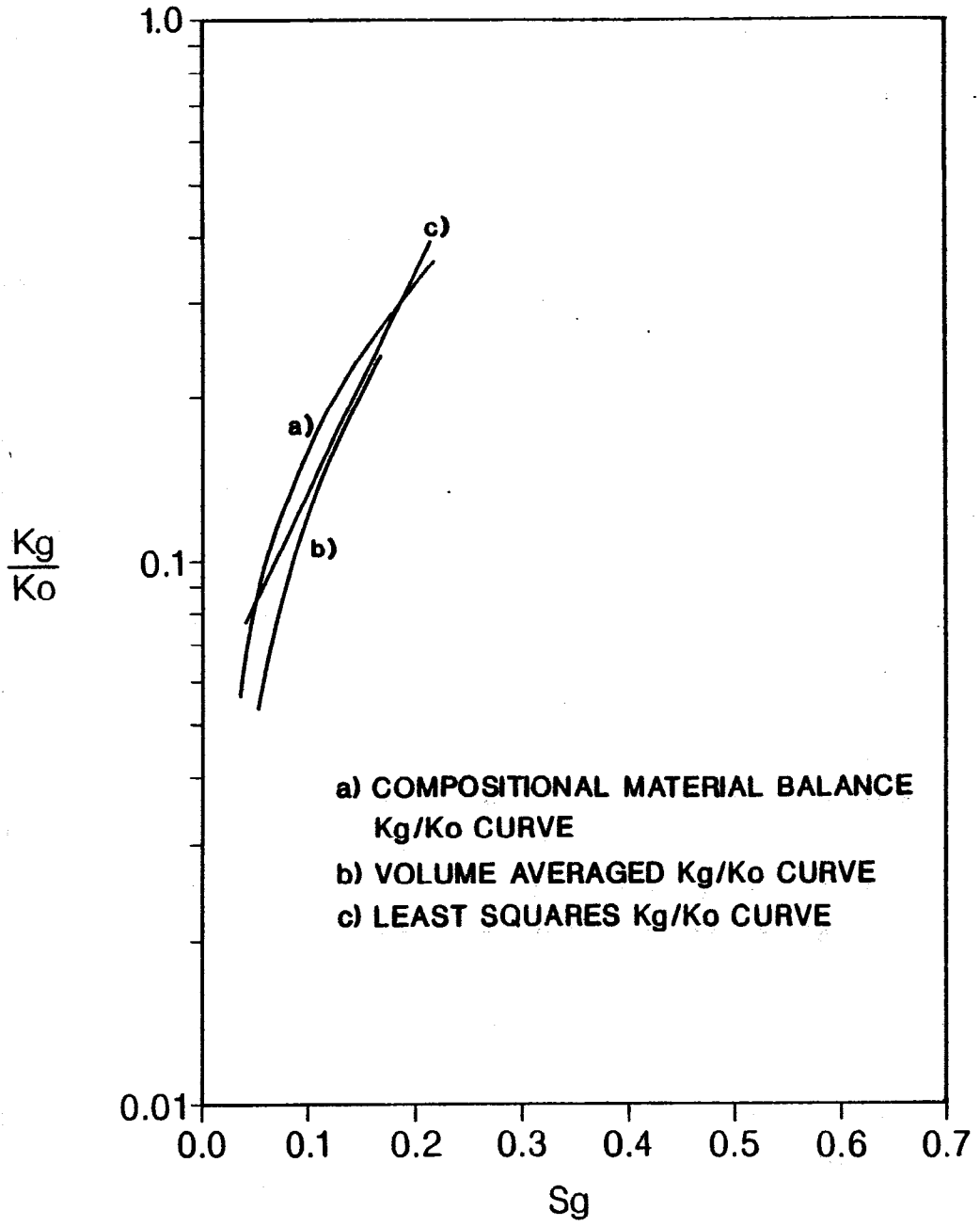

Fig. 33—South Edda total field K_g/K_o curve compared with a five-well volume averaged and a least square K_g/K_o curve.

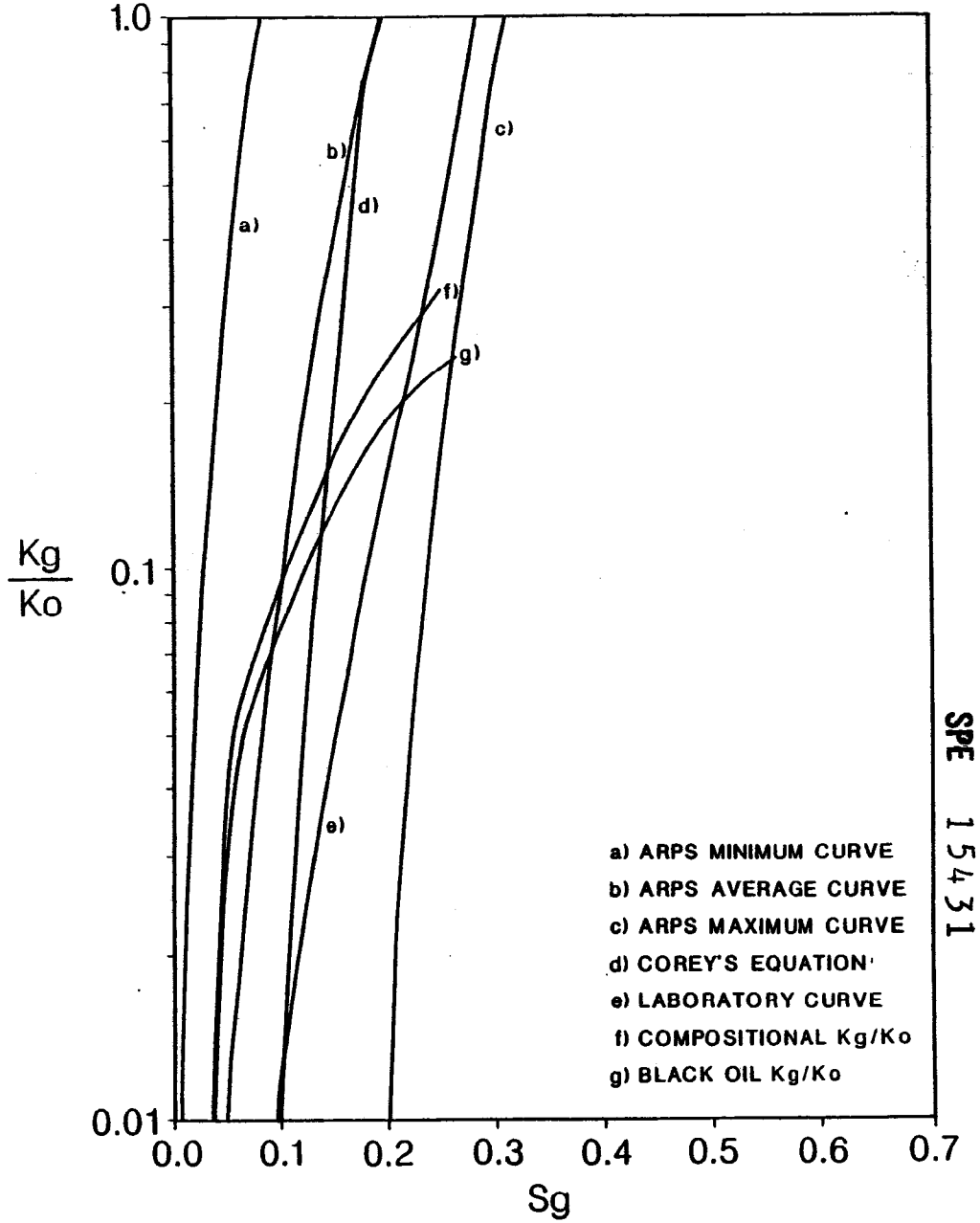

Fig. 34—Comparison of compositional material balance derived K_g/K_o curve with Corey's, Ar laboratory, and black oil—Well C-9.

SPE 15431

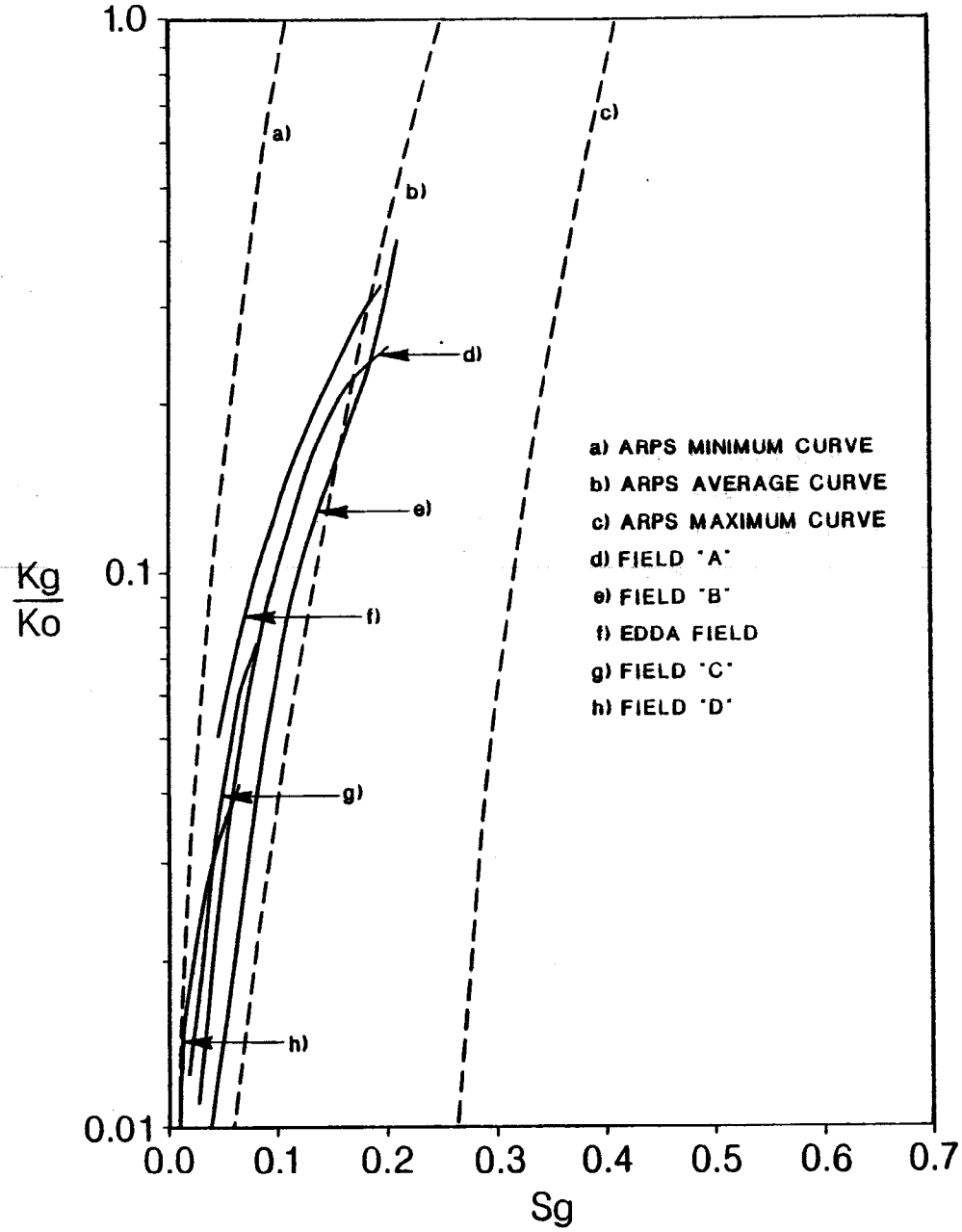

Fig. 35—Comparison of Greater Ekofisk area performance K_g/K_o curves with the South Edda field K_g/K_o curve—all normalized to $S_{wi} = 0.364$.

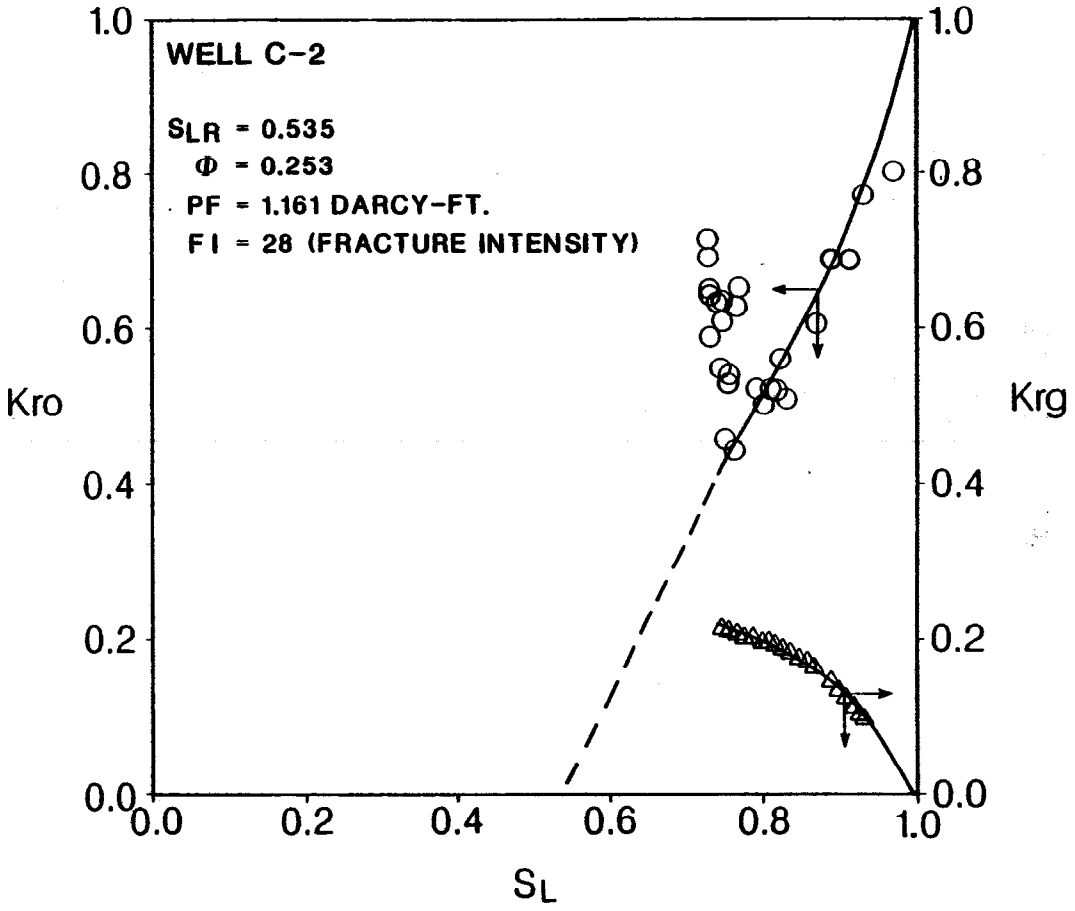

Fig. 36—Performance derived K_{ro} and K_{rg}.

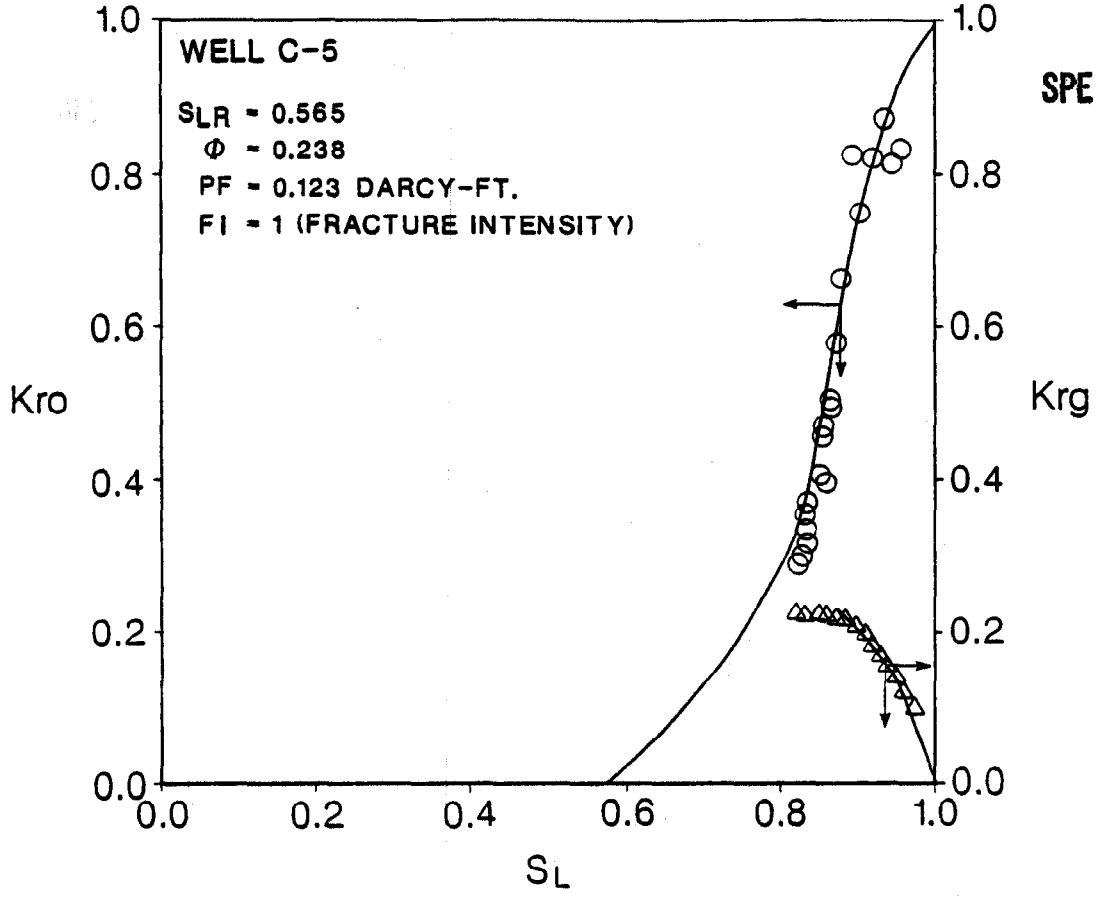

Fig. 37—Performance derived K_{ro} and K_{rg}.

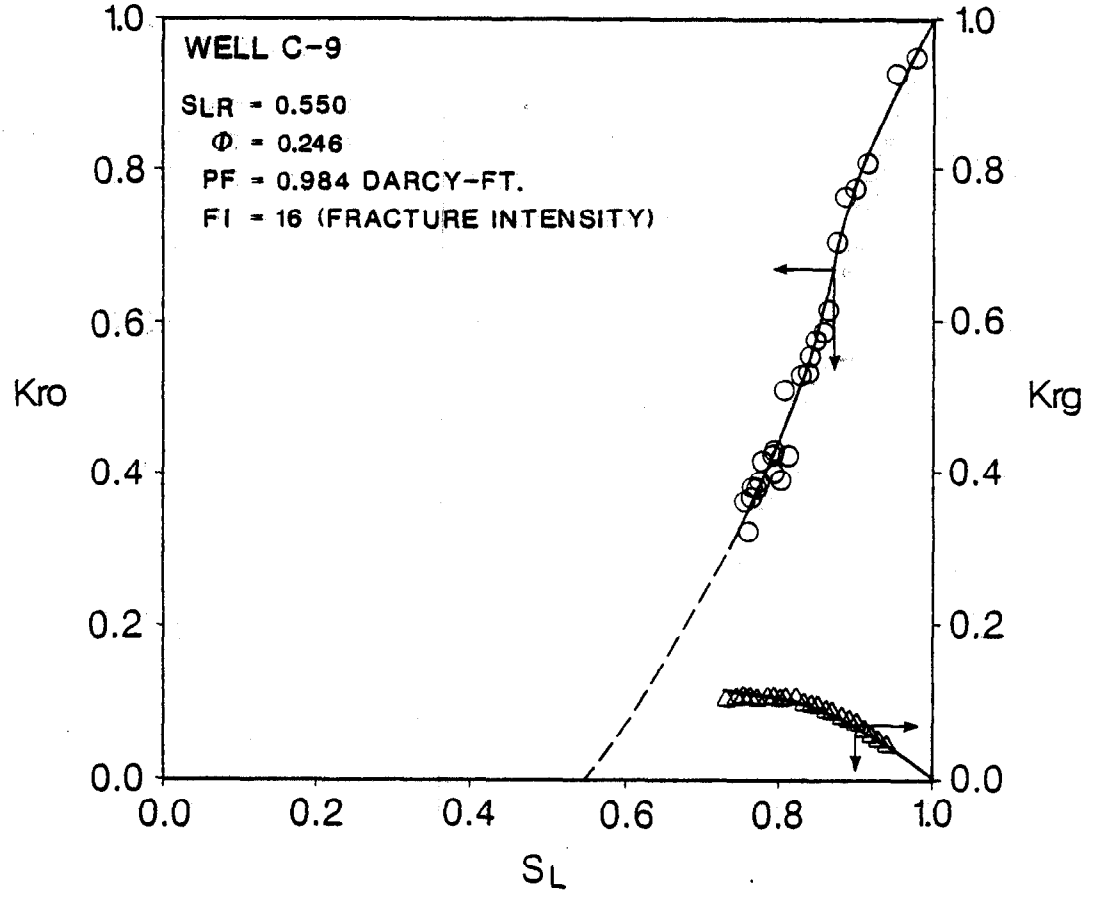

Fig. 38—Performance derived K_{ro} and K_{rg}.

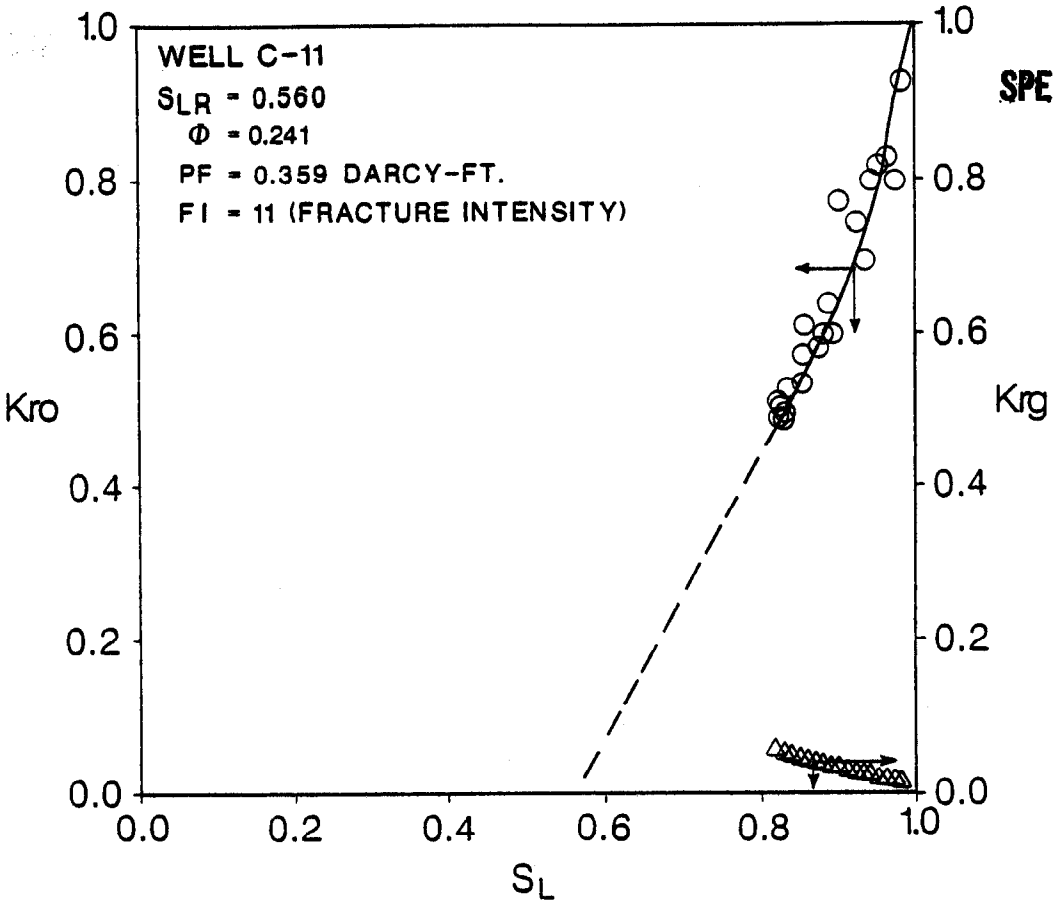

Fig. 39—Performance derived K_{ro} and K_{rg}.

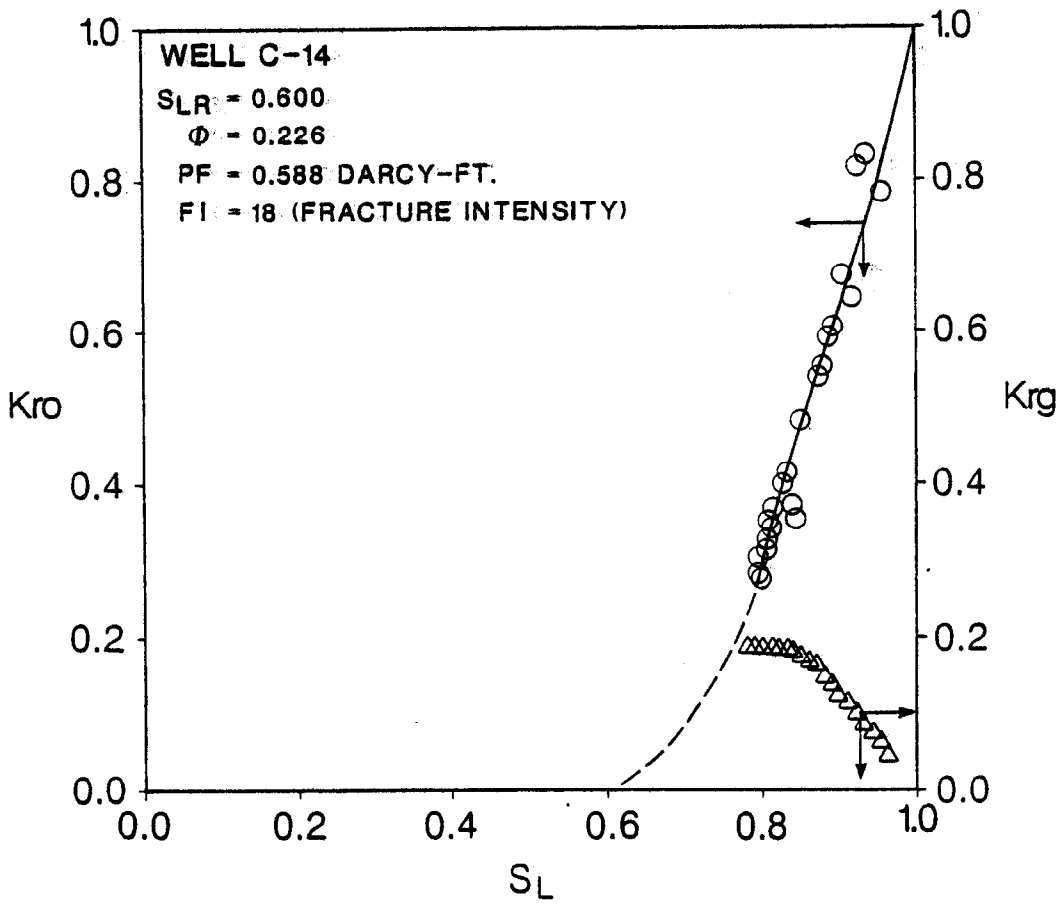

Fig. 40—Performance derived K_{ro} and K_{rg}.

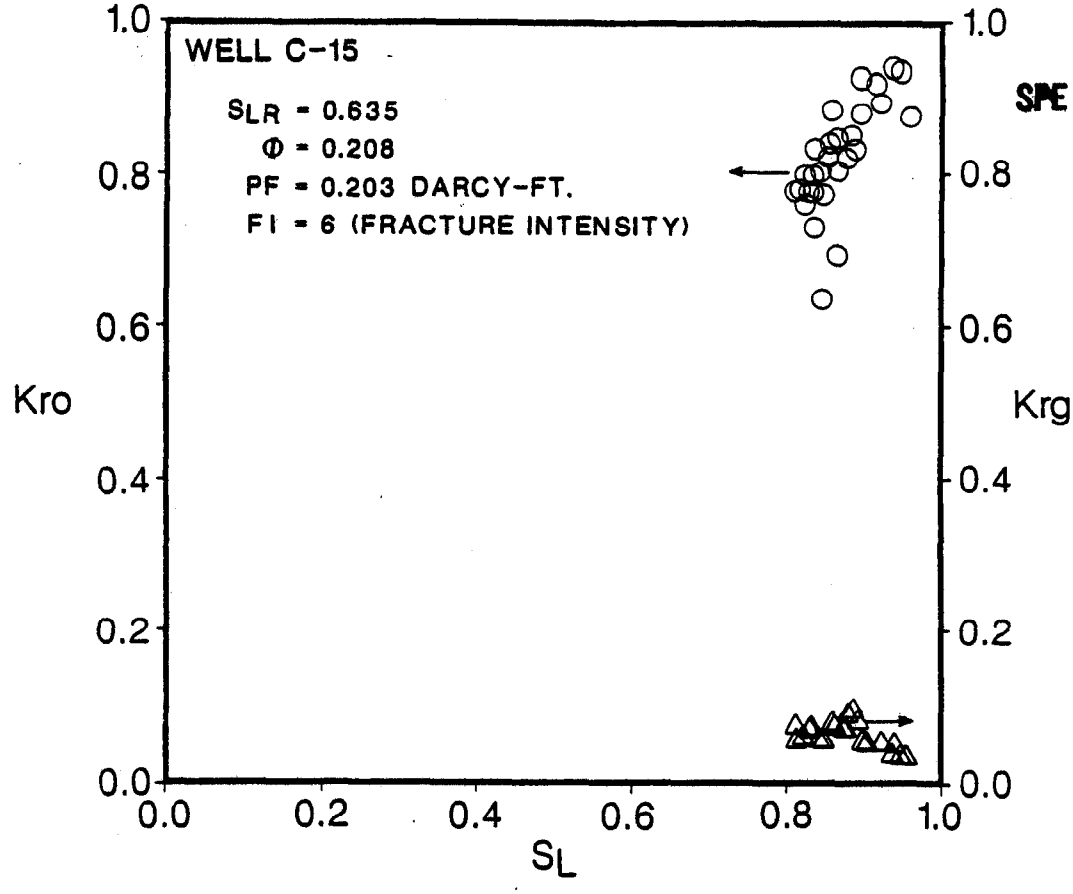

Fig. 41—Performance derived K_{ro} and K_{rg}.

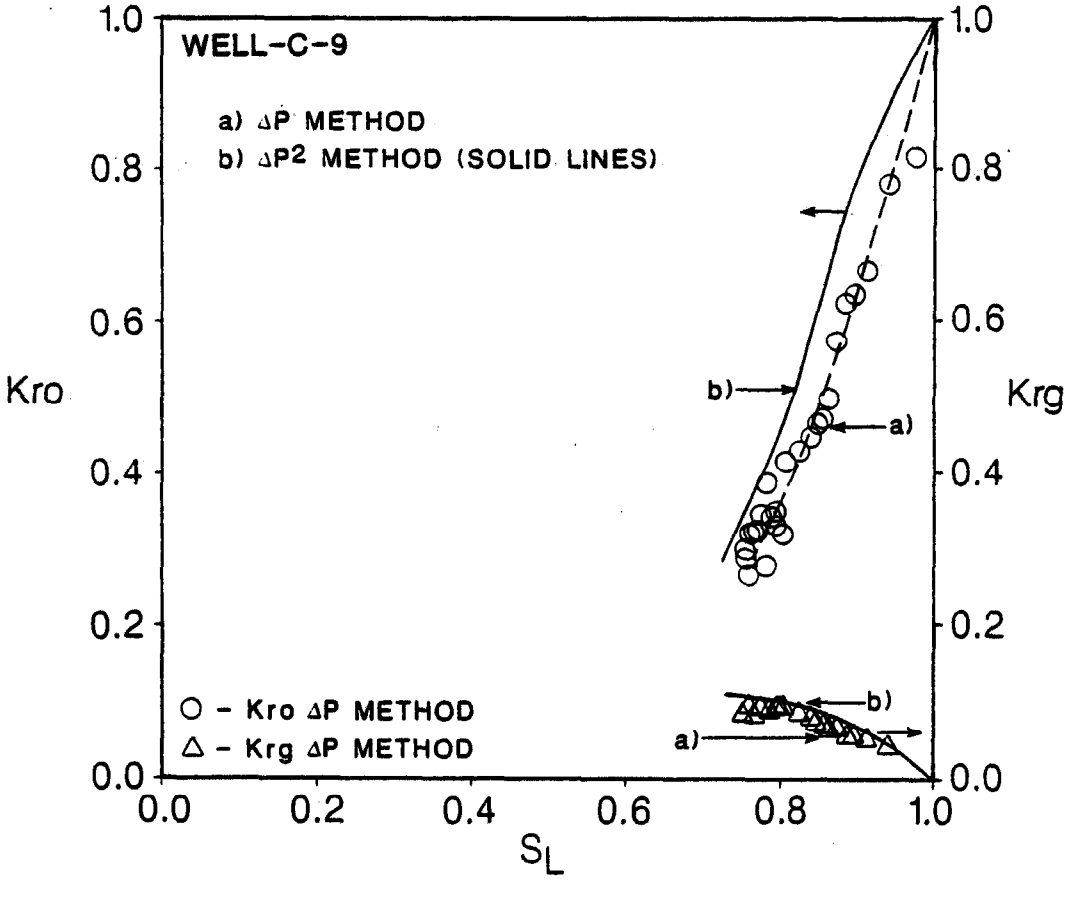

Fig. 42—Comparison of K_{ro} and K_{rg} using the ΔP^2 and Δp method.

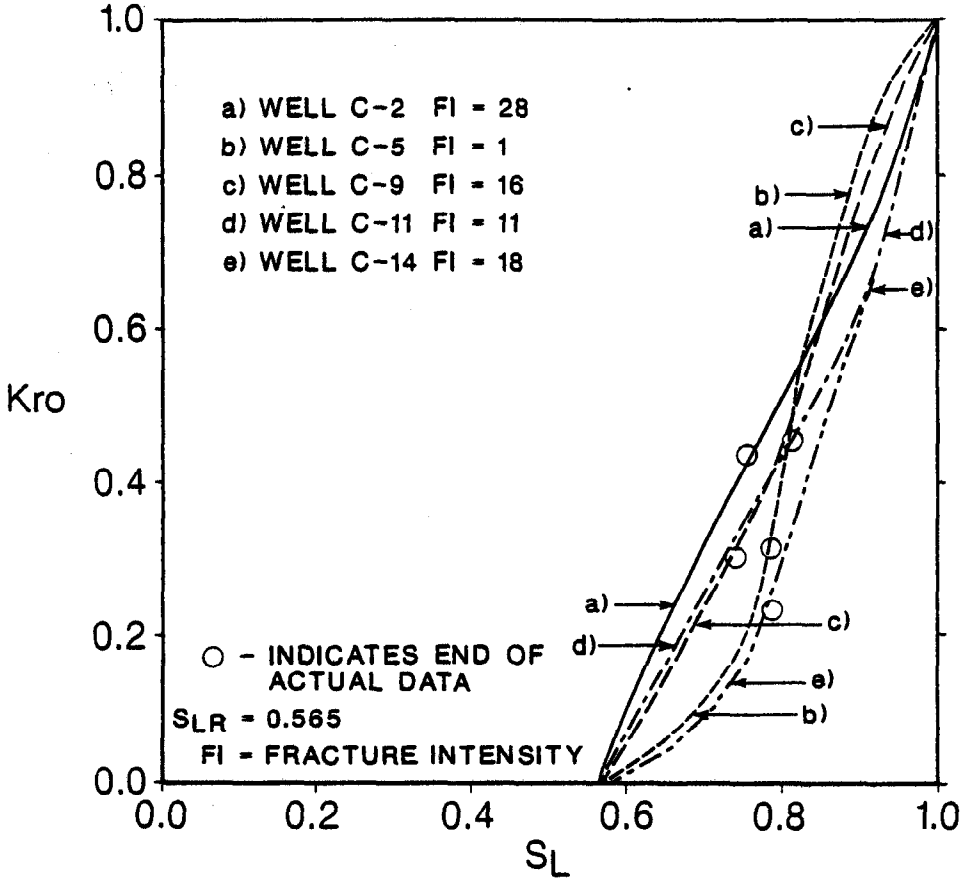

Fig. 43—Comparison of South Edda field wells performance derived K_{ro}, normalized to the same irreducible liquid saturation.

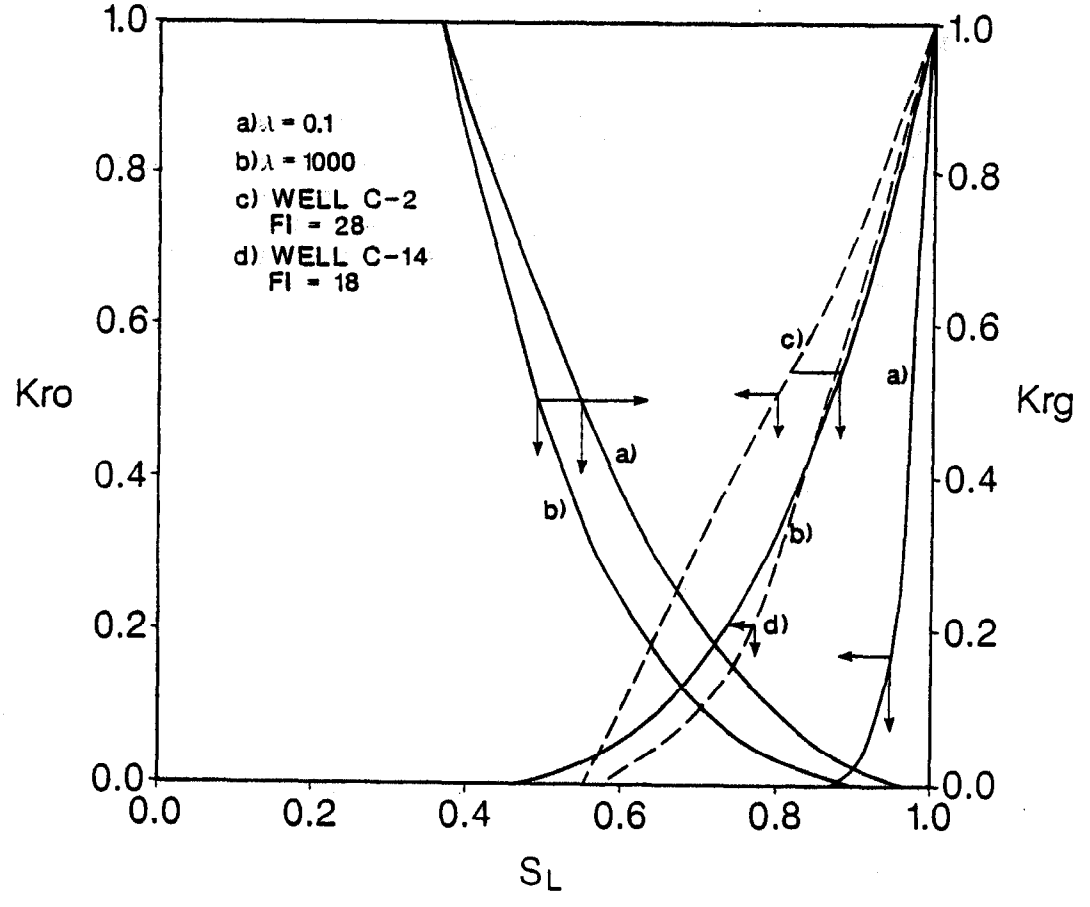

Fig. 44—Sensitivity of Corey's K_{ro} and K_{rg} curves to the pore-size distribution factor.

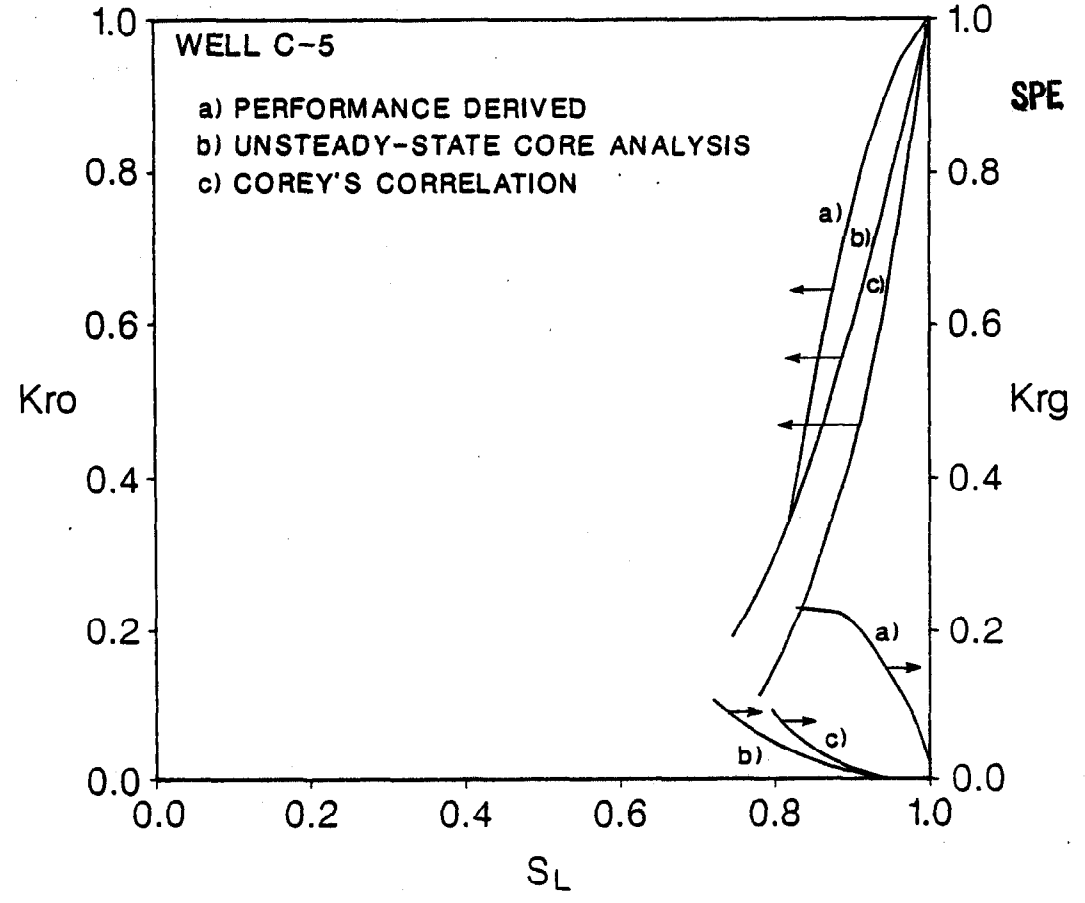

Fig. 45—Comparison of performance derived K_{ro} and K_{rg} curves with unsteady-state and Corey's derived curves.

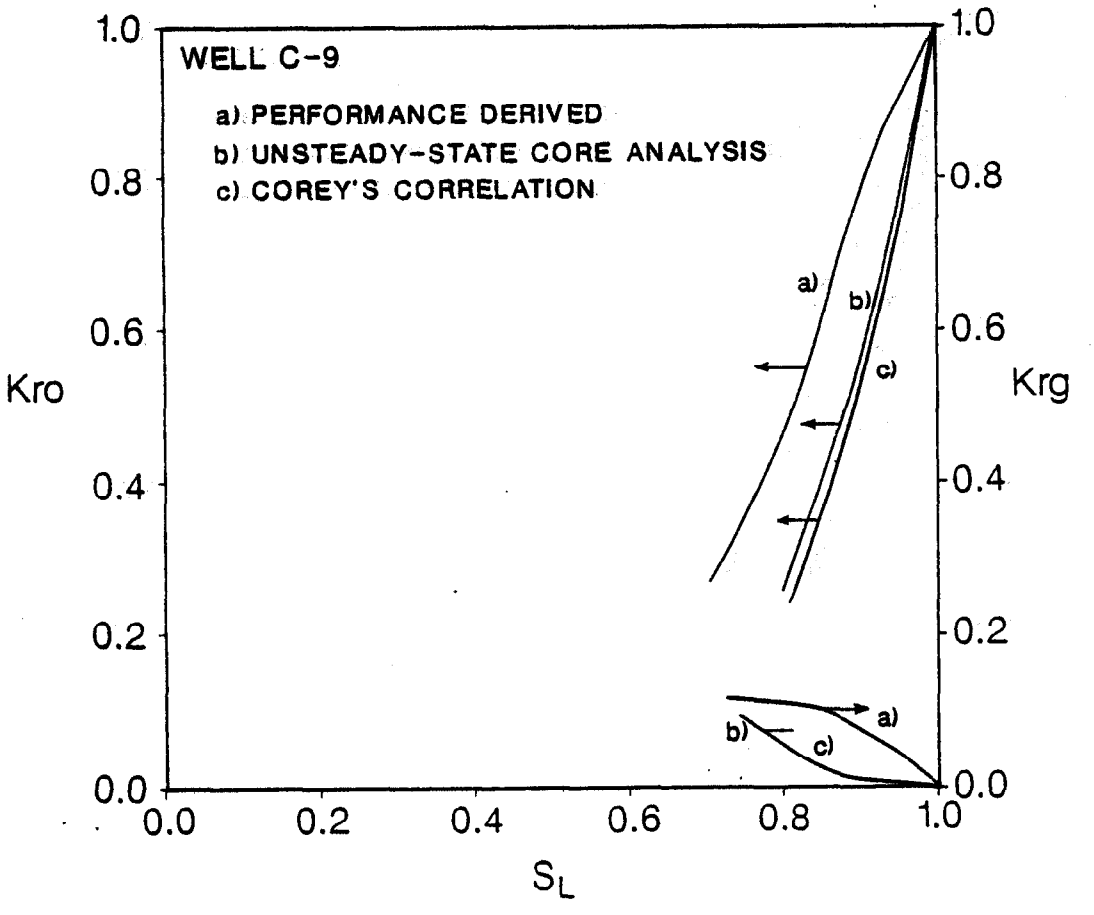

Fig. 46—Comparison of performance derived K_{ro} and K_{rg} curves with unsteady-state and Corey's derived curves.

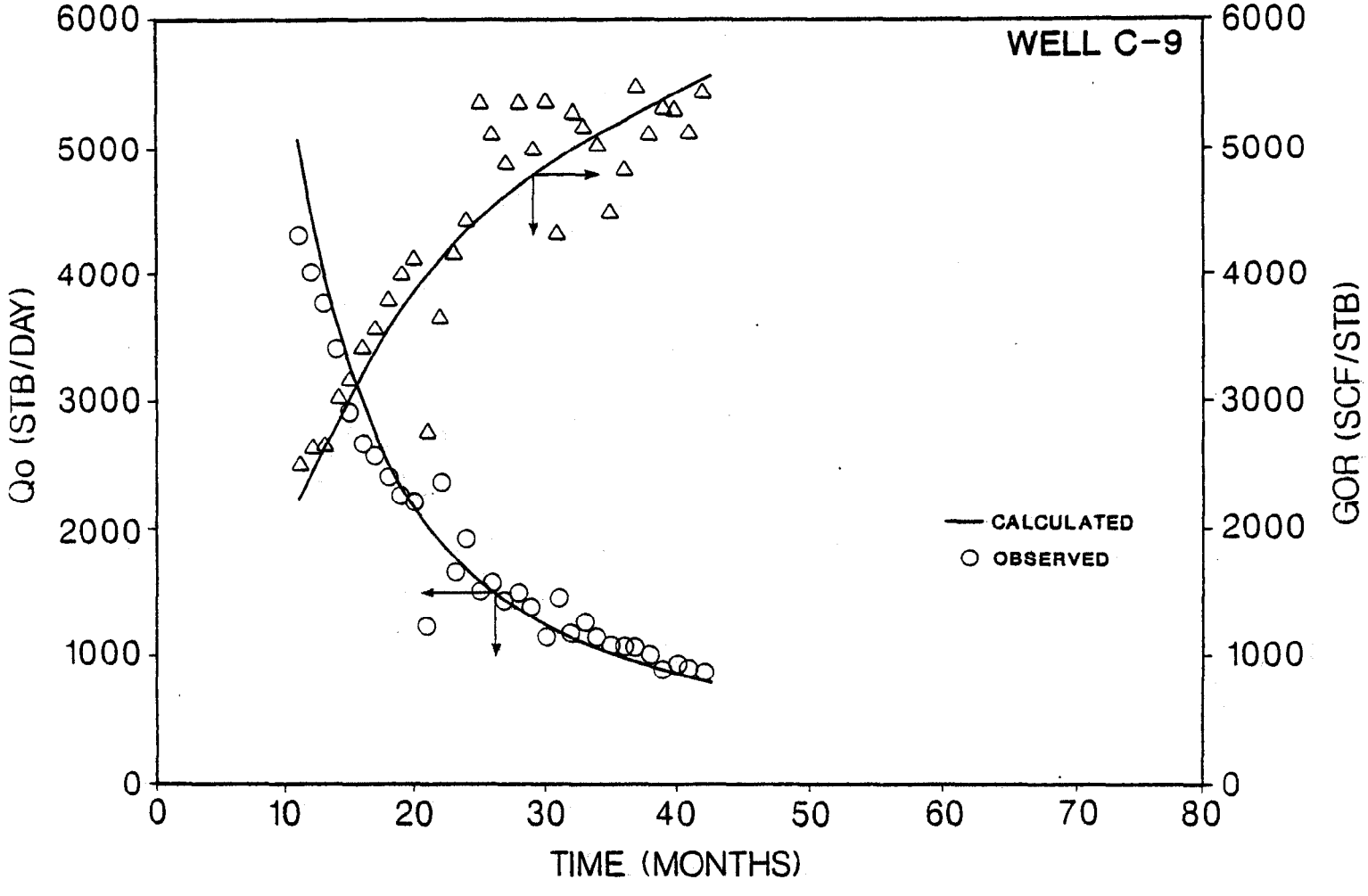

Fig. 47—Comparison of gas/oil ratio and oil rates (including condensate) obtained from performance derived K_{ro} and K_{rg} with actual oil rates and GOR.